AD-A082 851 PENNSYLVANIA STATE UNIV UNIVERSITY PARK APPLIED RESE--ETC F/G 20/4
A THEORY FOR CAVITATION INCEPTION IN A FLOW HAVING LAMINAR SEPA--ETC(U)
NOV 79 B R PARKIN N00024-79-C-6043
UNCLASSIFIED ARL/PSU/TM-79-198 NL

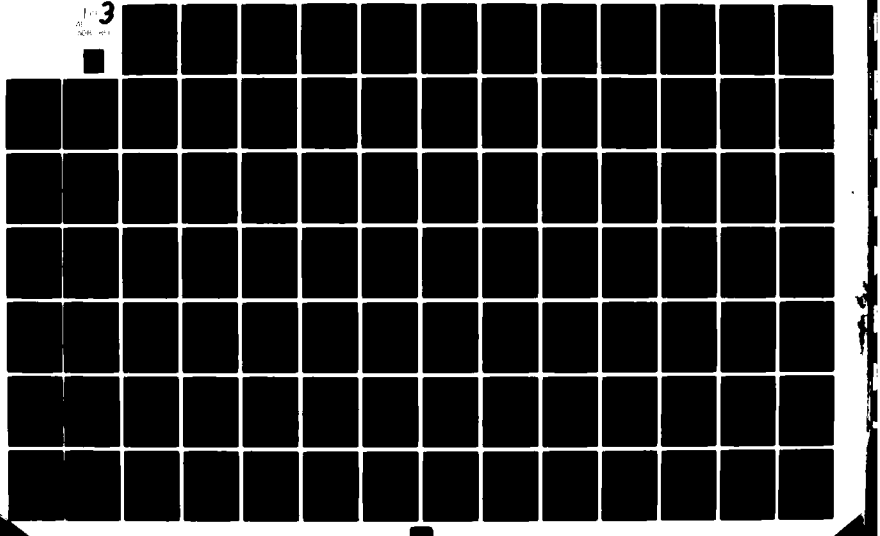

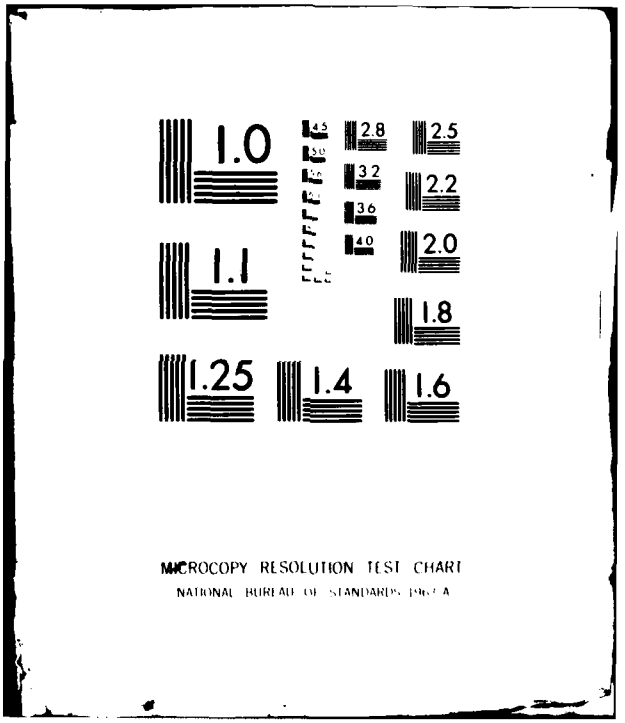
1.0
1.1
1.25
1.4
1.6
1.8
2.0
2.2
2.5
2.8
3.2
3.6
4.0
MICROCOPY RESOLUTION TEST CHART
NATIONAL BUREAU OF STANDARDS 1963 A

A THEORY FOR CAVITATION INCEPTION IN A FLOW HAVING LAMINAR SEPARATION

B. R. Parkin

Technical Memorandum
File No. TM 79-198
November 19, 1979
Contract No. N00024-79-C-6043

Copy No. 23

The Pennsylvania State University
APPLIED RESEARCH LABORATORY
Post Office Box 30
State College, PA 16801

Approved for Public Release
Distribution Unlimited

NAVY DEPARTMENT

NAVAL SEA SYSTEMS COMMAND

UNCLASSIFIED

SECURITY CLASSIFICATION OF THIS PAGE (When Data Entered)

REPORT DOCUMENTATION PAGE

READ INSTRUCTIONS BEFORE COMPLETING FORM

1. REPORT NUMBER: TM 79-198
2. GOVT ACCESSION NO.
3. RECIPIENT'S CATALOG NUMBER

4. TITLE (and Subtitle): A THEORY FOR CAVITATION INCEPTION IN A FLOW HAVING LAMINAR SEPARATION.
5. TYPE OF REPORT & PERIOD COVERED: Technical Memo[illegible]
6. PERFORMING ORG. REPORT NUMBER

7. AUTHOR(s): B.R. Parkin
8. CONTRACT OR GRANT NUMBER(s): N00024-79-C-6043

9. PERFORMING ORGANIZATION NAME AND ADDRESS:
Applied Research Laboratory
P. O. Box 30
State College, PA 1601
10. PROGRAM ELEMENT, PROJECT, TASK AREA & WORK UNIT NUMBERS

11. CONTROLLING OFFICE NAME AND ADDRESS:
Naval Sea Systems Command - Code SEA 63R-31
Washington, DC 20362
12. REPORT DATE: Nov[illegible]79
13. NUMBER OF PAGES: 170

14. MONITORING AGENCY NAME & ADDRESS (if different from Controlling Office)
15. SECURITY CLASS. (of this report): UNCLASSIFIED
15a. DECLASSIFICATION/DOWNGRADING SCHEDULE

12 175

16. DISTRIBUTION STATEMENT (of this Report)

Approved for Public Release. Distribution Unlimited.

Per NAVSEA - February 14, 1980

17. DISTRIBUTION STATEMENT (of the abstract entered in Block 20, if different from Report)

14 ARL/PSU/TM-79-198

18. SUPPLEMENTARY NOTES

19. KEY WORDS (Continue on reverse side if necessary and identify by block number)

reynolds number, cavitation, inception, prediction, theory, bubble, hemispherical

inception of

20. ABSTRACT (Continue on reverse side if necessary and identify by block number)

An approximate theory is developed to predict the onset of cavitation on hemispherical head forms for Reynolds numbers at which laminar separation is known to occur. Fairly good agreement is obtained between the cavitation desinence trends recently measured by Holl and Carroll and the present theory which is based upon first principles insofar as it is possible. Moreover, the observed occurrence of a lowest speed for "bubble-ring" cavitation, which is the only cavitation form considered here and the range of "cutoff" speeds

DD FORM 1 JAN 73 1473 EDITION OF 1 NOV 65 IS OBSOLETE

391007

UNCLASSIFIED

SECURITY CLASSIFICATION OF THIS PAGE (When Data Entered)

predicted by the present asymptotic theory show very encouraging agreement. Like the experiments, ~~the present~~ theory suggests that ~~this~~ cutoff speed and its accompanying cutoff cavitation number can also depend on ~~the~~ temperature ~~of the water~~ provided that the initial size attributed to a "typical" spherical free-stream air bubble nucleus also varies with ~~the~~ temperature. At 80°F (26.6°C) it is found that the typical nucleus from which bubble-ring cavitation originates has a radius of about seven microns. At higher temperatures the nucleus radius decreases from this value while at lower temperatures the initial radius exceeds the value noted. It is also found that: the onset cavitation number should be less than the magnitude of the pressure coefficient at the laminar separation point; and that the cavitation number increases with free-stream velocity. As long as there is an appreciable concentration of dissolved air in the water, it is also found, in agreement with experiment, ~~that~~ the onset of bubble-ring cavitation is practically independent of air content.

Subject: A Theory for Cavitation Inception in a Flow Having Laminar Separation

References: See page 139.

Abstract: An approximate theory is developed to predict the onset of cavitation on hemispherical head forms for Reynolds numbers at which laminar separation is known to occur. Fairly good agreement is obtained between the cavitation desinence trends recently measured by Holl and Carroll and the present theory which is based upon first principles insofar as it is possible. Moreover, the observed occurrence of a lowest speed for "bubble-ring" cavitation, which is the only cavitation form considered here, and the range of "cutoff" speeds predicted by the present asymptotic theory show very encouraging agreement. Like the experiments, the present theory suggests that this cutoff speed and its accompanying cutoff cavitation number can also depend on the temperature of the water, provided that the initial size attributed to a "typical" spherical free-stream air bubble nucleus also varies with the temperature. At 80°F (26.6°C) it is found that the typical nucleus from which bubble-ring cavitation originates has a radius of about seven microns. At higher temperatures the nucleus radius decreases from this value while at lower temperatures the initial radius exceeds the value noted. It is also found that the onset cavitation number should be less than the magnitude of the pressure coefficient at the laminar separation point and that the cavitation number increases with free-stream velocity. As long as there is an appreciable concentration of dissolved air in the water, it is also found, in agreement with experiment, that the onset of bubble-ring cavitation is practically independent of air content.

Acknowledgment: This study has been supported by the Naval Sea Systems Command under the cognizance of Code SEA 63R-31. The author wishes to acknowledge many useful discussions with Drs, J. W. Holl and M. L. Billet during the course of the study. Mr. Ross A. Kohler has been helpful with some of the numerical work and the bubble trajectory calculations were programmed for the Hewlett Packard Programmable calculator by Mr. W. R. Hall.

Contents

Contents - Continued

List of Tables

List of Figures

List of Figures - Continued

List of Figures - Continued

November 19, 1979
BRP:mmj

Nomenclature

a	magnitude of the dimensionless acceleration of the bubble wall
b	magnitude of the minimum pressure coefficient on the headform, $b = -C_{p_{min}}$
C	concentration of air dissolved in the water, moles of air per million moles of water (ppm) at any point in the flow
C_i	initial concentration of dissolved air measured in a sample of water tunnel water
C_p^*	measured pressure coefficient at an arbitrary upstream point on the body used for fitting approximating functions
C_p	pressure coefficient = $(p - p_o)/\frac{1}{2}\rho V_o^2$
$C_{p_{min}}$	static pressure coefficient in laminar separation bubble, $(p_s - p_o)/\frac{1}{2}\rho V_o^2$
C_{p_s}	static pressure coefficient in laminar
C_{p_1}	pressure coefficient at the point s_1 on the body
C_s	saturation concentration
C_σ	ratio of characteristic surface tension pressure to dynamic pressure, $= \frac{4\sigma}{R_o \rho V_o^2}$
D	diameter of the water tunnel model
dr	differential of dimensionless radius
$d\tau$	differential of dimensionless bubble time
$f(t)$	when laboratory time is used = $[p_o - p(t)]/\frac{1}{2}\rho V_o^2 = -C_p(t)$
$f_1(s)$, $f_2(s)$	parabolic approximations to the experimental pressure distribution on the head form
$f_2(\tau)$	an approximating function for the pressure distribution on the head form when dimensionless arc length has been transformed to dimensionless bubble time

Nomenclature - Continued

$F(\tau)$ dimensionless forcing function experienced by a cavitation bubble,

$$= - \frac{K + f(\tau)}{C_\sigma}$$

$F_a(\tau)$ dimensionless forcing function for the stepwise-autonomous approximation for cavitation bubble growth

H maximum height of the laminar separation bubble

I the impulse integral $\int r^2 F(\tau) d\tau$

I_a impulse integral for the stepwise-autonomous forcing function

$I(r_m)$ the value of the impulse integral at the maximum bubble radius

K cavitation number $= (p_o - p_v)/\frac{1}{2}\rho V_o^2$

K_c "critical" cavitation number

K_{co} cutoff cavitation number

K_e cavitation number when the bubble radius is the equlibrium radius

n surface tension parameter which governs the slope of the linearly increasing part of the surface tension law $S(r,\sigma)$

p static pressure at any point in the flow

p_a partial pressure of air in the free-stream nucleus at the measured dissolved air concentration

p_g partial pressure of air in the bubble when it is in the laminar separation zone

p_o static pressure at upstream infinity

$p_,$ pressure of the vapor inside the cavitation bubble

p_s static pressure of the liquid in the separation bubble

p_σ contribution of surface tension to the static pressure

$p(t)$ external static pressure as a function of laboratory time

Nomenclature - Continued

r	dimensionless radius $= R/R_o$
r_b	denotes the limiting value of r_m as limited by the height of the laminar separation bubble
r_c	critical dimensionless bubble radius
r_e	equilibrium dimensionless radius
r_m	maximum dimensionless bubble radius
r_{m_b}	maximum dimensionless radius as limited by height of laminar separation bubble $= r_b$
r_{max}	maximum dimensionless radius $= r_m$
r_o	value of dimensionless radius when $\tau = \tau_o$
r_ℓ	larger critical dimensionless radius
$r(\tau)$	dimensionless radius as a function of bubble time, τ
r_{vm}	the radius of minimum velocity very near the smaller critical radius
R	bubble radius
R_e	equilibrium bubble radius
Re	Reynolds number based on body diameter
R_m	maximum bubble radius
R_o	"radius" of typical nucleus
$R(t)$	bubble radius is time dependent
s	dimensionless arc length along the body surface = S/D
s_0, s_1, s_2, s_3	particular points on the body
s^*	dimensionless arc length at a point upstream of the minimum pressure point
S	arc length along surface of head form

Nomenclature - Continued

$S(n,\sigma)$	value of surface tension law when $r = n$ then $S = \sigma$
$S(r,\sigma)$	surface tension law
t	laboratory or "real" time
t_m	time available for vaporous growth
T	temperature
v	dimensionless bubble-wall velocity
v_o	dimensionless bubble-wall velocity when $\tau = \tau_o$
$v(r_o)$	dimensionless bubble-wall velocity when $r = r_o$
$v(\tau)$	dimensionless bubble-wall velocity as a function of dimensionless time
V_{co}	cutoff velocity
V_o	free-stream velocity
α	driving parameter, $\alpha = \frac{b - K}{C_\sigma}$
α_c	critical value of α corresponding to $r = r_c$
α_s	value of the bubble driving parameter at the smaller critical radius r_s as defined by Eq. (88a) in which case $r_s = r_c$
β	dimensionless parameter characterising static pressure in laminar separation zone, $\beta = \frac{K + C_{p_s}}{C_\sigma}$
β_e	value of β when $r = r_e$
β_c	value of β when $r = r_c$
γ	dimensionless air content parameter, $\gamma = p_a/(2\sigma/R_o)$
γ_c	critical value of γ corresponding to $r = r_c$
Γ	$\gamma - \beta$

Nomenclature - Continued

θ	ratio of maximum vapor bubble diameter to the maximum laminar separation bubble height
ρ	liquid density
σ	coefficient of surface tension
τ	dimensionless time, $t\sqrt{2\sigma/\rho R_o^3}$
τ_a	dimensionless lag time
τ_g	dimensionless growth time after the conclusion of favorable external pressure, $\tau > \tau_o$
τ_m	dimensionless time available for vaporous bubble growth
τ_o	duration of favorable environment for growth in which $F_a = \alpha$
$\phi(R)$	velocity potential at the bubble wall
$\lambda(T)$	constant of proportionality in Henry's law
μ	dynamic viscosity of liquid, symbol for micron
ν	kinematic viscosity of liquid
ξ	normalized radius, $\xi = r/\sqrt{\gamma}$
ξ_e	value of ξ when $r = r_e$
ξ_m	value of ξ when $r = r_m$

INTRODUCTION

In the following we shall attempt to estimate from first principles the onset of cavitation for a rather special flow on an axially symmetric body. The body consists of a hemispherical nose attached to an afterbody which is a right circular cylinder of diameter equal to that of the hemisphere. The free-stream flow velocity (V_o) is aligned with the body axis. The static pressure at upstream infinity is p_o, and the liquid density is ρ. This flow configuration is illustrated schematically in Figure 1.

It has been shown [1, 2]* that the flow about hemispherical bodies will often have a laminar separation bubble on the body downstream of the minimum pressure point. The laminar bubble is estimated to be present up to Reynolds numbers, based on body diameter, D, of about five million [1, 3]. This Reynolds number limit is greater than the Reynolds numbers of the majority of data reported from cavitation-tunnel experiments with such bodies. Therefore, there are considerable experimental data on cavitation inception or desinence in the presence of laminar separation which can be used to test the validity of theoretical findings. Our goal is to formulate a theory of cavitation onset which accounts for the main physical processes which appear to take place in this rather special flow and to compare our findings with experiment.

The present analysis is certainly not the first such study to appear in the literature. A concise review of a number of previous investigations has been given by Holl [4]. For our purposes, it seems sufficient to note that all features of the noncavitating flow, which may have a decisive influence on inception, were not as well-known when those earlier studies

*Numbers in brackets designate References, pp. 139-140.

were carried out as they are today. Therefore, previous theories for cavitation inception on bodies, which are now known to exhibit laminar separation, show at best only qualitative agreement with experiment. Our task will be to extract from the present more complete knowledge of the physical events which have been observed in the rather special flows of interest here, those features which seem to be most important with respect to the onset of cavitation. From such considerations one may then postulate a sequence of key events leading to cavitation onset. Next he can formulate a mathematical model which applies to each event. This system of mathematical relationships can then be used to estimate those flow parameters which determine cavitation inception. The estimated results can then be compared with experiment.

THE SEQUENCE OF EVENTS

Perhaps the most direct way to describe the several physical aspects of the theory is to list in sequence the key events or phases of bubble growth as they apply to a typical nucleus. Once we have given this sequence, the observational basis for each hypothesis will be discussed.

(a) It is assumed that cavitation bubbles originate from small nuclei which contain air or water vapor or both. Generally such nuclei are not visible to the unaided eye. In this study we will suppose that these nuclei are distributed throughout the liquid.

(b) A typical nucleus of radius R_o, once it is in the boundary layer on the body, will encounter a low pressure region which is favorable to vapororous bubble growth. That is, the local

static pressure on the body is less than p_v, the vapor pressure of the water. As it moves through this region of low pressure the bubble will grow from the initial radius R_o to some maximum radius R_m.

(c) The very small radius R_m is achieved at a point on the body where the local static pressure has risen to a value which is greater than the vapor pressure. Therefore, if left to itself the bubble would collapse.

(d) The bubble of radius R_m becomes stabilized on the body within the laminar bubble. After it has become fixed inside the laminar bubble its subsequent growth is caused by air diffusion from the liquid into the bubble.

(e) This gaseous growth continues until the bubble has become large enough to interact with the free shear layer between the outer flow and the inner region of the laminar bubble.

(f) The process of interaction with the shear layer, which causes further gaseous growth to cease, will lift the bubble from the surface of the body by a slight amount and permit it to move downstream with the flow. This motion will take place very close to the body and it will cover a very short distance because the bubble will soon find itself at the downstream end of the laminar bubble where the boundary layer becomes turbulent.

(g) When the bubble is exposed to the turbulent boundary layer flow, low pressures in the turbulent eddies cause a second short period of explosive vaporous growth. However, this final growth

phase can not proceed unchecked. As the bubble grows it will become large enough to experience the turbulent shearing motions in the boundary layer. These motions so distort the bubble that it is torn apart and it will appear to the observer as a part of the frothy narrow band of cavitation which appears at the downstream end of the laminar bubble. Indeed, it is the first appearance of this white band or cloud of extremely small bubbles which we identify as desinent or incipient cavitation. Some authors call this state of desinence or incipience "bubble-ring cavitation" because of its very limited streamwise extent.

The foregoing description of events outlines the occurrances which are of immediate concern in this study. However, it is worth noting that the events noted above have centered upon the history of a typical nucleus, which is only one of many nuclei, sharing the fate of the typical bubble. The number of nuclei which are similarly affected increases as the degree of cavitation is intensified and the extent of the cloud increases visibly. However, this intensification is limited by the extent of the laminar bubble because it will soon be filled by the cloud. When this filling reaches its limit the cloud is transformed into a cicumferential band of small clear cavities with their leading edges attached to the body just behind the point of laminar separation. Thus an entirely different cavitation flow regime is established. A region in which pressures are less than the vapor pressure of water no longer exists upstream in the vicinity of the minimum pressure point of noncavitating flow. The small cavities now on the body are actually cavity flows which are sustained by evaporation from the cavity wall and by air diffusion from the liquid

into the cavity. Presumably the methods of free-streamline theory could be adapted to the analysis of this flow. However, such considerations are outside the scope of this study.

Free-Stream and Surface Nuclei:

Let us consider next the observational basis for the preceding outline of the life of a typical cavitation bubble. It seems logical to start with a brief discussion of nuclei. This is a topic which has received considerable study. There is a rather extensive literature about the origin and the nature of cavitation nuclei. Rather than presenting a review of this material here we shall refer the reader to a few sources of further information. For relatively concise or somewhat longer discussions of the topic, one can consult Holl [4], Plesset [5], Beyer [6], Ross [7], or Knapp, Daily, and Hammit [8]. A fairly complete list of original sources is given in the last of these citations.

For our purposes it seems sufficient to note that it is known that ordinary water contains impurities, usually with some air stabilized upon them, which can act as "weak spots" in the liquid and form seats for cavitation bubble growth. When one performs cavitation experiments in a closed-circuit water tunnel, the events which take place in the test section can also produce small air-bubble nuclei unless the tunnel is equipped with a resorber which drives these bubbles into solution or it has some other device which removes such gas bubbles from the flow before they reenter the test section. The resorber offers the advantage that the dissolved air content of the water can be held constant in cavitation experiments of long duration. Air removal reduces the air content and can significantly change

the nuclei content when extended periods of cavitation testing are undertaken. In this situation one may simply put fresh water in the tunnel in order to restore the nuclei content to its original state.

It is known that a spherical air bubble in still water will dissolve because of surface tension if its radius is less than a critical value. On the other hand, if the radius is greater than this critical value a bubble can grow by air diffusion from the water into the bubble. Such a bubble will rise to the surface and will also be lost as a cavitation nucleus. Thus, much of the literature in the references cited above deals with reasons for the observed fact that cavitation nuclei are found in ordinary water even though it may have been quiescent for a very long time. On the other hand, we have noted that cavitation testing in a water tunnel, by its very nature, can generate very small bubbles which serve as cavitation nuclei. Although such nuclei may have short lives, their presence can affect water tunnel observations.

In order to account for the persistance of certain classes of nuclei, we shall employ a model in which the net surface energy is initially zero [9]. Such a nucleus could be composed of a microscopic solid particle which has absorbed air, which has a small crack, or which is porous so that air is stabilized on it. We will also want to account for some nuclei which are actually spherical air bubbles. We will use a simple analytical model which can accommodate both of these possibilities.

Those conditions which can cause stable nuclei in the flow can also pertain to the surface of the body. This fact has led to the concept of surface nuclei which consist of small crevices or pores which can act as

seats for the generation of air bubble nuclei on the body surface. Such surface imperfections become sources of air bubbles by a process of convective air diffusion [10]. In some ways such nuclei resemble free-stream nuclei because they produce bubbles which enter the boundary layer flow. However, if surface nuclei are the predominant source of nuclei in a flow and the water is supersaturated in the vicinity of such nuclei, inception is observed as patch cavitation even in regions where the local static pressure exceeds the vapor pressure.

Gupta [11] was among the first to perform systematic tests designed to compare the effects of cavitation inception from surface nuclei and free-stream nuclei. In experiments using Teflon and Polyethylene models, he found that surface nuclei on such porous bodies exhibit gaseous cavitation inception which is quite different from the kind of cavitation inception under consideration here. The cavitation process we plan to consider was observed on stainless steel hemispherical bodies. Stainless steel bodies were also tested by Gupta, and his observations of inception and desinence were considered to be consequences of free-stream nuclei. Subsequently, Van der Meulen [12] carried out boundary layer studies on hemispherical models made of stainless steel and Teflon which showed that the noncavitating flows about bodies of these materials were the same. He also found that the Teflon body exhibited gaseous cavitation and that the stainless steel model exhibited desinence and inception typical of free-stream nuclei. In this respect the findings of Gupta and Van der Meulen are in agreement. However, Van der Meulen found a strong cavitation hysteresis for the Teflon body and practically no hysteresis on the stainless steel model. Gupta's experiments showed the opposite. Reasons for these contradictory findings are as yet unknown.

Evidently, bodies which provide active sites of surface nuclei will exhibit cavitation inception characteristics which cannot be described by the sequence of events stated above. Therefore, we shall restrict our considerations to cavitation which originates from free-stream nuclei as stated in item (a) above.

Initial Vaporous Growth:

Interestingly enough, in spite of the many experimental investigations of cavitation bubble growth, no direct observations of vaporous growth of microbubbles in the boundary layer have been made. The difficulty of such experiments is manifest. Although larger traveling bubbles have been photographed and gaseous growth in the laminar bubble has been recorded, we only have indirect evidence that the microbubbles undergo a short period of vaporous growth prior to the time that a bubble becomes stabilized in the laminar bubble. Nevertheless, the evidence now available does argue for the existence of an initial phase of vaporous growth [10]. Four observations may be made in support of this argument:

(1) There are tensions in the liquid at the minimum pressure point on the body during inception. By tensions we mean static pressures less than vapor pressure.

(2) When the cavitation is observed to change from the incipient or desinent forms to sheet cavitation, the tension at the minimum pressure point is lost and no individual bubbles are found at any point in the boundary layer upstream of the cavity. Similarly, as the free-stream pressure is lowered, starting from noncavitating flow, no cavitation of any kind is observed on the body unless there is a tension at the minimum pressure point.

(3) In the experiments cited in Reference 10, the local pressures were such, just before a tension was produced at the minimum pressure point or just after it was lost, that the water in the vicinity of the minimum pressure point was still supersaturated with dissolved air.

(4) Thus, bubble growth by air diffusion would be only slightly affected by the above pressure changes if it could occur at all. Evidently the stream nuclei may be too small to permit such growth and one concludes tentatively that the bubble grows to a larger size than the original size of the nucleus before air diffusion starts. Presumably this increase in size occurs by means of a short period of vaporous growth prior to the onset of gaseous growth.

Bubble Size After Initial Growth:

Having indicated the reasons for vaporous growth one must now consider the smallest possible size that the bubble must attain and its location on the body after this growth has occurred. As we have noted, the smallest size must correspond to that radius which will just permit gaseous growth. We shall determine this radius, R_m, by using the theory of Epstein and Plesset [13]. This theory supposes that the bubble is at rest in an air-water solution which can be undersaturated or oversaturated. The rate at which a bubble dissolves or grows is calculated from the theory of diffusion. In Reference 10 it is noted that when the liquid flows past a fixed bubble the rate of air diffusion into or out of the bubble increases greatly compared to the quiescent fluid case of Reference 13. However, in the present study our interest centers on threshold conditions under which gaseous bubble growth is

possible. The subsequent growth rate is another matter and the Epstein-Plesset formulation is the correct one for the problem at hand. The location on the body where bubbles of at least the critical radius R_m are to be found is in the laminar bubble. It is in this location that subsequent gaseous growth has been observed [1], [10].

On the other hand, suppose that upon conclusion of vaporous growth the bubble is large enough to interact immediately with the free shear layer. Then it will be transported downstream into the region of the turbulent eddies, as noted in event (f) above. No gaseous growth will occur and visible inception will be observed. Thus, depending upon the height of the laminar bubble, there can be a second criterion for R_m. We will need to consider both of these possibilities below.

Finally, it must be confessed that events (e), (f), and (g) have been enumerated above for the sake of providing a reasonably complete picture of the inception process when laminar separation is present. If the cavitation bubble becomes stabilized in the laminar bubble at the radius R_m, as indicated in step (d), the subsequent events will occur automatically, Therefore, our theory of inception need not take the analysis beyond step (d).

Having drawn the picture of the basic physical factors to be considered in the theory, we now turn to its mathematical formulation.

A STABLE NUCLEUS

Previously we have noted that it may be desirable to allow for nuclei in the flow which can exist indefinitely as well as those which are small spherical air bubbles. In the latter form the nucleus will have a short life and there are situations of practical interest in which one would not expect such unstable nuclei to be present.

In most cases the water will contain dissolved air and the nuclei will contain both air and water vapor. As one can see from the literature cited previously by [4, 5, 6, 7, 8, 11], a number of physical alternatives have been proposed to explain the existence of persistent nuclei. For our purposes we will suppose that air or vapor bubbles are attached to small solid particles in the liquid. In this case we may take the effective surface energy to be zero initially so that the nuclei can exist indefinitely [13], and by Henry's law [14] the partial pressure of air in the gas pocket will be proportional to the concentration of air dissolved in the water. We will characterize the size of the initial gas pocket by an initial effective radius, R_o. At this radius the "effective surface tension" will be zero.

As the bubble grows from its initial size it will eventually assume a spherical shape and the effect of surface tension on the gases inside it will be given by $2\sigma/R$, where σ is the coefficient of surface tension. The required behavior of the surface tension may be approximated by $p_\sigma = 2S(R,\sigma)/R$ where the "surface tension law" $S(R,\sigma)$ is characterized by $S(R_o,\sigma) = 0$ and $S(R_1,\sigma) = \sigma$, in which we let R_1 be that bubble radius at which the surface tension law first achieves its full value, σ, and further, we let $R_1 = n\,R_o$ with $n \geq 1$. The simplest assumption which will approximate the complex variation of effective surface tension $S(R,\sigma)$ with bubble growth is that $S(R,\sigma)$ is a linear function of R. Then $S = (R-R_o)\sigma/R_o(n-1)$ for $R_o \leq R < n\,R_o$ and $S = \sigma$ when $R \geq n\,R_o$. If one puts $r = R/R_o$, then the surface tension law can be written as

$$S = \begin{cases} \dfrac{r-1}{n-1}\,\sigma \quad , & 1 \leq r < n \quad , \\ \sigma \quad , & n \leq r \quad . \end{cases} \tag{1}$$

Note that the interval of linearly increasing variation of S with r does not include the dimensionless radius r = n . This value of r is included with those values which can also be greater than n because we can then put n = 1 and get S = σ, corresponding to a spherical bubble for all physically attainable values of r.

The surface tension law of Eq. (1) is an attempt to account for an average behavior of a large number of nuclei of many possible initial sizes [15]. Compared to the molecular scale, bubble nuclei are macroscopic and ordinary concepts of surface tension for macroscopic systems apply. In order to obtain a stable nucleus we have introduced another parameter, n, which governs the slope of the linearly increasing part of $S(r,\sigma)$. We are encouraged to ascribe an average behavior to such a large number of nuclei of many possible initial sizes because experiments show that the zone of cavitation numbers at which cavitation starts is very narrow. Thus, we can approximate the observations by assigning a definite value of the cavitation number for inception (or desinence) for a given flow state.

CRITICAL BUBBLE RADIUS AFTER THE INITIAL VAPOROUS GROWTH

As we have indicated in previous discussions of steps (c) and (d), we shall take the radius R_m to be the maximum radius attained in the course of vaporous growth. At the same time it will be required that this radius be such that subsequent growth by air diffusion only is possible. We shall determine this critical condition for further gaseous growth under the assumption that R_m will be so small that the diameter, $2R_m$, is still small enough to avoid immediate interaction between the

cavitation bubble and the free shear layer at the edge of the laminar bubble. We will also neglect all convective effects of bubble-wall velocity upon the process of air diffusion into or out of the bubble. Moreover, we will neglect the effect of convective effects of the main stream over the body on diffusion rates. Our interest is restricted to ascertaining whether or not diffusion is possible in the first place, using only the simplest considerations.

However, we will study two possible situations with respect to the possibility for gaseous growth. For example, we suppose that the bubble starts to grow by air diffusion the instant it reaches its maximum radius at a fixed position in the separation bubble. The bubble-wall velocity will be zero and the bubble-wall acceleration will have a negative value at this instant. We will need to consider the effect of this acceleration upon the critical condition for diffusive growth in order to see if the transition from vaporous growth to gaseous growth is possible.

After transition to gaseous growth has been established can subsequent gaseous growth be maintained? This is the second question which must be considered. Since this question is the easier question of the two, we shall consider it first.

Subsequent Gaseous Growth:

Once the bubble has stabilized in the laminar separation bubble the velocity and acceleration of the bubble wall will be negligible. Therefore, the stability conditions of Epstein and Plesset [13] apply with almost no modification. In this case the static pressure in the liquid surrounding the cavitation bubble is uniform and equal to p_s.

Therefore, a balance of pressures at the bubble wall leads to

$$p_g(R_m) = p_s - p_v + 2\frac{S(R_m,\sigma)}{R_m} \quad , \tag{2}$$

where p_s is the static pressure of the liquid in the separation bubble, and p_v is the pressure of the vapor inside the cavitation bubble. The saturation concentration of dissolved air in the liquid at the bubble wall is given by Henry's law as

$$\lambda C_i = p_a \quad ,$$

where λ is the Henry's law constant, $\lambda = \lambda(T)$, and T is the temperature. Therefore,

$$\lambda(C_i - C_s) = p_a - p_s + p_v - 2\frac{S(R_m,\sigma)}{R_m} \geq 0 \quad . \tag{3}$$

For gaseous growth, the equality on the right-hand side of Eq. (3) is the threshold condition. But

$$p_s = p_o + C_{p_s}\frac{1}{2}\rho\ V_o^2 \quad ,$$

and

$$p_v = p_o - K\frac{1}{2}\rho\ V_o^2 \quad ,$$

where C_{p_s} is the static pressure coefficient in the laminar bubble, K is the cavitation number, V_o is the free-stream velocity, and ρ is the liquid density. Using these definitions we can write the critical condition from Eq. (3) as

$$0 = p_a - (K + C_{p_s})\frac{1}{2}\rho\ V_o^2 - 2\frac{S(R_m,\sigma)}{R_m} \quad . \tag{4}$$

Introducing the nucleus size R_o, we can define the following dimensionless quantities:

$$\gamma = p_a R_o/2\sigma \quad , \tag{5}$$

$$C_\sigma = 4\sigma/\rho R_o V_o^2 = 4/We^2 \quad , \tag{6}$$

where We is the Weber number based on nucleus size, and

$$\beta = (K + C_{p_s})/C_\sigma \quad . \tag{7}$$

Then, we can express Eq. (4) in dimensionless form as

$$\gamma - \beta = \frac{1}{r_m} \begin{cases} \dfrac{r_m - 1}{n - 1} & , \quad r_m < n \quad , \\ 1 & , \quad r_m \geq n \quad , \end{cases} \tag{8}$$

Since $r_m > 0$, it follows that $\gamma - \beta \geq 0$ in Eq. (8).

Equation (8) gives the desired result for the threshold of subsequent gaseous growth in dimensionless form. It must be supplemented by an additional condition based on the maximum height of the laminar bubble, H. Measured values of this quantity have been given by Van der Meulin [12], [17], and by Arakeri [18]. Their data are presented in Figure 2 which shows H/D plotted against Re, the Reynolds number based on body diameter, D. Also shown in Figure 2 is an analytical approximation for these data. The laminar bubble forms a kind of parabolic wedge-shaped region in the flow. Therefore, it may not be appropriate for us to equate the critical bubble diameter directly to the maximum bubble height. Instead, we will use one half of this value and put

$$4 R_m = 111 D/Re^{0.79} \quad ,$$

for the time being at least. In terms of the dimensionless bubble radius r_m, we have

$$r_m = \frac{27.8 D}{Re^{0.79} R_o} \quad . \tag{9}$$

Had we used the full laminar-bubble height in Eq. (9), the numerical constant would have been 55.5.

Since we are concerned with the transition to gaseous growth at the onset of cavitation, we would use either Eq. (8) or Eq. (9) to establish the maximum bubble radius which should be produced by the initial phase of vaporous growth. We would employ whichever of these equations gives the smaller value of r_m.

The nature of the relationships implied by Eqs. (8) and (9) is illustrated by Figure 3 which is drawn for a two-inch diameter body (0.0508 m) a water temperature of 70°F (21.1°C), and a nucleus size of 2μm (2×10^{-6} m). The vertical lines at the various Reynolds numbers in Figure 3 show the limiting values of r_m in accordance with Eq. (9). As an additional limiting value for $Re = 2 \times 10^4$, one finds $r_m = 282$ from Eq. (8). The line for $Re = 5 \times 10^6$ is included to show when the laminar bubble disappears. The outcome of Eq. (8) for several values of the surface tension parameter, n, is shown in Figure 3 by the solid lines. For each value of n there is a peak value of Γ at $r_m = n$. When $K + C_{p_s} = 0$, $\Gamma = \gamma$. For the assumed value of $R_o = 2\mu m$ the value of γ for saturation at one atmosphere and T = 21.1°C is $\gamma = 1.4$, corresponding to a saturation concentration of dissolved air of $C_i = 14.9$ parts per million. For a dissolved air concentration of seven parts per million, we find $\gamma = 0.656$. Continuing to assume that $K + C_{p_s} = 0$, we find from Figure 3 that if we consider an unstable nucleus (spherical bubble) the value of r_m, for $n = 1$ and $\gamma = 0.656$, is about 1.5. Had the water been saturated at one atmosphere, gaseous growth of the nucleus would be possible without any vaporous growth beforehand. In order for one to assess the effect of values of $K + C_{p_s}$ which differ from zero, we give the following table of values of $|\gamma - \Gamma| = |\beta|$ for $(K + C_{p_s}) = 0.05$ for several values of the free-stream velocity in Table I.

For magnitudes of $K + C_p$ other than the value assigned in Table I, we can simply ratio the values of $|\gamma - \Gamma| = |\beta|$ given in the table. As we see, for this case at least, the effect of $K + C_{p_s}$ on critical air content γ is not large.

For a stable nucleus at low dissolved air concentrations, one sees from Figure 3 that two values of r_m are possible. The question is, which value of r_m should be used? We shall argue that it is appropriate to use the larger value. If the smaller value, to the left of $r_m = n$, is used it can be seen that the positive slope of the Γ versus r_m curve requires that γ increase with r_m. However, γ is fixed because it is determined by the measured air content. Therefore, any bubble which arrives by vaporous growth at $r_m < n$ would represent a point (r,γ) below the curve of r_m versus γ for that particular value of n and its size would subsequently decrease by diffusion from the bubble into the surrounding water. On the other hand, if vaporous growth puts the bubble at a value of r_m to the right of the peak at $r_m = n$, further gaseous growth can take place. Therefore, we conclude that for stable nuclei one should always select that value of r_m to the right of $r_m = n$, but within the limit established by the height of the laminar separation bubble.

Transition from Vaporous Growth to Gaseous Growth:

The foregoing analysis applies to the last phase of a typical cavitation bubble life prior to the time that it moves from the laminar separation bubble into the turbulent boundary layer downstream of the separation zone. The phase which precedes this final stage of gaseous growth is when the vapor bubble just reaches its maximum radius and becomes stabilized in the laminar

separation bubble. The question to be investigated in connection with this event is whether or not air diffusion into the vapor bubble can start when the bubble wall has an appreciable acceleration.

In order to study this matter, let us assume that the static pressure in the liquid far from the bubble wall is p_s, the static pressure in the separation bubble. We also suppose that the bubble reaches its maximum radius, R_m, just as it enters the laminar bubble. The pressure in the liquid at the bubble wall will not be p_s. Instead it will be p(t) and it is given by the nonsteady Bernoulli equation which for the present situation is simply

$$p(R) = p_s - \rho \, \phi_t(R) \quad , \tag{10}$$

where the bubble radius R is time dependent, R = R(t) and $\phi(R)$ is the velocity potential at the bubble wall. But we know that the velocity potential at the bubble wall is

$$\phi(R) = -R\dot{R}$$

and when $R = R_m$, $\dot{R}_m = 0$. Therefore,

$$p(R) = p_s + \rho \, R_m \ddot{R}_m \quad . \tag{11}$$

On the other hand, the equation of motion for the bubble wall, as given by Reference [16], is

$$R\ddot{R} + \frac{3}{2}\dot{R}^2 = \frac{1}{\rho}\left[p_v + p_a\left(\frac{R_o}{R}\right)^3 - 2\,\frac{S(R,\sigma)}{R} - p_o - C_{p_s}\,\frac{1}{2}\,\rho\,V_o^2\right] \quad , \tag{12}$$

in which isothermal growth is assumed. At $R = R_m$, $\dot{R} = 0$, and the air pressure in the bubble is

$$p_g = p_a \left(\frac{R_o}{R_m}\right)^3 \quad .$$

Then if we also use the equation for p_v just preceding Eq. (4), we can write for Eq. (12) the specific result for R_m as

$$\rho R_m \ddot{R}_m = p_g - 2\frac{S(R_m,\sigma)}{R_m} - (K + C_{p_s})\frac{1}{2}\rho V_o^2 \quad . \tag{13}$$

This result also follows directly from Eq. (11) after the fluid pressures are balanced at the bubble wall. If the liquid at the bubble wall is saturated with dissolved air at concentration, C, we have from Henry's law that

$$p_g = \lambda C \quad ,$$

where as before, $\lambda(T)$ is the constant of proportionality in Henry's law. On the other hand, the partial pressure of air in the liquid is

$$p_a = \lambda C_i$$

as before. Then we can form the difference

$$\lambda(C_i - C) = p_a - \frac{2\sigma}{R_m} - (K + C_{p_s})\frac{1}{2}\rho V_o^2 - \rho R_m \ddot{R}_m \geq 0 \quad , \tag{14}$$

which is similar in form to Eq. (3) except that now we have restricted ourselves to the consideration of $R_m > n$ because of the discussion surrounding Figure 3. As we did for Eq. (4), we now restrict ourselves to the critical condition, $C_i - C = 0$, and write

$$0 = p_a - (K + C_{p_s}) \frac{1}{2}\rho V_o^2 - \frac{2\sigma}{R_m} - \rho R_m \ddot{R}_m \quad . \tag{15}$$

Next we introduce the dimensionless quantities defined in Eqs. (5), (6), (7), the dimensionless radius $r_m = R_m/R_o$, and the new parameter,

$$\tau^2 = t^2(2\sigma/\rho R_o^3) \tag{16}$$

in order to express Eq. (15) as

$$\gamma - \beta - \frac{1}{r_m} - r_m \frac{d^2 r_m}{d\tau^2} = 0 \quad . \tag{17}$$

But r_m is a maximum of $r(\tau)$. Therefore,

$$\frac{d^2 r}{d\tau^2} = -a \quad , \tag{18}$$

where a is the magnitude of the dimensionless acceleration. If we solve Eq. (17) for a we have

$$a = \frac{\gamma - \beta}{r_m} - \frac{1}{r_m^2} \tag{19}$$

For values of r_m and $\gamma - \beta$ shown in Figure 3, we see that when $r_m \geq n$ the value of a will certainly be less than unity. For the solutions of Eq. (12) of interest here the condition $a << 1$ will generally be satisfied.

Next we can write Eq. (18) as the quadratic

$$r_m^2 + \left(\frac{\gamma - \beta}{a}\right) r_m - \frac{1}{a} = 0 \quad ,$$

which has the positive root

$$r_m = \frac{1}{2}\left(\frac{\gamma - \beta}{a}\right)\left[-1 + \sqrt{1 + a\left(\frac{2}{\gamma - \beta}\right)^2}\right] \quad ; \qquad (20)$$

For sufficiently small values of a we can expand the radial in Eq. (20) and write Eq. (20) as

$$r_m = \frac{1}{\gamma - \beta} - \frac{a}{(\gamma - \beta)^3} + \frac{2a^2}{(\gamma - \beta)^5} - \ldots \quad , \qquad (20a)$$

which shows, when $r_m \geq n$ and as $a \to 0$, that we recover Eq. (8). Moreover, when there is bubble-wall acceleration the critical condition is less stringent than the case of no acceleration at the maximum radius. Therefore, if for $r_m \geq n$ gaseous growth is possible according to Eq. (8), air diffusion is certainly possible in accordance with respect to the criterion of Eq. (20).

Next let us consider the situation when $r \neq r_m$. In the neighborhood of r_{max} we will have $\ddot{r} = -a$ as before, but now $\dot{r} \neq 0$; and from Eq. (12) we see that the quadratic just above Eq. (20) is replaced by

$$r^2 + \frac{\left(\gamma - \beta - \frac{3}{2} v^2\right)}{a} r - \frac{1}{a} = 0 \quad ,$$

where $v(\tau)$ is the dimensionless bubble velocity. The critical condition for this case becomes

$$r = \frac{\gamma - \beta - \frac{3}{2} v^2}{2a} \left[-1 + \sqrt{1 + \frac{4a}{\left(\gamma - \beta - \frac{3}{2} v^2\right)^2}} \right] \quad , \qquad (21)$$

where now $\gamma - \beta - \frac{3}{2} v^2 > 0$ if $r > 0$. Moreover, if

$$\frac{4a}{\left(\gamma - \beta - \frac{3}{2} v^2\right)^2} \ll 1 \quad ,$$

we have

$$r = \frac{1}{\gamma - \beta - \frac{3}{2} v^2} - \frac{a}{\left(\gamma - \beta - \frac{3}{2} v^2\right)^3} + \frac{2a^2}{\left(\gamma - \beta - \frac{3}{2} v^2\right)^5} - \cdots \qquad (21a)$$

which shows that the present leading term dominates the first term in the expansion for r_m in Eq. (20a) and that there can be cases in which the value of r will exceed that from Eq. (8). Therefore, it appears that the process of transition from vaporous growth to gaseous growth will be more easily accomplished at $r = r_m$ than at neighboring values of r. Indeed, at such neighboring values the possibility of air diffusion may even be less likely than it is during the subsequent phase of gaseous growth as defined by the critical condition of Eq. (8), although this will not generally be true.

The Flaccid Bubble

There can be changes of nucleus size which may take place without any vaporous growth. At sufficiently high cavitation numbers, the nucleus can still travel in the boundary layer until it becomes stabilized in the separation zone on the body without experiencing vaporous growth. As in the example of a flaccid balloon, the size of the bubble would change by progressing through a succession of equilibrium thermodynamic states as it passes through regions of changing external pressure. It is assumed that these equilibrium size changes occur without appreciable air diffusion because there is insufficient time for such a comparatively slow process to take place. Under the isothermal assumption, the equilibrium size of interest here is that size which would be obtained in the separation bubble.

The essential relationship which governs the equilibrium size change of an isothermal bubble is

$$p_a R_o^3 = p_g R^3 \quad , \tag{22}$$

where p_a is the partial pressure of air in the free-stream nucleus and p_g is the partial pressure of air in the bubble when it is in the laminar separation zone. The balance of pressures on the bubble in the separation zone is

$$p_g + p_v = 2 \frac{S(R,\sigma)}{R} + p_s \quad . \tag{23}$$

Equations (22) and (23) can be combined to give

$$p_a R_o^3 = (p_s - p_v + \frac{2S}{R}) R^3 \quad . \tag{24}$$

Upon introducing the dimensionless quantities r, β, and γ from Eqs. (5), (6), and (7), we find

$$\frac{\gamma}{r^3} = \beta + \frac{S(r,\sigma)}{r} \quad . \tag{25}$$

Thus, the new radius is given by

$$\left.\begin{aligned} r^3 - \frac{r^2}{1 + (n-1)\beta} - \frac{(n-1)\gamma}{1 + (n-1)\beta} = 0 \quad , \quad r < n \quad , \\ r^3 + \frac{1}{\beta} r^2 - \frac{\gamma}{\beta} = 0 \quad , \quad r \geq n \quad . \end{aligned}\right\} \tag{26}$$

The equilibrium radius, r_e, is found from these cubics as the smaller real root for which $r_e \geq 1$. If this radius is less than r_m from Eq. (8) when $r_m \geq n$, the bubble will dissolve. Otherwise, subsequent diffusive growth is possible. In order to investigate the conditions leading to diffusive growth when $r_e \geq n$, let us rewrite the second of Eqs. (26) as

$$\beta \sqrt{\gamma} = \frac{\sqrt{\gamma}}{r_e} \left[\left(\frac{\sqrt{\gamma}}{r_e} \right)^2 - 1 \right] \quad , \quad n \leq r_e < r_b \quad , \tag{27}$$

where r_b denotes the limiting value of r_m given by Eq. (9). In terms of the variables $\beta\sqrt{\gamma}$ and $(r_e/\sqrt{\gamma})$, Eq. (27) defines a single curve. When this equation is satisfied, since r_e and γ are positive and $\gamma < r_e^2$ in

most instances, we see that this flaccid bubble result can give negative values of β although $\beta \geq 0$ if $r_e^2 \leq \gamma$. This result contrasts with the form of Eq. (8) for $r_m \geq n$; namely,

$$\beta = \gamma - \frac{1}{r_m} \quad . \tag{8}$$

As long as $\gamma - \beta > 0$ in Eq. (8), r_m will be positive and β can have positive or negative values. Moreover, β will be positive as long as $r_m^2 > 1/\gamma$. But the flaccid bubble equation (27) can be rewritten as

$$\beta + \frac{1}{r_e} = \frac{\gamma}{r_e^3} \quad ,$$

and from (8)

$$\beta + \frac{1}{r_m} = \gamma \quad .$$

In a particular flow these equations will apply for identical values of R_o, V_o, γ, and so forth. But the values of β will be different in these two cases. Designate them by β_e and β_c, respectively. We have argued above that the cavitation number K_c, corresponding to r_c, will be associated with a previous history of vaporous bubble growth even though Eq. (8) defines r_c as the critical radius with respect to air diffusion. Of course, r_c may not be the same as the maximum radius r_m actually achieved after vaporous growth. The equilibrium radius r_e for the flaccid bubble is not associated with vaporous growth and the cavitation number K_e will be greater than K_c. Therefore, $\beta_e > \beta_c$ as can be seen from the definition Eq. (7).

In order to investigate the implications of this state of affairs, Figure 4 presents a plot of $\beta\sqrt{\gamma}$ versus $\xi = r\sqrt{\gamma}$ of Eqs. (8) and (27). As noted above, the equilibrium condition for a spherical flaccid bubble, Eq. (27) with $n = 1$, is represented by a single curve in this plot. Equation (8), also for $n = 1$, appears as a one-parameter family of curves which depends upon $\gamma^{3/2}$. For negative values of β_e we expect the root of interest for the flaccid bubble to be along the dashed part of the curve in Figure 4 corresponding to $r_e > 1$. Nonetheless, we will consider radii on either side of $r = 1$. Figure 4 shows two members of the family of critical curves intersecting the equilibrium curve.

If we select an air content γ, we can draw a vertical line at a prescribed value of to the right of the intersection of the equilibrium curve and the prescribed critical curve. In this case the vertical will cut the critical curve at $\beta_c\sqrt{\gamma}$ and it cuts the equilibrium curve at $\beta_e\sqrt{\gamma}$ with $\beta_c > \beta_e$ in contradiction with the inequality noted above. The physical implication of this finding is that since $K_e < K_c$ and we have associated K_c with vaporous growth, it is not possible for a flaccid bubble to survive a passage through the low pressure region upstream of the separation zone on the head form without vaporous growth. Thus, we see that if $r_c = r_e$ and corresponding to the class of larger radii, this value lies to the right of the intersection. Then a flaccid bubble cannot reach the laminar separation zone and experience subsequent gaseous growth. On the other hand, suppose we imagine a horizontal line drawn through the point $(\xi_e, \beta_e\sqrt{\gamma})$ defined by the intersection of the vertical line with the equilibrium curve as noted above. This horizontal will cut the critical curve at a point at which $r_c < r_e$ and gaseous growth of

a flaccid bubble would certainly be possible except for the fact that in this case when $\beta_e = \beta_c$ the cavitation number is less than the onset cavitation number and the flaccid bubble would experience vaporous growth. If we consider a horizontal line through the point $(\xi_c, \beta_c\sqrt{\gamma})$ defined by the intersection of the vertical line above with the critical curve, we find that this upper horizontal cuts the equilibirum curve at a value of ξ_e such that $r_e < r_c$. In this case a flaccid bubble would dissolve even if it could reach the laminar bubble without first experiencing vaporous growth. Evidently, if the vertical reference line is to the right of the intersection, it is generally true that a flaccid bubble can not settle in the separation bubble, experience subsequent gaseous growth, and thereby cause the onset of cavitation.

Turning next to a reference line to the left of the intersection, we see that this line will cut the equilibrium and critical curves at points corresponding to $K_e > K_c$ and since K_c corresponds to cavitation onset, cavitation will not occur at K_e even though the flaccid bubble might experience gaseous growth in the laminar separation zone. A lower horizontal line through the intersection of this new reference vertical with the critical curve leads to two possible values for the flaccid bubble which have $r_e > r_c$ and gaseous growth is possible. But once again such a flaccid bubble would be interrupted in its passage to the laminar separation zone by vaporous growth. Along the upper horizontal we find $r_e < r_c$ and the flaccid bubble will dissolve.

We conclude therefore that flaccid bubbles which drift into the laminar bubble will not lead to incipient (or desinent) cavitation. Either they will dissolve or they will experience vaporous growth before reaching the laminar separation zone.

Recapitulation

Before taking up the topic of vaporous bubble growth we shall pause briefly to review the major findings on gaseous growth. It appears that when there is a laminar separation bubble on a hemispherical headform, the separation zone can provide a favorable environment of gaseous growth. We have also found that the gaseous growth must be preceded by a period of vaporous growth which starts in the low pressure region upstream of the laminar separation zone. In this study we have neglected the convective effects of bubble-wall motion on the conditions favorable for air diffusion. We have found that the most favorable condition for gaseous growth occurs at the time when a bubble undergoing vaporous growth just reaches its maximum radius. Therefore, the probability of bubble stabilization at a fixed point in the laminar separation zone would be highest at this instant. The conditions for subsequent gaseous growth, once the vapor bubble has become fixed on the body, are somewhat more demanding. Nevertheless, it is found that the liquid in the water surrounding the bubble in the separation zone is definitely supersaturated for most flows of experimental or practical interest. Therefore, gaseous growth is most likely to occur once the vapor bubble is in the separation zone.

CAVITATION BUBBLE CONVECTION

The arguments given thus far have established the limits for the initial phase of vaporous growth starting from a nucleus of size R_o and ending as a cavitation bubble of radius R_m. The radius R_m has been taken to be the maximum radius achieved in the vaporous growth phase and its value has been shown to depend on the dissolved air content in the water, the static pressure

in the laminar separation bubble and the height of the laminar separation bubble, as well as the initial nucleus size, and the surface tension.

We have not yet established the time available for this vaporous growth to occur. This interval is governed by the extent of the region on the body in which the local static pressure is less than the vapor pressure of the water and the location of the region of laminar separation. Since we suppose that the details of the noncavitating flow are known, the kinematics of the cavitation bubble translation along the surface of the body is easily determined if we assume that the bubble moves with the speed of the water. In our calculations we shall approximate the boundary layer on the body as a vortex sheet which moves with one half the local speed of the fluid at the edge of the boundary layer. Then if s is the arc length along the body surface and $C_p(s)$ is the local pressure coefficient, the speed of the bubble is

$$\frac{ds}{dt} = \frac{1}{2} V_o \sqrt{1 - C_p(s)} \quad . \tag{28}$$

A typical pressure distribution in the neighborhood of the separation bubble and minimum pressure point is shown schematically in Figure 5. The experimental values of the pressure coefficient, C_p, plotted in Figure 5 are averages of measurements made by J. A. Carroll [3]. These points, tabulated in Table II, pertain to experiments in which the water temperature was 78°F (25.56°C) and the free-stream velocity ranged from 20 fps (6.096 m/sec) to 60 fps (18.288 m/sec). The arc length along the body is denoted by s and the diameter of the water tunnel model is denoted by D. The value of C_p at s/D = 0.798 gives the average value of the pressure coefficient in the

laminar separation bubble. Two parabolic approximations to these data are shown in Figure 5 as $f_1(s)$ and $f_2(s)$ which apply in the regions illustrated. Moreover, two values of C_{p_s} are shown by horizontal lines. The higher value, $C_{p_s} = -.613$ is intended to represent the pressure in a fairly short bubble. But since the bubble length varies with Reynolds number, Figure 5 also shows the value $C_{p_s} = -0.630$ intended to represent the upstream edge of the bubble. This value does not appear to depend upon free stream-velocity as long as there is a laminar bubble [3]. Also shown in Figure 5 is the region on the body, below the line $C_p(s) < -K$, where the static pressure is less than the vapor pressure of water. The illustration shows an example in which $K + C_{p_s} > 0$ for reasons discussed in the previous section. We will assume that vaporous growth of the cavitation bubble ends at the point s_3 inside or at the start of the laminar bubble and that the subsequent gaseous growth occurs at this fixed point. Then the transit time between s_0 and s_3 will be set equal to t_m, the time available for vaporous growth. At t_m the bubble radius will be R_m. Therefore, from Eq. (28) we have

$$t_m = \frac{2}{V_o} \int_{s_0}^{s_3} \frac{ds}{\sqrt{1 - C_p(s)}} \quad . \tag{29}$$

One might choose to evaluate Eq. (29) in a number of ways. In this study we shall stress simplicity rather than high accuracy because data on cavitation inception show some scatter and our aim is to isolate the main parameters which seem to be responsible for the observed trends. This viewpoint has already been applied to the derivation of Eq. (28).

Suppose for the moment that we are given a value of the cavitation number, K. Then we can locate approximately the point s_0 to be on the parabolic curve near $C_p(s)$. This is the first point, as s increases from s^*, that $K + C_p = 0$. Moreover, at the minimum pressure point, s_1, let $C_{p_1} = -b$. Now let us fit a parabola between the point s, (s^*, C_p^*), and $(s_1, -b)$. We will choose the point C_p^* to be just a bit above C_{p_s} in order that we can select various values of K as we may wish. The approximating parabola for this part of $C_p(s)$ is

$$f_1(s) = -b + \frac{(b + C_p^*)s_1^2}{(s_1 - s^*)^2}\left(1 - \frac{s}{s_1}\right)^2 \quad , \quad s^* \leq s \leq s_1 \quad , \tag{30}$$

and since $f_1(s_0) = -K$, we have

$$s_0 = s_1\left\{1 - \frac{s_1 - s^*}{s_1}\sqrt{\frac{b - K}{b + C_p^*}}\right\} \quad . \tag{31}$$

For the arc segment between the minimum pressure point and the point in the laminar bubble or just upstream of it at (s_2, C_{p_s}), we will fit another parabola

$$f_2 = -b + \frac{(b + C_{p_s})s_1^2}{(s_2 - s_1)^2}\left(\frac{s}{s_1} - 1\right)^2 \quad , \quad s_1 \leq s \leq s_2 \quad . \tag{32}$$

For $s_2 \leq s \leq s_3$, we take $C_p(s) = C_{p_s}$.

Equations (30), (31), and (32), which have been used in Figure 5 to approximate the hemisphere data, can now be used to approximate Eq. (29) in terms of the key parameters which control vaporous bubble growth. Moreover, we will also need to convert spatial coordinates into time coordinates in subsequent calculations and we will use our parabolic approximations for this purpose.

For those values of s governed by Eq. (30), we have

$$t = \frac{2s_1}{V_o\sqrt{1+b}} \int_{\frac{s_0}{s_1}}^{s/s_1} \frac{d\xi}{\sqrt{1 - \frac{b + C_p^*}{1+b}\left[\frac{s_1}{s_1 - s^*}(1-\xi)\right]^2}}$$

$$= \frac{2(s_1 - s^*)}{V_o\sqrt{b + C_p^*}} \left\{ \sin^{-1}\sqrt{\frac{b-K}{1+b}} - \sin^{-1}\frac{s_1 - s}{s_1 - s^*}\sqrt{\frac{b + C_p^*}{1+b}} \right\} . \tag{33}$$

If we introduce the dimensionless time, $\tau = t\sqrt{\frac{2\sigma}{\rho R_o^3}}$, from Eq. (16), we can write the inverse of Eq. (33) as

$$s = s_1 - (s_1 - s^*)\sqrt{\frac{1+b}{b + C_p^*}} \sin\left[\sin^{-1}\sqrt{\frac{b-K}{1+b}} - \frac{\tau V_o}{2(s_1 - s^*)}\sqrt{\frac{\rho R_o^3}{2\sigma}(b + C_p^*)}\right] , \tag{34}$$

where $s_0 \leq s \leq s_1$ and s_0 is given by Eq. (31). This inverse can be used to transform $f_1(s)$ into $f_1(\tau)$.

In that arc-length interval within which $s_1 \leq s < s_2$, we have

$$t - t_1 = \frac{2s_1}{V_o \sqrt{1 + b}} \int_1^{s/s_1} \frac{d\xi}{\sqrt{1 - \frac{b + C_{p_s}}{1 + b} \left[\frac{s_1}{s_2 - s_1} (\xi - 1)\right]^2}}$$

$$= \frac{2(s_2 - s_1)}{V_o \sqrt{b + C_{p_s}}} \sin^{-1} \frac{s - s_1}{s_2 - s_1} \sqrt{\frac{b + C_{p_s}}{1 + b}} \quad .$$

The value of t_1 is found from Eq. (33) with $s = s_1$. Therefore,

$$t = \frac{2}{V_o} \left\{ \frac{(s_1 - s^*)}{\sqrt{b + C_p{}^*}} \sin^{-1} \sqrt{\frac{b - K}{1 + b}} \right.$$

$$\left. + \frac{(s - s_1)}{\sqrt{b + C_{p_s}}} \sin^{-1} \frac{s - s_1}{s_2 - s_1} \sqrt{\frac{b + C_{p_s}}{1 + b}} \right\} \quad , \tag{35}$$

and when $s_1 < s \leq s_2$ and $\tau > \frac{2(s_1 - s^*)}{V_o} \sqrt{\frac{2\sigma}{\rho R_o{}^3 (b + C_p{}^*)}}$, the inverse of Eq. (35) is

$$s = s_1 + (s_2 - s_1)\sqrt{\frac{1+b}{b+C_{p_s}}}\sin\left\{\frac{\sqrt{b+C_{p_s}}}{s_2 - s_1}\left[\frac{\tau V_o}{2}\sqrt{\frac{\rho R_o^3}{2\sigma}} - \frac{(s_1 - s^*)}{\sqrt{b+C_p^*}}\sin^{-1}\sqrt{\frac{b-K}{1+b}}\right]\right\} . \tag{36}$$

Equation (36) can be used to transform $f_2(s)$ into $f_2(\tau)$. Finally we can find t_2 directly from Eq. (35). Transforming from t_2 to τ_2, we have

$$\tau_2 = \frac{2}{V_o}\sqrt{\frac{2\sigma}{\rho R_o^3}}\left\{\frac{(s_1 - s^*)}{\sqrt{b+C_p^*}}\sin^{-1}\sqrt{\frac{b-K}{1+b}} + \frac{s_2 - s_1}{\sqrt{b+C_{p_s}}}\sin^{-1}\sqrt{\frac{b+C_{p_s}}{1+b}}\right\} . \tag{37}$$

In that part of the body downstream of s_2 and upstream of the point s_3, we shall assume the static pressure to be constant and equal to C_{p_s}. At s_3 the cavitation bubble is stabilized in the laminar bubble. Thus in the arc length between s_2 and s_3, we can take the translational velocity of the bubble to be constant and we have

$$\tau - \tau_2 = \frac{2(s - s_2)}{V_o\sqrt{1 - C_{p_s}}}\sqrt{\frac{2\sigma}{\rho R_o^3}} , \tag{38}$$

where $\tau_2 \leq \tau \leq \tau_m$ ans $s_2 \leq s \leq s_3$.

In some cases we will want to put $s_2 = s_3$ in which case τ_m is given by Eq. (37). Generally, however, we can write

$$\tau_m = \frac{2}{V_o}\sqrt{\frac{2\sigma}{\rho R_o^3}}\left\{\frac{s_1 - s^*}{\sqrt{b + C_p^*}}\sin^{-1}\sqrt{\frac{b - K}{1 + b}}\right.$$

$$\left. + \frac{s_2 - s_1}{\sqrt{b + C_{p_s}}}\sin^{-1}\sqrt{\frac{b + C_{p_s}}{1 + b}} + \frac{s_3 - s_2}{\sqrt{1 - C_{p_s}}}\right\} . \qquad (39)$$

The choice for the dimensionless time τ can be rewritten as

$$\tau = \frac{t}{R_o}\sqrt{\frac{2\sigma}{R_o \rho}} . \qquad (40)$$

The square root term is a velocity which is characteristic of cavitation-bubble motions when the bubble is small. Since our interest centers on the early part of vaporous bubble growth, it is natural to use a unit of time which is appropriate to this phase of the motion. A plot of the ratio τ/t for a range of nucleus sizes of interest in this study is given in Figure 6 in order to illustrate quantitatively the relationship between dimensionless time and real time.

Equations (30) through (37) provide the basic kinematic relationships caused by the translation of the cavitation bubble along the surface of the body. They can now be used to determine the changes in static pressure with respect to time in the water surrounding the bubble which can cause vaporous growth.

CAVITATION BUBBLE DYNAMICS

In Eq. (12) we have already displayed a particular form of the equation which governs isothermal cavitation bubble growth and collapse when the static pressure in the liquid far from the bubble wall has been set equal to the constant static pressure in the laminar separation bubble as prescribed by the equation following Eq. (3). In the following, we shall take the static pressure to be a function of time in accordance with

$$p(t) = p_o + \frac{1}{2} \rho V_o^2 f(t) \quad , \tag{41}$$

where f(t) is determined from Eqs. (30) or (32) with the help of the transformations given by Eqs. (34), (36), or (38), respectively. If we introduce the dimensionless radius, r, and time, τ, into the equation of motion, it can now be written as

$$r \frac{d^2 r}{d\tau^2} + \frac{3}{2} \left(\frac{dr}{d\tau}\right)^2 = \frac{\gamma}{r^3} - \frac{S(r,n)}{r} - \frac{K + f(\tau)}{C_\sigma} \quad , \tag{42}$$

As before, $\gamma = p_a/(2\sigma/R_o)$, $C_\sigma = (2\sigma/R_o)/\frac{1}{2}\rho V_o^2$, and where now

$$S(r,n) = \begin{cases} \dfrac{r-1}{n-1} & , \quad 1 \leq r < n \quad , \\ 1 & , \quad n \leq r \quad . \end{cases} \tag{43}$$

The term $-[K + f(\tau)]/C_\sigma$ is a forcing function, $F(\tau)$, which causes the bubble to grow from r = 1 to r = r_m during the time τ_m. We can write F in terms of the parabolic approximations, (30) and (32), as

$$F(\tau) = \begin{cases} \dfrac{-f_1(\tau) - K}{C_\sigma} & , \quad 0 \leq \tau \leq \tau_1 \quad , \\ \dfrac{-f_2(\tau) - K}{C_\sigma} & , \quad \tau_1 < \tau \leq \tau_2 \, , \end{cases} \tag{44}$$

where the use of the argument τ in f_1 and f_2 implies that $f_1(s)$ and $f_2(s)$ have been transformed in accordance with Eqs. (34) and (36), respectively. In the interval $s_2 \leq s \leq s_3$, we use the transformation of Eq. (38) and take $F(\tau) = -[K + C_{p_s}]/C_\sigma = \text{const}$. In the folllwing we shall call this constant $-\beta$ in order to be consistant with the definition of Eq. (7). When the static pressure first falls to the vapor pressure, we start to count the dimensionless time, τ. That is, $F(0) = 0$. The diagram of Figure 7 shows schematically the form of $F(\tau)$. The interval in τ for which $F > 0$ corresponds to tensions in the water; that is, the static pressure is less than vapor pressure. The value of F for $\tau \geq \tau_m$ is taken as constant because the cavitation bubble has become stabilized in the laminar separation region and the equation for p_s following Eq. (3) applies.

A solution of Eq. (42) when a forcing function of the form $F(\tau)$ acts could be that for a growing bubble, although other possibilities exist. Since Eq. (42) is nonautonomous and nonlinear, there is little that one can do to solve it analytically. In such circumstances one uses a suitable numerical method with such initial conditions as may seem reasonable. In this study we shall employ the initial conditions,

$$\left.\begin{aligned} r(0) &= 1 \quad , \\ \frac{dr}{d\tau}\bigg|_{\tau = 0} &\quad . \end{aligned}\right\} \tag{45}$$

In past numerical studies* of Eq. (42), with the solution being subject to Eq. (45) and in which forcing functions similar to $F(\tau)$ were used, it was found that four classes of solutions were produced.

In Class 1, a typical bubble undergoes small-scale oscillations in which the major part of the motion, if not all of it, occurs for values of $r < n$.

---

*Unpublished

In Class 2, a bubble motion of Class-1 type is followed by another periodic motion involving significantly larger amplitudes than the initial oscillation with the maximum radius r_m considerably larger than n.

In Class 3, periodic solutions are found but all amplitudes of $r(\tau)$ are large. If necessary, these amplitudes can be made very large indeed if appropriate values of the key parameters are selected.

In Class 4, the bubble is observed to grow without limit.

For reasons already discussed in the section on THE SEQUENCE OF EVENTS, Class-2 and Class-3 solutions are of interest here. This fact brings out a problem which follows from working directly with Eq. (42). It has proved difficult to determine analytically the ranges of the physical parameters for which Class-3 or Class-2 solutions can be expected. This lack of a-priori criteria applies to Eq. (42) in spite of extensive studies of the stability of nonlinear ordinary differential equations summarized in the literature [19, 20]. Therefore, we shall employ certain additional simplifications in order to find some approximate conditions which will separate the various classes of solutions. Our aim is to find criteria which relate the values of a few key physical parameters to the class of solution being sought whilst retaining enough generality in the analysis to permit practically useful cases to be studied.

THE PIECEWISE-AUTONOMOUS APPROXIMATION

In order to secure the simplicity which autonomous dynamical systems have compared to those defined by differential equations depending explicitly on the time, we shall replace $F(\tau)$ as defined by Eq. (44) by a sequence of step functions. This further simplification is illustrated

schematically by the heavy dashed lines in Figure 7. The first step function of amplitude,

$$\alpha = (b - K)/C_\sigma \quad , \tag{46}$$

is applied at a delayed time, $\tau_a \geq 0$. The second step function, of negative amplitude is applied at $\tau = \tau_a + \tau_o \leq \tau_m$. The amplitude of this step is adjusted so that the value of F is $-\beta$, where the parameter β has already been defined by Eq. (7). In passing we observe that the parameters α and β are linearaly dependent. Thus we see that

$$\alpha + \beta = (b + C_{p_s})/C_\sigma \tag{47}$$

and

$$\alpha - \beta = (b - C_{p_s} - 2K)/C_\sigma \quad . \tag{48}$$

In any event, for the pulsed bubble the driving function is

$$F_a(\tau) = \begin{cases} 0 \quad , & 0 \leq \tau \leq \tau_a \quad , \\ \alpha \quad , & \tau_a < \tau \leq \tau_a + \tau_o \quad , \\ -\beta \quad , & \tau_a + \tau_o < \tau \leq \tau_m \quad . \end{cases} \tag{49}$$

When using the approximation (49), we apply the initial conditions of Eq. (45) at $\tau = \tau_a$ instead of at $\tau = 0$. When the start of the solution is delayed in this way we can consider the interval $(0, \tau_a)$ during which $r = 1$ as an approximate way of representing Class-2 solutions which contain an initial interval of small amplitude oscillations before oscillations of larger amplitude occur. Class-3 solutions would correspond to $\tau_a = 0$.

Matching Conditions:

The way in which the forcing function, Eq. (49), of the piecewise-autonomous system is used to match the parabolic approximation for the forcing function of the nonautonomous system of Eqs. (42) and (44) is illustrated in Figure 7. The quantities τ_a and τ_o remain to be determined by the matching procedure. One condition which is required for matching is that a bubble will move downstream in the boundary layer from the point s_0, where the static pressure on the body first falls to vapor pressure and $\tau = 0$, to the point s_3, where it is stabilized in the boundary layer, within the time interval, τ_m as given by Eq. (39). The distance along the arc of the body which is traversed by the nucleus during this time is $s_3 - s_0$. In terms of the piecewise autonomous approximation, this distance is the sum of three subintervals,

$$(s_3 - s_0)\sqrt{\frac{2\sigma}{\rho R_o^3}} = (\tau_a V_o\sqrt{1 + K})/2 + (\tau_o V_o \sqrt{1+ K + \alpha C_o})/2$$

$$+ [(\tau_m - \tau_o - \tau_a) V_o \sqrt{1 + K - \beta C_\sigma}]/2 \quad .$$

Therefore we can solve for τ_m and introduce the values of αC_σ and βC_σ from the definitions of β, Eq. (7), and α, Eq. (46), in order to write

$$\tau_m = \frac{2(s_3 - s_0)}{V_o\sqrt{1 - C_{p_s}}}\sqrt{\frac{2\sigma}{\rho R_o^3}} - \tau_a\left(\sqrt{\frac{1 + K}{1 - C_{p_s}}} - 1\right) - \tau_o\left(\sqrt{\frac{1 + b}{1 - C_{p_s}}} - 1\right) \quad . \tag{50}$$

As we have noted, the value of τ_m is given by Eq. (39) so that the matching condition (50) contains only two unknows, τ_a and τ_o.

In following sections the value of radius, r_o, when $\tau = \tau_a + \tau_o$ will be needed. Strictly, this value should be obtained from the integration of the equation of motion in the interval, $\tau_a \leq \tau \leq \tau_a + \tau_o$, with $F_a = \alpha$ as indicated by Eq. (49) and with $r(\tau_a) = 1$, $v(\tau_a) = 0$. However, as we have noted, τ_m is prescribed. Moreover, $r_m = r(\tau_m)$ is also specified and r_m is a maximum radius so that $v(\tau_m) = 0$. Therefore, a simple approximation for the solution in the interval $\tau_a \leq \tau \leq \tau_m$ could be given by the parabola,

$$r = 1 + (r_m - 1) \frac{\tau - \tau_a}{\tau_m - \tau_a} \left(2 - \frac{\tau - \tau_a}{\tau_m - \tau_a} \right) \quad . \tag{51}$$

Evidently Eq. 51 does satisfy the conditions that $r(\tau_a) = 1$ and that $r(\tau_m) = r_m$. Moreover,

$$\frac{dr}{d\tau} = \frac{2(r_m - 1)}{\tau_m - \tau_a} \left[1 - \frac{\tau - \tau_a}{\tau_m - \tau_a} \right] \quad . \tag{52}$$

Equation (52) shows that $v(\tau_m) = 0$ as anticipated, but that $v(\tau_a) \neq 0$. In view of the approximations already noted with respect to the piecewise autonomous representation, the violation of the initial condition that $v(\tau_a) = 0$ can be accepted. The appropriate inversion of Eq. (51), after we put $r = r_o$ and $\tau = \tau_a + \tau_o$, is

$$\tau_o + \tau_a \left[1 - \sqrt{\frac{r_m - r_o}{r_m - 1}} \right] = \tau_m \left[1 - \sqrt{\frac{r_m - r_o}{r_m - 1}} \right] \quad . \tag{53}$$

Equations (51) and (53) contain three unknows: τ_a, τ_o, and r_o.

Continuing with the matching, we employ the dynamical Equations (42), (43), and (45). We see that if we write $v = dr/d\tau$, then the differential operator on the left-hand side of Eq. (42) can be written as

$$r \frac{dv}{d\tau} + \frac{3}{2} v^2 = \frac{1}{2r^2} \frac{d}{dr}(r^3 v^2) \quad . \tag{54}$$

Then we can write the first integral of Eq. (42) in terms of indefinite integrals as

$$r^3 v^2 = 2 \int r^2 F(\tau) \frac{dr}{d\tau} d\tau + 2 \gamma \ln r - 2 \int r S(r,n) dr + \text{const} \quad , \tag{55}$$

where the function $S(r,n)$ is given by Eq. (43). Consider the nonautonomous system, in which case $F(\tau)$ is given by Eq. (41), or at least it is closely approximated by Eq. (44). Using the initial conditions (45) and the surface tension law of Eq. (43), we can evaluate the constant of integration in Eq. (55) as well as the second integral on the right-hand side of the equation. Denoting the first integral on the right-hand side of Eq. (55) by $I(r)$, we have

$$r^3 v^2 = 2I(r) + 2 \gamma \ln r - \begin{cases} \frac{2}{n-1} \left(\frac{r^3 - 1}{3} - \frac{r^2 - 1}{2} \right) & , \quad 1 < r < n \quad , \\ \left(r^2 - \frac{n^2 + n + 1}{3} \right) & , \quad n \leq r \quad . \end{cases} \tag{56}$$

But when $r = r_m$, $v = 0$ as we have noted. Therefore, when $r_m \geq n$, in accordance with the discussion surrounding Figure 3, we have

$$2I(r_m) = -2\gamma \ln r_m + r_m^2 - \frac{n^2 + n + 1}{3} \quad . \tag{57}$$

Since our interest is centered upon the maximum radius, $r_m \geq n$, we shall use Eq. (57) in order to evaluate $I(r_m)$.

In order to check the proposed use of Eq. (57), we have considered the case in which the forcing function $F(\tau)$ is a simple step function of strength α. In this case

$$I = \frac{\alpha}{3}(r_m^3 - 1) \quad .$$

We have integrated a number of bubble histories, $r(\tau)$, for various values of air content parameter γ, driving parameter α, and with $n = 5$ using a Hewlett-Packard HP 97 programmable calculator. Many of these trajectories exhibited a maximum radius r_m. For such trajectories values of α, γ, and r_m obtained for three values of air content are entered in the first three columns of Table III. The value of I, which can be computed directly in this case, is shown in the fourth column of Table II. The right-hand side of Eq. (56) is evaluated for $n = 5$ in the fifth column. Comparison of the values contained in the fourth and fifth columns shows excellent agreement. As a further check we have integrated Eq. (42) using a Runge-Kutta routine. The initial values were $r(0) = 1$, $v(0) = 0$, and we put $n = 5$. For the forcing function we took

$$F(\tau) = \begin{cases} \alpha \sin(\pi\tau/\tau_a) & \text{for } \tau \leq \tau_b = \tau_a[1 + \frac{1}{\pi}\tan^{-1}(\beta/\sqrt{\alpha^2 - \beta^2})] \\ -\beta & \text{for } \tau > \tau_b \end{cases} ,$$

For these calculations we took $\alpha = 0.3, \beta = 0.08, \gamma = 0.2, \tau_a = 30$, and τ_b turned out to be $\tau_b = 32.5776$. The routine gave $r(\tau)$ and $v(\tau)$ with $r_m = 8.058$. The integral I was found by a numerical integration of $v(\tau)r^2(\tau)F(\tau)$ to be I = 26.9527. The formula (57), using the calculated r_m, gave I = 26.8817. The relative difference is less than 0.3 percent.

We return now to the piecewise autonomous system governed by the forcing function F_a of Eq. (49). We note that the first integral on the right-hand side of Eq. (55) must be evaluated in three steps. In the interval $0 \leq \tau < \tau_a$ there will be no contribution. In the interval $\tau_a \leq \tau \leq \tau_o + \tau_a$ we know that $1 \leq r \leq r_o$, so that the appropriate result, accounting for the initial conditions, $r(\tau_a) = 1$ and $v(\tau_a) = 0$, is

$$r_o^3 v_o^2 = \frac{2}{3}\alpha(r_o^3 - 1) + 2\gamma \ln r_o - \begin{cases} \frac{2}{n-1}\left(\frac{r_o^3 - 1}{3} - \frac{r_o^2 - 1}{2}\right), & 1 \leq r_o \leq n \\ \left(r_o^2 - \frac{n^2 + n + 1}{3}\right), & n \leq r_o \end{cases} , \quad (58)$$

where $v(r_o) = v_o$. Finally, from formulae holding in the interval, $r_o \leq r \leq r_m$ or $\tau_a + \tau_o \leq \tau \leq \tau_m$, and then when $r = r_m$, $\tau = \tau_m$, $v(r_m) = 0$, we will have

$$-r_o^3 v_o^2 = \frac{2}{3}\beta(r_m^3 - r_o^3) + 2\gamma \ln \frac{r_m}{r_o} - \begin{cases} r_m^2 - \frac{n^2+n+1}{3} - \frac{2}{n-1}\left(\frac{r_o^3-1}{3} - \frac{r_o-1}{2}\right) & , \quad r_o < n \\ r_m^2 - r_o^2 & , \quad r_o \geq n \end{cases} .$$

In this last formula, $r_m \geq n$. The product $r_o v_o^2$ can be eliminated from these last two equations simply by adding them. Thus,

$$0 = \frac{2}{3}(\alpha + \beta) r_o^3 - \frac{2}{3}\alpha - \frac{2}{3}\beta r_m^3 + 2\gamma \ln r_m - r_m^2 + \frac{n^2 + n + 1}{3} . \tag{59}$$

Equation (59) holds for both $1 \leq r_o < n$ and $r_o \geq n$ and only when $r_m \geq n$, as we have noted already.

We have found it useful to obtain Eq. (59) by a somewhat circuitous route because the intermediate equations leading to Eq. (58) can be of use. A more direct derivation results from the observation that for the piecewise-autonomous case, the integral

$$I(r_m) = \int_o^{\tau_m} r^2 F(\tau) v(\tau) d\tau ,$$

with $F(\tau) = F_a$ from Eq. (41), becomes

$$I_a = \alpha \int_{r_o}^{r_o} r^2 dr - \beta \int_{r_o}^{r_m} r^2 dr = \frac{1}{3}[(\alpha + \beta)(r_o^3 - 1) - \beta(r_m^3 - 1)] .$$

This result can be used in Eq. (56) with $r = r_m$, from which Eq. (59) follows at once.

The value of r_m appearing in Eq. (59) must be identical to that appearing in Eq. (57); that is, $I(r_m) = I_a$. Therefore, the third matching condition is

$$r_o = \left[\frac{\alpha + \beta\, r_m^{\,3} + 3\, I(r_m)}{\alpha + \beta}\right]^{1/3} = \left[1 + \frac{(K + C_{p_s})(r_m^{\,3} - 1) + 3\, C_\sigma\, I(r_m)}{b + C_{p_s}}\right]^{1/3} . \tag{60}$$

Since α and β follow from an estimate for K and because γ and r_m are prescribed, thereby permitting $I(r_m)$ to be found from Eq. (57), it follows for the prescribed value of K that r_o is determined once and for all by Eq. (60). Since $1 < r_o < r_m$, Eq. (60) implies that the permissible range of K is limited. In order to find the upper bound, we write (60) as

$$(r_o^{\,3} - 1)(b + C_{p_s}) = (K + C_{p_s})(r_m^{\,3} - 1) + 3\, C_\sigma\, I(r_m) < (r_m^{\,3} - 1)(b + C_{p_s}) .$$

The inequality follows from the fact that $r_o \leq r_m$, as noted. Working with this inequality we find that

$$K \leq b - \frac{3\, C_\sigma\, I}{r_m^{\,3} - 1} \tag{60a}$$

if r_o is not to exceed the permissible upper bound. A similar expression can be found for the lower bound:

$$K > -C_{p_s} - \frac{3\, C_\sigma I}{r_m^{\,3} - 1} . \tag{60b}$$

The value of r_o from (60) can be used in Eq. (53), which reduces Eqs. (50) and (53) to a pair of linear equations in the unknows τ_a and τ_o. The solution of these simultaneous equations is

$$\tau_a = \frac{1}{\Delta}\left\{\frac{s_3 - s_0}{\sqrt{1 - C_{p_s}}}\left(\frac{2}{V_o}\sqrt{\frac{2\sigma}{\rho R_o^3}}\right) - \tau_m\left[1 + \left(1 - \sqrt{\frac{r_m - r_o}{r_m - 1}}\right)\left(\sqrt{\frac{1 + b}{1 - C_{p_s}}} - 1\right)\right]\right\} \tag{61}$$

and

$$\tau_o = \frac{1}{\Delta}\left[\tau_m\sqrt{\frac{1 + K}{1 - C_{p_s}}} - \frac{s_3 - s_0}{\sqrt{1 - C_{p_s}}}\left(\frac{2}{V_o}\sqrt{\frac{2\sigma}{\rho R_o^3}}\right)\right]\left(1 - \sqrt{\frac{r_m - r_o}{r_m - 1}}\right) , \tag{62}$$

where the determinate Δ is given by

$$\Delta = \sqrt{\frac{1 + K}{1 - C_{p_s}}} - 1 - \left(\sqrt{\frac{1 + b}{1 - C_{p_s}}} - 1\right)\left(1 - \sqrt{\frac{r_m - r_o}{r_m - 1}}\right) . \tag{63}$$

Of course, the above solution contains the approximation introduced by the parabolic representation of bubble growth from Eq. (51).

A more exact matching can be obtained if we use a more exact expression for pulsed-bubble growth in the stepwise autonomous case than that of Eq. (51). However, we can continue to use Eq. (60) in order to find r_o because it is exact. The bubble growth expression needed for a more precise calculation is obtained from the differential equation form of Eq. (58). In that

expression we replace r_o by $r(\tau)$, v_o by $dr/d\tau$, and integrate (58) from $r = 1$ to $r = r_o$. This step gives

$$\tau_o = \begin{cases} \displaystyle\int_1^{r_o} \frac{dr}{\sqrt{\frac{2\alpha}{3}\left(1 - \frac{1}{r^3}\right) + \frac{2\gamma}{r^3}\ln r - \frac{2}{n-1}\left[\frac{1}{3}\left(1 - \frac{1}{r^3}\right) - \frac{1}{2}\left(\frac{1}{r} - \frac{1}{r^3}\right)\right]}}, & r_o < n \\ \displaystyle\int_1^{n} \frac{dr}{\sqrt{\frac{2\alpha}{3}\left(1 - \frac{1}{r^3}\right) + \frac{2\gamma}{r^3}\ln r - \frac{2}{n-1}\left[\frac{1}{3}\left(1 - \frac{1}{r^3}\right) - \frac{1}{2}\left(\frac{1}{r} - \frac{1}{r^3}\right)\right]}} & \\ \quad + \displaystyle\int_n^{r_o} \frac{dr}{\sqrt{\frac{2\alpha}{3}\left(1 - \frac{1}{r^3}\right) + \frac{2\gamma}{r^3}\ln r - \frac{1}{r} + \frac{n^2 + n + 1}{3r^3}}}, & r_o \geq n \end{cases} . \tag{64}$$

The value of r_o in the upper limit of Eqs. (64) comes from Eq. (60). Thus, τ_o is now found by a numerical quadrature.

The value of τ_a, which is the only unknown remaining follows from Eq. (50):

$$\tau_a = \left[\frac{s_3 - s_0}{\sqrt{1 - C_{p_s}}}\frac{2}{V_o}\sqrt{\frac{2\sigma}{\rho R_o^3}} - \tau_m - \tau_o\left(\sqrt{\frac{1+b}{1 - C_{p_s}}} - 1\right)\right]\left(\sqrt{\frac{1+K}{1 - C_{p_s}}} - 1\right)^{-1} . \tag{65}$$

The preceding discussion outlines an "exact" calculation for the matching although it does require a numerical integration. The approach prior to this one provides an approximate algebraic matching which sacrifices

accuracy for ease of calculation. The general framework of these matching procedures is not the only way one might wish to achieve a correspondence between nonautonomous and stepwise-autonomous representations for bubble growth. The particular method presented here has been selected because it seems to be the more convenient of the two approaches considered in the course of this research. It now remains to compare the algebraically and quadrature-matched bubble growths with a corresponding nonautonomous growth in order to get some idea of the relative performance of the two matching methods.

In order to check the matching procedures, we have integrated numerically Eq. (42) for a parabolic bubble driving function $f(\tau)$ and a stable nucleus, having $n = 5$ in the surface-tension law $S(r,\sigma)$. A standard Runge-Kutta method was used for this calculation. The particular driving function is

$$F(\tau) = \begin{cases} 4\alpha \dfrac{\tau}{\tau_\alpha}\left(1 - \dfrac{\tau}{\tau_\alpha}\right) & , \quad \tau \leq \tau_\beta \, , \\ \\ -\beta & , \quad \tau > \tau_\beta \, , \end{cases}$$

with

$$\tau_\beta/\tau_\alpha = \frac{1}{2}\left[1 + \sqrt{1 + (\beta/\alpha)}\right] = 1.0627$$

In this example $\alpha = 0.3$, $\beta = 0.08$, $\gamma = 0.2$, and $\tau_\alpha = 30$. The outcome of these calculations gave $\tau_m = 36.71$ and $r_m = 8.490$ for the coordinates of the maximum-growth point. Equation (48) shows that when both α and β are given, the value of K is determined from the ratio α/β. A short calculation gives $K = 0.632$. Then it follows that $\alpha C_\sigma = 0.1184$ and $\beta C_\sigma = 0.0136$.

As we have seen, one aspect of the matching is based upon a kinematic equivalence between distance of nucleus travel and the time required for this travel. The other aspect is that the radius at the maximum-growth point must be the same for the piecewise-autonomous and nonautonomous cases.

Turning now to the kinematics, we recall that the basic relationship between the distance and time at any point on the arc of the body is

$$\left(\sqrt{\frac{2\sigma}{\rho R_o^3}} \right) ds = \frac{V_o}{2} \sqrt{1 + K + F(\tau)\, C_\sigma}\; d\tau \quad ,$$

where the factor of 1/2 accounts approximately for the fact that the nucleus is in the boundary layer. As a result of our particular choice for $F(\tau)$, we have

$$\frac{2\Delta s}{V_o} \sqrt{\frac{2\sigma}{\rho R_o^3}} = 2\tau_\alpha \sqrt{\alpha C_\sigma} \int_0^{\tau_b/\tau_\alpha} \sqrt{(\lambda + \tfrac{1}{4}) - (\tfrac{1}{2} - x)^2}\; dx$$

$$+ (\tau_m - \tau_b) \sqrt{1 + K - \beta C_\sigma} \quad ,$$

where

$$\lambda = \frac{1 + K}{4\alpha C_\sigma} = 3.446 \quad .$$

The final expression for the parabolic driving function is

$$\frac{\Delta s}{V_o\sqrt{\alpha C_\sigma}}\sqrt{\frac{2\sigma}{\rho R_o^3}} = \frac{\tau_\alpha}{2}\left[x - \frac{1}{2}\sqrt{(\lambda+\frac{1}{4}) - (x-\frac{1}{2})^2} + (\lambda+\frac{1}{4})\sin^{-1}\frac{x-\frac{1}{2}}{\sqrt{\lambda+\frac{1}{4}}}\right]_0^{1.0627}$$

$$+ (\tau_m - \tau_b)\sqrt{\lambda - \frac{\beta}{4\alpha}} = 67.4755 \quad .$$

The corresponding kinematic relationship for the piecewise-autonomous representation is found just above Eq. (50). In terms of the present notation, we can write it as

$$\frac{\Delta s}{V_o\sqrt{\alpha C_\sigma}}\sqrt{\frac{2\sigma}{\rho R_o^3}} + \tau_a\sqrt{\lambda} + \tau_o\sqrt{\lambda+\frac{1}{4}} + (\tau_m - \tau_o - \tau_a)\sqrt{\lambda - \frac{\beta}{4\alpha}} \quad ,$$

where τ_a is a pulse delay time, τ_o is the positive-phase duration and these quantities are to be determined. The final expression for the piecewise-autonomous bubble is

$$\frac{\Delta s}{V_o\sqrt{\alpha C_\sigma}}\sqrt{\frac{2\sigma}{\rho R_o^3}} = 0.0180\,\tau_a + 0.0842\,\tau_o + 65.5904 \quad .$$

The expressions for the parabolic and piecewise-autonomous bubble cases can be equated in accordance with the kinematic matching requirement. This step gives

$$0.0180\,\tau_a + 0.0842\,\tau_o = 1.8851 \quad ,$$

or

$$\tau_o + 0.2133\,\tau_a = 22.39 \quad .$$

Next we shall use the algebraic matching procedure as provided by the parabolic-bubble-growth approximation of Eq. (53). First, Eq. (60) is used to calculate r_o. The result is

$$r_o = 7.179 \quad .$$

When this value of r_o and the value of r_m is used in Eq. (53), we get

$$\tau_o + 0.5816\, \tau_a = 21.35 \quad .$$

Thus we have two equations in the unknowns τ_a and τ_o. The solution is $\tau_a = -2.824$ and $\tau_o = 22.99$. These parameters define the pulse shape for the algebraic matching. We now turn to the alternate method which uses an integration of $r(\tau)$ when the bubble experiences a step function input of strength α.

For this matching by quadrature we recall that r_o is determined once and for all by Eq. (60). We replace Eq. (53) by the tabulation $r(\tau)$ when there is a step function driving function. From this table we find by interpolation that

$$\tau(r_o) = \tau(7.179) = 19.445 = \tau_o \quad .$$

In the present case it is only necessary to put this value of τ_o into the final kinematic condition (a) given above in order to find the value for τ_a. The result is

$$\tau_a = 13.81 \quad .$$

In Figure 8 the three trajectories for the cases discussed above are plotted with delay times and locations of the maxima marked for emphasis. This figure shows that the quadrature matching gives a good estimate for the r_{max} actually obtained for the parabolic test case but that the value of τ_{max} is not well reproduced. The algebraic matching

gives a better agreement for τ_{max}, but misses the desired r_{max} by a considerable amount. Numerical data pertaining to these check cases are tabulated in Table IV. The values of τ_m and r_m shown in Table IV were found from the Runge-Kutta routine. For the "test case" the parabolic forcing function applies. For the algebraic and quadrature cases, the forcing function, F_a of Eq. (49), is used. The values of τ_a and τ_o were found from the two matching procedures as discussed above and these were part of the input to the stepwise-autonomous pulsed-bubble routine.

As the theory develops further, it will become evident that s o m e error in the outcome for τ_m can probably be tolerated. On the other hand, it is important that the matching procedure gives a reasonably good value for r_m. Evidently the method which uses a quadrature is considerably better in this regard than the algebraic method. The result of all of this is to show that one can find a useful equivalence between a nonautonomous system and its piecewise-autonomous counterpart. This finding leads us to hope that in this study it may be possible to use this fact to devise a relatively simple approach to the calculation of cavitation inception.

It is important to note that τ_o has been defined in such a way that τ_o is nonnegative. On the other hand, τ_a can be positive or negative, although one ordinarily expects τ_a to signify a positive time lag. In addition, it does not seem reasonable to permit negative values of τ_a because this implies a pulsed-bubble growth time exceeding τ_m, which is the time actually available for bubble growth, and this is contrary to the rationale of the matching scheme. Moreover, further numerical studies

of the algebraic matching have shown that both positive and negative values of τ_o can occur. The negative values appear in those cases for which τ_o, if known precisely, would be small. Therefore, it seems best to restrict all matching calculations to those which depend upon a quadrature.

Singular Points and Stability:

The rules relating to translation of the cavitation bubble along the surface of the body and for matching the forcing functions of the piecewise-autonomous and nonautonomous systems have been established. It is now necessary for us to explore the properties of the piecewise-autonomous system because its use in place of the more exact nonautonomous formulation will allow us to develop some criteria about ranges of the physical parameters leading to the various classes of solution, $r(\tau)$. The development of such conditions from autonomous forms of Eq. (12) certainly contains no novelty, [9], [21], and [22], but the piecewise-autonomous representation adopted here requires further study.

In order to carry out the following analysis, we return to Eq. (42), the initial conditions (45), and we use the transformation of Eq. (54). In this way we can rewrite (42) as

$$\frac{d}{dr}\,(r^3\,v^2) = 2\frac{\gamma}{r} - 2rS(r,n) + 2r^2F_a(\tau) \quad , \qquad (66)$$

where the forcing function $F_a(\tau)$ is illustrated in Figure 7 and defined by Eq. (49). When $0 \leq \tau \leq \tau_o$ the first integral of Eq. (66) which satisfies the initial conditions (45) is given by Eq. (56). Since $v = dr/d\tau$ the solution in terms of r and τ is given by

$$\tau = \int_1^r \frac{x^{3/2}\,dx}{\sqrt{\frac{2}{3}\alpha(x^3 - 1) + \gamma \ln x - \begin{cases} \frac{2}{n-1}\left(\frac{x^3 - 1}{3} - \frac{x^2 - 1}{2}\right), & x < n \\ x^2 - \frac{n^2 + n + 1}{3}, & x < n \end{cases}}} \quad . \tag{67}$$

In Eq. (67) when $r = r_o$, $\tau = \tau_o$, and $v_o = v(r_o)$ in accordance with Eq. (58). The quantities r_o and v_o are the initial conditions for the second part of the solution in which $\tau > \tau_o$ and $F_a = -\beta$. From Eq. (60) we can write the first integral of Eq. (66), accounting for these new initial conditions, as

$$r^3 v^2 = r_o v_o^2 - \frac{2}{3}\beta\,(r^3 - r_o^3) + 2\gamma \ln \frac{r}{r_o} + \begin{cases} -\frac{2}{n-1}\left(\frac{r^3 - r_o^3}{3} - \frac{r^2 - r_o^2}{2}\right), & r < n \\ -r^2 - \frac{2}{n-1}\left(\frac{r_o^3}{3} - \frac{r_o^2}{2}\right) + \frac{n^3}{3(n-1)}, & r \geq n \end{cases} . \tag{68}$$

and from Eq. (68) we have

$$\tau - \tau_o = \int_{r_o}^r \frac{x^{3/2}\,dx}{g(\beta, \gamma, v_o, r_o; x)} \quad , \tag{69}$$

in which g is of obvious definition. Although we have reduced the problem to a quadrature, the solutions must be obtained numerically. Therefore, questions relating to the stability of various solutions are certainly of interest and we shall examine this matter further.

In order to investigate the matter of stability, we shall write Eq. (66) as a pair of first order differential equations:

$$\frac{dr}{d\tau} = v$$

$$r\frac{dv}{d\tau} = -\frac{3}{2}v^2 + \alpha + \frac{\gamma}{r^3} - \begin{cases} \dfrac{r-1}{(n-1)r} & , \quad r < n \\ \dfrac{1}{r} & , \quad r \geq n \end{cases} \tag{70}$$

with $r(0) = 1$, $v(0) = 0$ as before. This set of equations applies when $0 \leq \tau \leq \tau_o$. Now consider solutions for which $r < n$. The phase-plane trajectories of Eq. (70) are defined in this case by

$$\frac{dv}{dr} = \frac{[\alpha(n-1) - 1]r^3 + r^2 + \gamma(n-1) - \frac{3}{2}(n-1)v^2 r^3}{v r^4 (n-1)} = \frac{P(r,v)}{Q(r,v)} \tag{71}$$

and these trajectories are given by Eq. (70) for $r < n$ simply by solving it for $v(r)$.

On the other hand, the singular points of Eq. (71) are located in the phase plane at those points for which $Q = P = 0$. Since $r > 0$ we see that $Q = 0$ when $v = 0$. That is, all singular points will be on the r-axis. Therefore, in order to find the affix of these points, we need only put

$$P(r,0) = [\alpha(n-1) - 1]r^3 + r^2 + \gamma(n-1) = 0 \quad . \tag{72}$$

In the special case when $\gamma = 0$, we see that there are three real roots. Two of these roots are the double root at $r = 0$. There is one real root for $r > 1$ at

$$r = \frac{1}{1 - (n-1)\alpha} \quad , v = 0 \quad . \tag{73}$$

This root will lie in the interval $1 \leq r \leq n$ if $0 \leq \alpha \leq 1/n$. If $\alpha \to 1/(n-1)$, $r \to \infty$.

In the general case $\gamma > 0$ we must solve the cubic given by Eq. (72). If we divide this equation by the coefficient of r^3, we can use Tartaglia's method [23] to obtain the general solution. It is found for $\gamma > 0$ that there is only one real root. Its affix can be found from the formula

$$r = \frac{1}{3[1 - (n-1)\alpha]} + A + B \quad , \tag{74}$$

where

$$\left\{ \begin{matrix} A^3 \\ B^3 \end{matrix} \right\} = \frac{1}{27} \left\{ \frac{1}{[1 - (n-1)\alpha]^3} + \frac{27\gamma(n-1)}{2[1 - (n-1)\alpha]} \right\}$$

$$\pm \frac{1}{27[1 - (n-1)\alpha]} \left\{ \frac{27\gamma(n-1)}{[1 - (n-1)\alpha]^2} + \frac{[27\gamma(n-1)]^2}{4} \right\}^{1/2} . \tag{75}$$

One can verify that Eq. (74) reduces to Eq. (73) when $\gamma \to 0$.

In order to classify these roots we can apply Liapounoff's method (see [20] p. 317). Thus we must find the characteristic roots of the Jacobian matrix,

$$\begin{bmatrix} Q_r(r,0) & P_r(r,0) \\ Q_v(r,0) & P_v(r,0) \end{bmatrix}$$

where the value of r in the argument of each function denotes the value of the real root according to Eq. (73). In the special case for which $\gamma = 0$, we find the characteristic equation to be given by

$$\lambda^2 + \frac{n - 1}{[1 - (n - 1)\alpha]^5} = 0 \quad . \tag{77}$$

But we consider only $1 - (n - 1)\alpha > 0$ so that λ is purely imaginary,

$$\lambda = \pm i \sqrt{\frac{n - 1}{[1 - (n - 1)\alpha]^5}} \quad ,$$

and the real root given by Eq. (73) is a vortex point. In a sufficiently small neighborhood of this singularity the trajectories in the phase plane will be closed curves "focused on" or "centered about" the singular point. Such trajectories represent periodic solutions for $r(\tau)$.

When $\gamma > 0$, the characteristic equation becomes

$$\lambda^2 + (n - 1)\, r^4\, (3[1 - (n - 1)\alpha]\, r^2 - 2r) = 0 \quad , \tag{78}$$

with the value of r being given by Eq. (74). If λ is real the singularity will be a saddle point. This would require that

$$2 - 3\,[1 - (n - 1)\alpha]\, r > 0 \quad . \tag{79}$$

But from Eq. (74) one can see that $r > \frac{1}{1 - (n - 1)\alpha}$ which is in the right half of the r-v plane as long as $1 - (n - 1)\alpha > 0$. But (79) would require $r < \frac{2}{3} \frac{1}{1 - (n - 1)\alpha}$ which contradicts Eq. (74). This contradiction will be resolved if λ is imaginary. Therefore, if $1 - (n - 1)\alpha > 0$, the singularity will be a vortex point, provided $\gamma \geq 0$. We shall see from examples to be presented later that, in fact, $1 - (n - 1)\alpha > 0$. Another observation is that the value of λ appears to be independent of air content γ.

However, the affix of the singular point r does depend on γ as indicated by Eqs. (74) and (75) and so there is an implicit dependence of λ upon γ.

When $r \geq n$ the forms of P and Q are changed to read [see Eqs. (70)] $P(r,v) = \alpha r^3 - r^2 + \gamma - \frac{3}{2} v^2 r^3$ and $Q(r,v) = vr^4$. As before $Q = 0$ for $r > 0$ only if $v = 0$. Therefore the affixes of the singularities are obtained from $P(r,0) = 0$ or

$$\alpha r^3 - r^2 + \gamma = 0 \quad . \tag{80}$$

When $\gamma = 0$ one finds a double root at the origin and a distinct real root at $r = 1/\alpha$. Moreover, the characteristic equation pertaining to the distinct root is $\lambda = \pm 1/\alpha^{5/2}$. Since both characteristic values are real, the singularity is a saddle point. The motion $r(\tau)$ will generally be unstable in the neighborhood of a saddle point because the phase-plane trajectories will be open curves. However, the motion in the large may or may not be divergent. If a trajectory cuts the r-axis between the initial point and the saddle point, a periodic motion could still take place. When $\gamma > 0$, we can examine Eq. (80) using Tartaglia's method as before. In this instance one must distinguish between three cases:

(i) when $\frac{27\gamma}{4} - \frac{1}{\alpha^2} > 0$ or $\alpha > \frac{2}{\sqrt{27\gamma}}$, there is one real root;

(ii) when $\frac{27\gamma}{4} - \frac{1}{\alpha^2} = 0$ or $\alpha = \frac{2}{\sqrt{27\gamma}}$, there is one real distinct root and a real double root;

(iii) when $\frac{27\gamma}{4} - \frac{1}{\alpha^2} = 0$ or $\alpha < \frac{2}{\sqrt{27\gamma}}$, there are three real and unequal roots.

When one applies Liapounoff's method to the real root for case (i), this root being at v = 0 and

$$r = \frac{1}{3\alpha} + \left[\frac{1}{27\alpha^3} - \frac{\alpha}{2\alpha} + \frac{1}{27}\sqrt{\left(\frac{27\gamma}{2\alpha}\right)^2 - \frac{27\gamma}{\alpha 4}}\right]^{1/3}$$

$$+ \left[\frac{1}{27\alpha^3} - \frac{\gamma}{2\alpha} - \frac{1}{27}\sqrt{\left(\frac{27\gamma}{2\alpha}\right)^2 - \frac{27\gamma}{\alpha 4}}\right]^{1/3} , \qquad (81)$$

he finds that the two characterisitc values are real. Therefore, the singularity is a saddle point as it was in the case of $\gamma = 0$. We also note that Eq. (81) leads to $r = 1/\alpha$ when $\gamma = 0$ in agreement with the initial consideration of Eq. (80) for $\gamma = 0$.

For case (ii) the distinct root is found to be negative at $r = -1/3\alpha = -\sqrt{3\gamma/2}$. In this study all trajectories start from r = 1, v = 0, and proceed to phase-plane regions for which r > 1. Therefore this negative root will have little or no influence on the trajectory v(r). On the other hand, the double root is found to be at $r = 2/3\alpha = \sqrt{3\gamma}$. Because this is a double root and the associated characteristic values are both zero, this singularity is not an elementary singularity which can be investigated by the usual methods. We shall therefore be content with the observation that for cases (i) and (ii) the defining condition, $\gamma\alpha^2 \geq \frac{4}{27} = 0.1481$, implies values of γ and α which will not be encountered in the examples of interest here.

In case (iii) there are real and unequal roots which are located at

$$\left.\begin{aligned} r_i &= \frac{1}{3\alpha} - \frac{2}{3\alpha}\cos\psi_i \quad , \quad i = 1, 2, 3, \\ \text{with} \quad \psi_i &= \frac{\phi + 2\pi(i-1)}{3} \text{ and } \phi = \cos^{-1}\left[\frac{27\gamma\alpha^2}{2} - 1\right] \quad . \end{aligned}\right\} \tag{82}$$

Study of these roots shows that r_1 and r_2 are saddle points and that r_1 is negative. We also find that r_3 is a vortex point. Thus in the right half of the phase plane there are two singularities which are at locations on the r-axis given by r_2 and r_3 in Eq. (82). We will find that the vortex point is nearer to the origin than the saddle point in most of the examples which we shall consider. Moreover, the root r_3 changes character, from vortex point to saddle point when $\alpha = 0$. Also when $\gamma = 0$ it becomes a double root at the origin as already discussed in connection with case (i).

The foregoing discussion summarizes the situation with respect to the similarities of the piecewise-autonomous system, Eq. (70), which corresponds to that phase of the bubble motion for which $F_a = \alpha$ (see Eq. 57). Because of the surface tension law employed in the theory, two separate phase-plane characteristics are required. For early phases of bubble growth when $1 \leq r(\tau) < n$, the only singularity in the right half of the r-v plane is a vortex point, located on the r-axis in accordance with the formulae of Eqs. (74) and (75). For bubble radii larger than n the preceding situation no longer applies. Instead the phase-plane picture changes instantaneously when $r = n$ to one in which there are two singularities in the right half plane. The singularity on the r-axis and the origin will generally be a

vortex point. The second singularity, which is more distant from the origin than the first will generally be a saddle point. Depending on the air content this situation can be reversed. This is the case (for $n = 1$) studied previously by Dergarabedian [21] and by Ma and Wang [22]. The present study is more restrictive than those cited in the sense that the only trajectories of interest here will be those which start from $r = 1$, $v = 0$. We may also claim an extension of previous work because of the inclusion of the surface tension law $S(n,\sigma)$ and the fact that here a piecewise-autonomous system is being considered. In fact, our next step is to study that part of the solution for which $F_a = -\beta$ in Eq. (55).

The phase-plane trajectories for this case are indicated by Eq. (60) if r_m and v_m are replaced by r and v and we do not set the product $r^3 v^2$ equal to zero. Alternatively if we replace the zero on the left-hand side of Eq. (61) by $r^3 v^2$ and put r instead of $r_\square$ on the right-hand side, we have the trajectories resulting from Eq. (52) after the term $r_o^3 v_o^2$ has been eliminated from Eq. (60) by using Eq. (59). The relationship $\tau = \tau(r)$ for this phase of the motion is an obvious extension of Eq. (67).

The analysis for stability of the system parallels that given above for $F_a = \alpha$. In this case, since $F_a = -\beta$, the equations indicated by Eq. (70) can be changed by replacing the term $+\alpha$ by $-\beta$. Therefore we have for $r < n$

$$\left.\begin{aligned} P(r,v) &= -[(n-1)\beta + 1]\, r^3 + r^2 + \gamma (n-1) - \tfrac{3}{2}(n-1)\, v^2 r^3 \\ \text{and} \\ Q(r,v) &= -vr^4 (n-1) \quad . \end{aligned}\right\} \tag{83}$$

Or when $r \geq n$ we have

$$\left.\begin{aligned} P(r,v) &= -\beta r^3 - r^2 + \gamma - \frac{3}{2} v^2 r^3 \\ \text{and} \\ Q(r,v) &= vr^4 \quad . \end{aligned}\right\} \tag{84}$$

In either case, when $r < n$ or $r \geq n$, the fact that $F_a = -\beta$ indicates that the cavitation bubble will collapse provided that β is a sufficiently large positive number. Thus it is not surprising when we find for the case $r < n$ that there is only one singular point on the r-axis and that it is a vortex located at

$$r = \frac{1}{3[1 + (n-1)\beta]} [\, 1 + A + B] \quad , \tag{85}$$

where

$$\left\{ \begin{matrix} A^3 \\ B^3 \end{matrix} \right\} = 1 + \frac{27}{2} \gamma (n-1) [1 + (n-1)\beta]^2$$

$$\pm [1 + (n-1)\beta] \sqrt{27(n-1)\gamma \left\{ 1 + \frac{27}{4} (n-1)\gamma [1 + (n-1)\beta]^2 \right\}} \quad .$$

when $\gamma = 0$, Eq. (85) reduces to

$$r = \frac{1}{1 + (n-1)\beta} \quad . \tag{86}$$

When $r \geq n$ one must consider the three cases corresponding to those studied above when $F_a = \alpha$. However, in the present case it turns out that only one of the several possible real roots is in the positive half of the plane and

this root is a vortex point when $(27\gamma\beta^2/4) > 1$ and it is located at

$$r = -\frac{1}{3\beta}(1 + 2\cos\psi) \quad , \text{with } \psi = \frac{1}{3}\left[2\pi + \cos^{-1}\left(1 - \frac{27\gamma\beta^2}{2}\right)\right] \quad . \quad (87)$$

This finding is consistent with the physical behavior one expects in a region having an unfavorable environment for bubble growth. The other singular points, being in the negative half of the phase plane, should have no effect on the solution.

Thus far the analysis has been restricted to $\beta > 0$. If β should change sign, it is evident that the general features of the phase plane studied previously for $\alpha > 0$ will be regained. If one makes the change in sign of the β term in the various formulae given above, he can see the ranges for the various parameters which lead to a single vortex for $r > 1$ or for vortex and saddle points on the r-axis as before.

Limiting Trajectories:

While the locations and the character of the singularities in the phase plane help us to understand the stability and general shapes of the trajectories near these points, we still need to know what particular type of solution we might expect for prescribed values of the governing physical parameters α, β, γ, and τ_o. We can obtain some guidance in this matter by using an approach suggested previously in Ref. [9].

For example, it is clear from the development of Eq. (59) that the first integral of the equation of motion is an energy integral. The left-hand side of this equation is the change in kinetic energy. The right-hand side is the work done by the external environment, the air inside the bubble

and the surface tension forces. As long as we maintain a constant value of α the formulation adopted here allows for no change in the total energy of the system.

As the bubble grows, the logarithmic effect of air content in Eq. (59) will be much smaller than the polynomial terms on the right-hand side of Eq. (59). Therefore, the work done will have a general shape of a cubic in r. In a plot of work done against the radius r, one would see a curve which starts from $W(1) = 0$. As r increases $W(r)$ rises to a maximum and subsequently decends to an isolated minimum at some critical radius, $r = r_c$. It can be shown for n greater than unity that the minimum of W occurs at a value of r_c greater than n as long as $\tau_o \to \infty$. Since the kinetic energy is zero for $r = 1$ it will be zero again if $W_{min} = 0$. The fact that r_c is a minimum of W insures that the time required for the bubble to grow to r_c is logarithmically infinite. Thus, if α and γ are chosen so as to make $W_{min} = 0$, appreciable growth will not occur, although Class-1 solutions are certainly not ruled out. Then for the step function input, corresponding to $\tau_o \to \infty$, we might say that cavitation might not occur for values of α and γ which are less than or equal to these critical values. However, this statement requires some further qualification.

We can denote these critical values of α and γ, corresponding to $r = r_c$, by α_c and γ_c. Moreover, within the range of bubble radii under consideration here, the phase-plane trajectories must share the cubic appearance of $W(r)$. Therefore they too often have isolated minima at certain radii r_c and when a particular trajectory is just tangent to the r-axis in the phase plane the values of α and γ will have assumed their critical values as described above. Generally we envisage that this limiting trajectory will be approached from a sequence of trajectories upon which $\alpha > \alpha_c$. On any one of these

trajectories a bubble would grow without limit and we would say for the step function driving parameter that Class-4 solutions are obtained. On the other hand, as we shall see when $\alpha < \alpha_c$, the phase plane trajectories are closed and Class-1 solutions are found. Evidently the critical trajectory, upon which $\alpha = \alpha_c$ and $\gamma = \gamma_c$, is a separatrix between Class 1- and Class-4 solutions for a step function driving parameter. Therefore we should not necessarily regard these values of α_c and γ_c as being those which would preclude cavitation in all circumstances. We must await the outcome of the entire analysis before we can decide this point.

Continuing with the case in which $\tau_o \to \infty$, we must find the specific relationships between the critical values of r, α, and γ. These follow from the conditions

$$v(r_c) = 0$$

and

$$\left.\frac{dv}{dr}\right|_{r_c} = 0 \quad .$$

The two equations which result from these conditions are

$$\frac{2\alpha_c}{3}(r_c^3 - 1) + 2\gamma \ln r_c - r_c^2 + \frac{n^2 + n + 1}{3} = 0$$

and

$$\alpha_c r_c^3 - r_c^2 + \gamma = 0 \quad .$$

These equations account for the fact that $r_c \geq n$ as noted previously, and these conditions will certainly apply to spherical bubble nuclei when $n = 1$. We observe that these equations, being linear in α_c and γ_c, can be solved for these parameters in terms of r_c. The solution is

$$\alpha_c = \left[(2\ln r_c - 1)\, r_c^2 + \frac{n^2 + n + 1}{3}\right]/(2\Delta) \tag{88}$$

and

$$\gamma = r_c^2 \left[r_c^3 - (n^2 + n + 1)\, r_c + 2\right]/(6\Delta) \quad , \tag{89}$$

where

$$\Delta = (\ln r_c - \tfrac{1}{3})\, r_c^3 + \tfrac{1}{3} \quad . \tag{90}$$

When $r_c < n$ we can proceed formally using the same criteria on v and dv/dr as for $r_c \geq n$. In this case the fundamental equation becomes

$$\alpha_c\, r_c^3 + \gamma = \frac{r_c^2 (r_c - 1)}{n - 1} \qquad \text{(from dv/dr = 0)}$$

and

$$\alpha_c\, (r_c^3 - 1) + 3\gamma \ln r_c = \frac{(r - 1)^2\, (2r + 1)}{2\,(n - 1)} \qquad \text{(from v = 0)} \quad .$$

Solving for α_c and γ as before, we get

$$\alpha_c = \frac{(r_c - 1)}{\Delta\,(n - 1)} \left[3 \ln r_c - \frac{(r_c - 1)(2r_c + 1)}{2}\right] \tag{88a}$$

and

$$\gamma = - \frac{r_c^2\, (r_c - 1)^2\, (r_c + 2)}{2\Delta\,(n - 1)} \quad , \tag{89a}$$

where the value of Δ is given by Eq. (90). These results will be used at another point in the argument.

trajectories a bubble would grow without limit and we would say for the step function driving parameter that Class-4 solutions are obtained. On the other hand, as we shall see when $\alpha < \alpha_c$, the phase plane trajectories are closed and Class-1 solutions are found. Evidently the critical trajectory, upon which $\alpha = \alpha_c$ and $\gamma = \gamma_c$, is a separatrix between Class 1- and Class-4 solutions for a step function driving parameter. Therefore we should not necessarily regard these values of α_c and γ_c as being those which would preclude cavitation in all circumstances. We must await the outcome of the entire analysis before we can decide this point.

Continuing with the case in which $\tau_o \to \infty$, we must find the specific relationships between the critical values of r, α, and γ. These follow from the conditions

$$v(r_c) = 0$$

and

$$\left.\frac{dv}{dr}\right|_{r_c} = 0 \quad .$$

The two equations which result from these conditions are

$$\frac{2\alpha_c}{3}(r_c^3 - 1) + 2\gamma \ln r_c - r_c^2 + \frac{n^2 + n + 1}{3} = 0$$

and

$$\alpha_c r_c^3 - r_c^2 + \gamma = 0 \quad .$$

These equations account for the fact that $r_c \geq n$ as noted previously, and these conditions will certainly apply to spherical bubble nuclei when $n = 1$. We observe that these equations, being linear in α_c and γ_c, can be solved for these parameters in terms of r_c. The solution is

November 19, 1979
BRP:mmj

Returning to the physically important case of $r_c \geq n$ [Eqs. (88) and (90)], we see that the smallest physically admissible value of the air content parameter is $\gamma = 0$. From Eq. (89) we see when $\gamma = 0$ that r_c values are found as roots of a cubic. The root of interest must satisfy $r_c \geq n$ and it can be found numerically. Figure 9 shows values of α_c and r_c versus n when $\gamma = 0$ in accordance with Eqs. (88), (89), and (90). Figure 10 shows α_c and γ as functions of r_c for a spherical nucleus, $n = 1$, and for a stable nucleus, $n = 5$.

It remains to make good our assertion that the separatrix corresponding to α_c, γ which passes through the phase-plane point $(r_c,0)$ does separate Class 1 from Class-4 solutions when the external driving parameter $F_a(t)$ is a step function. In order to illustrate these points, we have simply obtained some numerical results for zero air content and for a stable nucleus having $n = 5$. These trajectories were calculated on a Hewlett-Packard HP 97 programmable calculator. Since the calculator is limited to programs which contain no more than 125 steps, the step function input, $F_a(t) = \alpha(t)$ (for $\tau_o = 0$), is about the most elaborate trajectory calculation that could be performed using only a single program. The program was designed to calculate the phase-plane trajectories for various values of α and γ in accordance with Eq. (56) and to determine the growth time to any $r(\tau)$ by a numerical integration as discussed in connection with Eq. (58) and shown explicitly in Eq. (67). An example of several phase-plane trajectories at $\gamma = 0$ and with $n = 5$ is shown in Figure 11. Only the upper half of the phase plane is shown in Figure 11. If the trajectories shown are reflected in the r-axis, the phase-plane representation would be complete.

A general finding illustrated by this figure is that the critical trajectory corresponding to $\alpha_c = 1/r_c = 0.180661$ and $r_c = 5.5352$ does separate the form of solutions to be expected from the autonomous equation of motion. When $\alpha < \alpha_c$, Figure 11 shows that the complete trajectories are closed loops so that these solutions are periodic. The amplitudes r_m and the half-periods, τ_m, for these solutions are shown in Figure 12. This figure shows how the amplitude and half-period increase with increasing α until the critical value $\alpha_c = .180661$ is reached. It can also be seen that τ_m does not vanish at $\alpha = 0$. In order to see how this nonzero limit occurs, we return to the autonomous form of Eq. (42) and write $r = 1 + x$. Near $\alpha = 0$, r is close to one so that we can assume that $x \ll 1$. Therefore, if we retain only first order terms in x, the equation of motion is linearized. These steps result in

$$\frac{dx^2}{d\tau^2} + \left(\alpha + \frac{1}{n-1} + 4\gamma\right) x = \alpha + \gamma$$

and

$$x(0) = \dot{x}(0) = 0 \quad .$$

The solution of this equation is

$$x = \frac{\alpha + \gamma}{\alpha + \frac{1}{n-1} + 4\gamma} \left[1 - \cos\left(\tau \sqrt{\alpha + \frac{1}{n-1} + 4\gamma}\right)\right] \quad .$$

The maximum value of x occurs when

$$\tau_{max} \sqrt{\alpha + \frac{1}{n-1} + 4\gamma} = \pi$$

so that

$$x_{max} = \frac{2(\alpha + \gamma)}{\alpha + \frac{1}{n-1} + 4\gamma} \quad .$$

For the situation of present interest we have $\alpha = \gamma = 0$ and $n = 5$. Therefore $x_{max} = 0$ and $\tau_{max} = \pi\sqrt{n-1} = 2\pi$ as shown in Figure 12.

We also note from Eq. (73) and the considerations which follow from it that the "closed loops" in Figure 11 are centered about vortex points which are positioned at $r = [1 - (n-1)\alpha]^{-1}$, $v = 0$, provided that $r_m < 5$. Locations of the singular points on the r-axis for various values of α are given in Table V. The location r given for the last entry at $\alpha = 0.8066$ in Table V is valid only for those points along the trajectory for which $r(\tau) < n$. When $r \geq n$, the singularities are located in accordance with Eq. (80). In the case $\gamma = 0$, we have seen that the singularity is a saddle point at $r = 1/\alpha = 5.5353$. This saddle point is nearly coincident with the critical value r_c corresponding to $\alpha_c = 0.80661$. We note, however, that $r_m = 5.52886$ lies inside the position of the saddle point for this case so that this particular trajectory must be a closed loop. It is worth noting that as $\alpha \to \alpha_c$ the saddle point location coincides with the critical point location $r_c = 1/\alpha_c$ as indicated in the discussion leading to Eq. (88). Evidently the critical point is a saddle point and the limiting trajectories through this point are separatricies which, for the case of $\tau_o = \infty$, separates Class 1 from Class-4 solutions. Solutions of this latter type are shown in Figure 11 by the trajectories for $\alpha = 0.1807$ and 0.1875. The trajectory denoted by $\alpha = 0.18066$ is one of the Class-1 solutions used previously in Table II.

Continuing with the example for $\tau_o = \infty$, but extending our considerations to air contents exceeding zero, we find phase-plane plots to have trajectories of the same general appearance as those of Figure 11. All considerations discussed above for the case when $\gamma = 0$ apply as well to these more general cases. The chief difference pertains to the location of the critical point r_c and the value of α_c as γ varies. Again, these critical values separate solutions of Class 1 from those of Class 4. Previously we had discussed Figure 10 which shows plots of α_c and r_c for a range of air contents. These data permit one to place a lower bound on conditions for significant vaporous bubble growth because we shall, for the most part, be interested in how the solutions corresponding to unlimited growth, such as those trajectories for $\alpha > \alpha_c = 0.180661$ in Figure 11, are converted into Class-3 solutions when τ_o is finite. However, as we have seen from the preceding considerations on gaseous growth, there will be cases in which only modest vaporous growth will be needed to initiate vaporous cavitation. In such cases solutions of Class 1 may be of interest.

Suppose next that $\alpha > \alpha_c$ and that τ_o has a prescribed finite value and that n and γ are prescribed as before. Then one can inquire as to the values of β and a new value of r_c for which the time required for growth is infinite. As will be shown later, the preceding critical values of r_c and α_c and the new pair of critical values, $\beta_c(\alpha,\gamma)$ and $r_c(\alpha,\gamma)$, put limits on the range of physical parameters within which Class-3 solutions are to be expected. (See the discussion of solution types following Eq. (45).) The second pair of critical values are determined from the first integral of the equation of motion as indicated by Eq. (56). The form of the equation of interest here is

$$r^3v^2 = r_o^3v_o^2 - \frac{2\beta}{3}(r^3 - r_o^3) + 2\gamma \ln \frac{r}{r_o}$$

$$- \begin{cases} \frac{2}{n-1}\left[\frac{r^3-r_o^3}{3} - \frac{r^2-r_o^3}{2}\right] , & r_o \leq r < n , \\ (r^2 - r_o^2) , & r_o \leq n \leq r , \; n \leq r_o \leq r , \end{cases} \tag{91}$$

Alternatively, we could have patterned Eq. (91) after Eqs. (68) and (56) in order to make the dependence of r_c and β_c upon α more explicit. However, we shall use the present form because of its convenience. Moreover, our interest centers on those cases in which $r_c > n$ because of the auguments given previously regarding the stability of cavitation bubbles with respect to air diffusion. This restriction does not rule out the possibility that τ_o is such that $r_o < n$. In this latter situation we will simply match the trajectories for $r < n$ or $r \geq n$ in the customary way in order to seek critical values (β_c, r_c) for which $r_c > n$. In any event, the conditions which determine the critical values are $v(r_c) = 0$ and $\left.\frac{dv}{dr}\right|_{r_c} = 0$ as before.

Therefore, when $r_o < n$ and $r_c > n$, the condition $v(r_c) = 0$ can be written as

$$0 = r_o^3v_o^2 + 2\left[\gamma \ln \frac{r_c}{r_o} - \frac{\beta_c}{3}\left[1 - \frac{r_o^3}{r_c^3}\right]\right] - \frac{r_c^2}{3}\left[1 - 2\frac{r_o^3}{r_c^3}\right] + \frac{1}{n+1}\left[\frac{n^3}{3} - r_o^2 + \frac{2}{3}r_o^3\right] . \tag{92}$$

The condition that the phase-plane trajectory has vanishing slope at $r = r_c$ follows directly from Eq. (82) with $r \geq n$. Thus

$$\beta_c = \frac{\gamma}{r_c^3} - \frac{1}{r_c} \quad . \tag{93}$$

Once the value of the product $r_o^3 v_o^2$ has been found from Eq. (58) and r_o has been determined from Eq. (64) with the prescribed value of τ_o, it is possible to find r_c and β_c by an iteration based upon Eqs. (92) and (93).

When $r_o \geq n$ the condition that $v(r_c) = 0$ is

$$0 = r_o^3 v_o^2 - \frac{2}{3}\beta_c (r_c^3 - r_o^3) + 2\gamma \ln \frac{r_c}{r_o} - (r_c^2 - r_o^2) \quad , \tag{94}$$

where r_o is given by Eq. (64) and v_o follows from Eq. (68) with $r = r_c \geq n$ and $v(r_c) = 0$. The critical values, r_c and β_c result from an iteration based on Eqs. (93) and (94).

It is interesting to note from Eq. (93) that, depending upon the value prescribed for the air content, γ, β_c can be negative. In the particular case $\beta_c = 0$, we have $r_c = \sqrt{\gamma}$. If we require that $r_c > n$, then for this case at least, we see that $\gamma > n^2$. This condition will seldom be satisfied and we expect negative values of β_c to be the rule. For example, when $\gamma = 0$, $\beta_c = -1/r_c$. Thus, if a large value of r_c is to be expected, it will be accompanied by a negative β_c of small magnitude. Note that β_c has no explicit dependence on n.

For use in subsequent applications it is convenient to express α_c and β_c in the forms $\alpha_c(\gamma, r_c, r_o)$ and $\beta_c(\gamma, r_c, r_o)$. The formula for β_c, given in Eq. (93) is already in the desired form. In the case of α_c we may simply

replace r_m in Eq. (59) with r_c. Then we use Eq. (93) in order to eliminate β_c from this result. As is also true for Eq. (59), this modified equation is valid for $r_c \geq n$ and for both $r_o < n$ and $r_o \geq n$. The desired relationship is

$$\alpha_c = \frac{1}{r_o^3 - 1}\left[\frac{2r_o^3 + r_c^3}{2r_c} + \gamma\left(1 - \frac{r_o^3}{r_c^3} - 3\ln r_c\right) - \frac{n^2 + n + 1}{2}\right] . \tag{95}$$

Although the time available for vaporous bubble growth is very short as measured in the laboratory time scale, when we consider the pace of this event in terms of bubble time, τ, the time available is quite long. As a consequence, our interest must center on phase-plane trajectories which are fairly close to the separatricies analyzed above. In particular, we will want to know how those portions of such "nearly-critical" trajectories contribute to the total growth time because the largest contributions to the total time will come from those parts of a phase-plane trajectory which are closest to a critical radius point and at the same time are in the vicinity of an isolated minimum of the trajectory.

For example, in the case of a minimum associated with a smaller critical radius we have

$$r^3 v^2 = \frac{2}{3}\alpha(r^3 - 1) + 2\gamma \ln r - r^2 + \frac{n^2 + n + 1}{3} . \tag{96}$$

We are interested in the radius r_s and the value $v^2(r_s)$ at the minimum point for which $dv/dr = 0$. We find that this radius is given by

$$r_s^2 - 6\gamma \ln r_s + 2(\alpha + \gamma) - (n^2 + n + 1) = 0 , \tag{97}$$

from which it follows that

$$v^2(r_s) = 2\left[\alpha - \frac{1}{r_s}\left(1 - \frac{\gamma}{r_s^2}\right)\right] \quad . \tag{98}$$

As $\alpha \to \alpha_c$ and $r_s \to r_c$, the smaller critical radius, we see from the equation preceding Eq. (88) that $v^2(r_s) \to 0$ in Eq. (98).

Now consider points in the neighborhood of the minimum point on this noncritical trajectory. Using Eqs. (97) and (98), one can put Eq. (96) into the form

$$v^2 = 2\left[\alpha - \frac{1}{r_s}\left[1 - \frac{\gamma}{r_s^2}\right]\right] + \frac{3}{r_s}\left[1 - \frac{\gamma}{r_s^2}\right]\left[\frac{r - r_s}{r_s}\right]^2 + 0\left[\left[\frac{r - r_s}{r_s}\right]^3\right] \quad . \tag{99}$$

Then if we put

$$x = \frac{r - r_s}{r_s} \quad , \quad A = 2\left[\alpha - \frac{1}{r_s}\left[1 - \frac{\gamma}{r_s^2}\right]\right] \quad , \quad B = \frac{3}{r_s}\left[1 - \frac{\gamma}{r_s^2}\right] \quad ,$$

and discard third and higher-order terms, we have

$$\Delta\tau = 2\, r_s \int_0^{x_o} \frac{dx}{\sqrt{A + B\, x^2}} = \frac{2r_s}{\sqrt{B}} \ln \frac{x_o\sqrt{B} + \sqrt{A + B\, x_o}}{\sqrt{A}} \quad , \tag{100}$$

where x_o is a point still in a small neighborhood of $x = 0$ and $\Delta\tau$ is the time added by that part of the trajectory between $-x_o$ and $+x_o$.

For phase-plane trajectories which lie very close to the separatrix passing through the smaller critical radius r_c, the incremental time $\Delta\tau$ can easily exceed the time required for the bubble to grow from $r = 1$ to $r = (1 - x_o)r_s$ because the value of A will be very close to zero. The growth time from $r = 1$ to $r = (1 - x_o)r_s$ can be found by a numerical integration based upon Eqs. (64) and the incremental time $\Delta\tau$ can be added to it. The remaining time between $r = (1 + x_o)r_s$ and r_o can be found by a numerical integration and this last part added to the other two in order to get τ_o. The time increment from τ_o where $r = r_o$ to $r = r_m$ is τ_g and it is given by Eq. (69). Then we may put $\tau_m = \tau_o + \tau_g$ ($\tau_a = 0$) in order to get the longest period of vaporous growth and presumably at the largest cavitation number. In those cases corresponding to very large $\Delta\tau$, very small changes in K (or α and β) will produce large changes in $\Delta\tau$, while those contributions to the total growth time from regions of the trajectory remote from r_s will show very little change. Therefore, for cases in which the smaller critical radius is very close to r_s, the final matching of total growth time to τ_m, the time available for vaporous bubble growth, can be accomplished using Eq. (100).

In order to see how this last step can be carried out, suppose that an initial series of calculations of the sort just described has been executed. Then we will have found an incremental time from Eq. (100) which can be designated by $\Delta\tau_1$. We will also have found a value of $(\tau_o + \tau_g)_1$ which generally will not agree with the desired value τ_m. The difference $\tau_m - (\tau_o - \tau_g)_1$ is to be made up by varying the cavitation number K. But since we are already very close to the lower critical radius, the only possible changes in τ will come from Eq. (100) as a new value of $\Delta\tau$,

which can be called $\Delta\tau_2$. The difference between these two incremental times will be given by

$$\Delta\tau_2 - \Delta\tau_1 = \tau_m - (\tau_o + \tau_g)_1 \quad . \tag{101}$$

The next step requires that the coefficients A and B, defined for use in Eq. (100), be expressed in terms of $(\alpha - \alpha_c)$. Equation (97) is very useful for this purpose because it not only holds when $r = r_s$ as written, it must also be true when $r_s \to r_c$. Therefore one can write

$$r_s^2 - r_c^2 - 6\, r \ln \frac{r_s}{r_c} = 2(\alpha_c - \alpha)$$

or

$$\left(\frac{r_c - r_s}{r_c}\right)^2 - 2\,\frac{r_c^2 - 3\gamma}{r_c^2 + 3\gamma}\left(\frac{r_c - r_s}{r_c}\right) + \ldots = 2(\alpha_c - \alpha) \quad .$$

Therefore

$$\frac{r_c - r_s}{r_c} = \frac{r_c^2 - 3\gamma}{r_c^2 + 3\gamma} - \sqrt{\left(\frac{r_c^2 - 3\gamma}{r_c + 3\gamma}\right)^2 - 2(\alpha_c - \alpha)}$$

$$= (\alpha_c - \alpha)\,\frac{r_c^2 + 3\gamma}{r_c^2 - 3\gamma} + \ldots \quad , \tag{102}$$

where the negative root is used because $\dfrac{r_c - r_s}{r_c} \ll 1$. Turning to the coefficient A, one sees after some manipulation that

$$A = 2\left[\alpha - \alpha_c + \left(\alpha_c - \frac{2}{r_c}\right)\frac{r_c - r_s}{r_c} + \ldots\right] \quad .$$

Using Eq. (102) we get

$$A = 2(\alpha - \alpha_c)\left[1 - \left(\alpha_c - \frac{2}{r_c}\right)\left(\frac{r_c^2 + 3\gamma}{r_c^2 - 3\gamma}\right)\right] + O\left[\left(\alpha - \alpha_c\right)^2\right] \quad . \tag{103}$$

The coefficient B can also be written as

$$B = 3\left[\alpha_c + \left(\alpha_c - \frac{2\gamma}{r_c^2}\right)\frac{r_c - r_s}{r_c} + \ldots\right] \quad ,$$

from which it follows that

$$B = 3\,\alpha_c\left[1 + (\alpha_c - \alpha)\left(1 - \frac{2\gamma}{\alpha_c\, r_c^2}\right)\left(\frac{r_c^2 + 3\gamma}{r_c^2 - 3\gamma}\right) + O\left[(\alpha_c - \alpha)^2\right]\right] \quad . \tag{104}$$

These results can now be used after Eq. (91) has been written so as to express the incremental difference, $\Delta\tau_2 - \Delta\tau_1$ as indicated by Eq. (101). Retaining only the dominant terms, one can write

$$\frac{(\Delta\tau_2 - \Delta\tau_1)}{r_c}\sqrt{3\alpha_c} = \ln\frac{\alpha_1 - \alpha_c}{\alpha_2 - \alpha_c}$$

or

$$\alpha_2 = \alpha_c - (\alpha_c - \alpha_1)\exp\left[-\frac{\tau_m - (\tau_o + \tau_{g_1})}{r_c}\sqrt{3\alpha_c}\right] \quad . \tag{105}$$

For some purpose it is convenient to use Eq. (47) in order to write (105) in terms of the parameter β instead of α. The foregoing analysis permits

the development of more refined version of Eq. (105) although such refinement should not often be required.

The situation with respect to the larger critical radius is analogous to that described for the smaller critical radius except that now we consider only Class-3 solutions and we assume that the maximum radius, r_m, will just fall short of the larger critical radius, r_c. The fact that both r_m and r_c correspond to zeros of $v^2(r)$ permits some simplifications in the analysis as compared to that given above. For example, we can start with the second form of Eq. (56) in which $r \geq n$, so that

$$r^3 v^2 = \frac{2}{\beta}(\alpha + \beta)\, r_o^3 - \frac{2}{3}\beta r^3 - \frac{2}{3}\alpha + 2\gamma \ln r - r^2 + \frac{n^2 + n + 1}{3} \quad .$$

On a trajectory having prescribed values of α, β, and γ, this equation will certainly hold when $r = r_m$ and $v(r_m) = 0$. Subtracting $v^2(r_m)$ from the preceding equation we find that

$$r^3 v^2 = \frac{2}{3}\beta (r_m^3 - r^3) + 2\gamma \ln \frac{r}{r_m} + r_m^2 - r^2 \quad . \qquad (106)$$

Equation (106) can be expanded in powers of the quantity $x = (r_m - r)/r_m$. The result of this step is

$$v^2 = x \left\{ 2\left[\beta + \frac{1}{r_m}\left(1 - \frac{\gamma}{r_m^2}\right)\right] + \left[4\beta + \frac{1}{r_m}\left(5 - \frac{7\gamma}{R_m^2}\right)\right] x \right\} + O(x^3) \quad . \qquad (107)$$

The zeroth order term inside the curly bracket of Eq. (107) vanishes in the limit as $r_m \to r_c$ and $\beta \to \beta_c$ because of Eq. (93). For the same reason,

AD-A082 851 PENNSYLVANIA STATE UNIV UNIVERSITY PARK APPLIED RESE--ETC F/G 20/4
A THEORY FOR CAVITATION INCEPTION IN A FLOW HAVING LAMINAR SEPA--ETC(U)
NOV 79 B R PARKIN N00024-79-C-6043
UNCLASSIFIED ARL/PSU/TM-79-198 NL

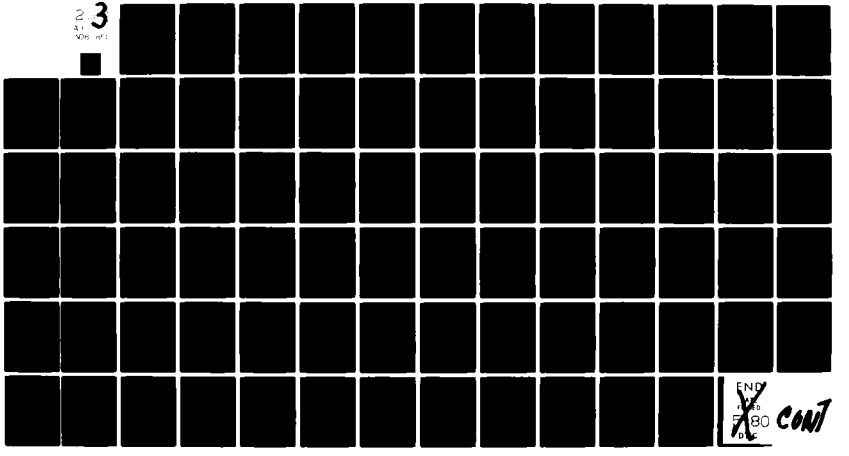

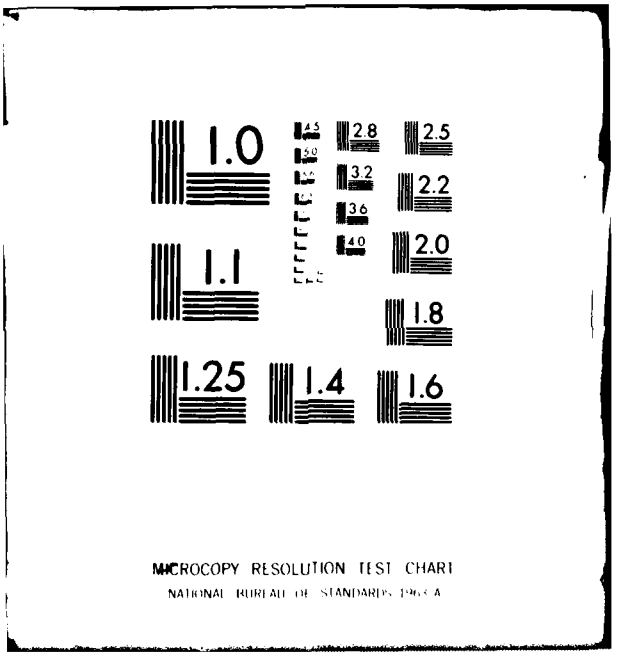
1.0
1.1
1.25
1.4
1.6
1.8
2.0
2.2
2.5
2.8
3.2
3.6
4.0
MICROCOPY RESOLUTION TEST CHART
NATIONAL BUREAU OF STANDARDS 1963-A

the coefficient of the first order term in the curly bracket becomes $\frac{1}{r_c}\left(1 - \frac{3\gamma}{r_c^2}\right)$ and Eq. (100) reduces to

$$v^2(x) = \frac{x^2}{r_c}\left[1 - \frac{3\gamma}{r_c^2}\right] + 0\ (x^3) \quad .$$

On the other hand, coefficients in Eq. (107) can be expanded in terms of the small parameter

$$\lambda = \frac{r_c - r_m}{r_c}$$

with the result that

$$2\left[\beta + \frac{1}{r_m}\left[1 - \frac{\gamma}{r_m^2}\right]\right] = 2\left[\beta + \frac{1}{r_c}\left[1 - \frac{\gamma}{r_c^2}\right] + \frac{\lambda}{r_c}\left[1 - \frac{3\lambda}{r_c^2}\right] + \frac{\lambda^2}{r_c}\left[1 - \frac{6\lambda}{r_c^2}\right]\right]$$

and

$$4\ \beta + \frac{1}{r_m}\left[5 - \frac{7\gamma}{r_m^2}\right] = 4\left[\beta + \frac{1}{r_c}\left[1 - \frac{\gamma}{r_c^2}\right] + \frac{\lambda}{r_c}\left[1 - \frac{3\gamma}{r_c^2}\right] + \frac{\lambda^2}{r_c}\left[1 - \frac{6\gamma}{r_c^2}\right]\right]$$

$$+ \frac{1}{r_c}\left[1 - \frac{3\gamma}{r_c^2}\right] + \frac{\lambda}{r_c}\left[1 - \frac{9\gamma}{r_c^2}\right] + \frac{\lambda^2}{r_c}\left[1 - \frac{18\gamma}{r_c^2}\right] \quad .$$

If we discard terms of order λ and higher compared to those remaining and use Eq. (84) again, we can approximate Eq. (107) by

$$v^2(x) = x \left\{ 2(\beta - \beta_c) + \left[4(\beta - \beta_c) + \frac{1}{r_c} \left(1 - \frac{3\gamma}{r_c^2} \right) \right] x \right\} \quad . \tag{108}$$

From Eq. (108) it follows that the incremental time contributed by a bubble-radius interval in which $0 \leq x \leq x_o$, will be

$$\Delta\tau = r_m \int_0^{x_o} \frac{dx}{\sqrt{x\,(A + B\,x)}} = 2\,\frac{r_c}{\sqrt{B}}\,(1 - \lambda)\,\ln \frac{\sqrt{Bx_o} + \sqrt{A + Bx_o}}{\sqrt{A}} \quad , \tag{109}$$

where terms of order x^3 have been discarded, and we have put $A = 2(\beta - \beta_c)$ and $B = 4(\beta - \beta_c) + (1 - 3\gamma/r_c^2)/r_c$. Note that Eq. (109) shows that $\Delta\tau$ becomes logarithmically infinite as $\beta \to \beta_c$. If one discards the small parameter λ compared to unity and inverts Eq. (109), he finds that

$$\left[\frac{\sqrt{Bx_o} + \sqrt{A + Bx_o}}{\sqrt{A}} \right]^2 = \exp \left(\frac{\Delta\tau\sqrt{B}}{r_c} \right) \quad . \tag{110}$$

As before, we can consider two cavitation numbers, K_1 and K_2, which lead to corresponding values of β, β_1, and β_2, and which are close to β_c. These values will define corresponding values of $\Delta\tau_1$, $\Delta\tau_2$, A_1, A_2, B_1, and B_2. Then Eq. (110) can be written approximately as

$$\beta_2 = \beta_c + (\beta_1 - \beta_c) \exp - \left(\frac{\Delta\tau_2 - \Delta\tau_1}{r_c^{3/2}} \right) \quad , \tag{111}$$

where we have put

$$B \approx \frac{1}{r_c} \quad \text{and} \quad \frac{\sqrt{B_1 x_o} + \sqrt{A_1 + B_1 x_o}}{\sqrt{B_2 x_o} + \sqrt{A_2 + B_2 x_o}} \approx 1 \quad .$$

As in the case of the smaller critical radius considered above, Eq. (111), enables one to obtain a final matching between available growth time and that needed to achieve the prescribed vaporous growth to the maximum radius (r_m). This matching can be more plainly seen if in place of the factor $r_c^{3/2}$ we were to put $r_m = r_c$ in Eq. (111). As Eq. (109) shows, this alternative is certainly a permissible mode of expression. However, it would have very little effect on the outcome of the calculations.

CALCULATIONS FOR CAVITATION INCEPTION

In preceding sections we have developed mathematical formulations for key events which lead to cavitation inception in the presence of laminar separation on the body. We must now order these various formulas so that K, the cavitation number for inception, can be determined if various flow parameters such as body geometry, free-stream velocity, and so forth are known.

Review of Basic Formulae:

We shall start the calculations by selecting a value for K. The way in which K is chosen will be considered below. All other quantities such as ρ, ν, σ, R_o, C_p^*, b, C_{p_s}, D, s^*, s_1, s_2, and s_3 will have been prescribed. The dissolved air content and water temperature will also be given so that Henry's law can be used to find p_a, the saturation partial pressure of dissolved air in the water. From these data we can calculate the parameters

$$\gamma = p_a R_o/2\sigma \quad \text{and} \quad C_\sigma = 4\sigma/R_o \rho V_o^2 \quad . \qquad (5), (6)$$

We can also obtain first estimates for

$$\alpha = (b - K)/C_\sigma \quad \text{and} \quad \beta = (K + C_{p_s})/C_\sigma \quad . \qquad (46), (7)$$

The time available for vaporous growth can also be estimated from Eq. (50):

$$\tau_m = \frac{2}{V_o}\sqrt{\frac{2\sigma}{\rho R_o^3}}\left\{\frac{s_1 - s^*}{\sqrt{b + C_p^*}}\tan^{-1}\sqrt{\frac{b - K}{1 + K}}\right.$$

$$\left. + \frac{s_2 - s_1}{\sqrt{b + C_{p_s}}}\tan^{-1}\sqrt{\frac{b + C_{p_s}}{1 - C_{p_s}}} + \frac{s_3 - s_2}{\sqrt{1 - C_{p_s}}}\right\} \quad . \qquad (50a)$$

If $r_m \geq n$, the maximum radius at the end of vaporous growth is the smaller of

$$r_m = \frac{27.8\ D}{Re^{0.79} R_o} \qquad (\sim \text{laminar bubble height}) \quad , \qquad (9)$$

or

$$r_m = \frac{1}{\gamma - \beta} \qquad (\text{subsequent gaseous growth, } r_m \geq n) \quad . \qquad (8)$$

As a result of the stability considerations which were given in our discussion of Figure 3, we know that Eq. (8) can be used only if it gives $r_m \geq n$. Otherwise gaseous growth can not take place after the initial vaporous growth. On the other hand, if r_m equals or exceeds that given by Eq. (9), we would expect bubble cavitation to occur instead of the band cavitation associated with gaseous bubble growth in the separated region. Thus, for the present calculations, we conclude that

$$n < r_m \leq 27.8\ D/(Re^{0.79} R_o) \qquad (112)$$

and that the final determination of r_m must await other considerations which are given later.

Once r_m is prescribed, we must match the nonautonomous and the piecewise-autonomous systems. We shall replace the nonautonomous equations with those derived for the piecewise-autonomous system on the basis that the matching between the two identifies the values of r_m and τ_m as being equals. Thus we calculate

$$I = \frac{1}{2} r_m^2 - \gamma \ln r_m - \frac{n^2 + n + 1}{6} \quad . \tag{57a}$$

Then we have

$$r_o = \left[\frac{\alpha - \beta r_m^3 - 3 I(r_m)}{\alpha + \beta} \right]^{1/3} \quad . \tag{59}$$

Since α and β are known (at least for the value of K selected), Eq. (51) determines r_o "once and for all." The time for the first phase of vaporous growth (in the region of favorable environment for growth where $F_a = \alpha$) is

$$\tau_o = \begin{cases} \displaystyle\int_1^{r_o} \frac{dr}{\sqrt{g_1(\alpha,\gamma,n;r)}} \quad , & r_o < n \quad , \\ \displaystyle\int_1^{n} \frac{dr}{\sqrt{g_1(\alpha,\gamma,n;r)}} + \int_n^{r_o} \frac{dr}{\sqrt{g_2(\alpha,\gamma,n;r)}} \quad , & r_o \geq n \quad , \end{cases} \tag{64}$$

where

$$g_1(\alpha,\gamma,n;r) = \frac{2\alpha}{3}\left(1 - \frac{1}{r^3}\right) + \frac{2\gamma}{r^3}\ln r - \frac{2}{n-1}\left[\frac{1}{3}\left(1 - \frac{1}{r^3}\right) - \frac{1}{2}\left(\frac{1}{r} + \frac{1}{r^3}\right)\right] ,$$

and

$$g_2(\alpha,\gamma,n;r) = \frac{2\alpha}{3}\left(1 - \frac{1}{r^3}\right) + \frac{2\gamma}{r^3}\ln r - \frac{1}{r} + \frac{n^2+n+1}{3r^3} .$$

The next phase of growth takes place when $F_a = -\beta$ and the bubble attains its maximum radius. Let this interval be designated by τ_g. Then

$$\tau_g = \int_{r_o}^{r_m} \frac{dr}{g(\beta,\gamma,v_o,r_o;r)} \tag{69a}$$

and from Eq. (69) when suitable modifications are introduced, g is defined by

$$g^2 = \frac{2}{3}(\alpha+\beta)\frac{r_o^3}{r^3} - \frac{2}{3}\alpha\frac{1}{r^3} - \frac{2}{3}\beta + \frac{2\gamma}{r^3}\ln r - \frac{1}{r} + \frac{n^2+n+1}{3r^3} , \quad r_o \leq r \leq r_m .$$

(69b)

Equation (69b) holds for $1 \leq r_o < n$ for $r_o \geq n$, but with $r \geq n$. The matching is completed when we put

$$\tau_m = \tau_a + \tau_o + \tau_g , \tag{113}$$

where τ_m is given by (31a), τ_a is the interval between the time when the static pressure outside the bubble first equals the vapor pressure and

the piecewise-autonomous forcing function jumps to $F_a = \alpha$. τ_o and τ_g are given by Eqs. (64) and (69a),* respectively. For the time beeing, τ_a is not determined except by Eq. (113). Generally we expect $\tau_a \geq 0$. Indeed, for the longest possible vaporous growth we would, in principle, expect $\tau_a = 0$ to correspond to the cavitation number at inception in which case (113) reduces to $\tau_m = \tau_o + \tau_g$. However, imposition of this requirement would not lead to a proper distance-time matching.

Once the piecewise-autonomous equations for vaporous growth have been matched to the nonautonomous system for vaporous growth, we shall use the properties of the former in order to continue the calculations. The next step in these calculations depends upon the fact that τ_m is often a rather large number. For example, we can estimate roughly the magnitude of τ_m by means of the formula

$$\tau_m \sim \frac{2(s^* - s_3)}{V_o} \sqrt{\frac{2\sigma}{\rho R_o^3}} \quad .$$

Then if D = 2 inches (.0509 m), we find from Table II that

$$\frac{s^* - s_3}{D} \doteq 0.241 \quad .$$

If we assume that $R_o = 2\mu m$ and $V_o = 20$ fps (6.095 m/s), it follows that

$$\tau_m \doteq 17{,}000 \quad .$$

If the free-stream velocity should increase to 80 fps (24.380 m/s), the value of τ_m would decrease to about

$$\tau_m \doteq 4{,}200$$

---

*See page 98

If in addition, the diameter of the body were reduced to 1/4-inch (0.00626 m), we would find then that

$$\tau_m \doteq 528 \quad .$$

If in addition to the above changes, the nucleus radius were increased to 10μm the total bubble time would be reduced to about

$$\tau_m \doteq 47 \quad .$$

The foregoing example shows that in laboratory experiments the bubble time available for vaporous growth can vary widely. The results also show that in many situations of practical interest, the bubble time available will be very large so that the need to match the nonautonomous with the stepwise-autonomous model must certainly account for this important case.

Classification of Solutions and the Role of Critical Radii:

Continuing the analysis of vaporous growth, we have seen that Eqs. (93) and (95) give critical values of α and β which separate Class-3 from Class-4 solutions. Since we require Class-3 solutions once the bubble starts its vaporous growth, it follows from (93) that

$$\beta > -\frac{1}{r_m}\left[1 - \frac{\gamma}{r_m^2}\right] \tag{114}$$

or that

$$K > -C_{p_s} - (1 - \gamma/r_m^3)\, C_\sigma/r_m \quad . \tag{114a}$$

The limiting condition between these two solution classes corresponds to an equality in Eq. (114). Thus

$$\beta\sqrt{\gamma} = -\frac{1}{\xi}\left(1 - \frac{1}{\xi^2}\right) \quad , \tag{115}$$

where $\xi = r_m/\sqrt{\gamma}$. Equation (115) is plotted in a ξ, $\beta\sqrt{\gamma}$ - plane in Figure 13. Since $r_m \geq n$, ξ will generally be found on that branch of Eq. (115) which is to the right of the minimum and K will be such that $\beta\sqrt{\gamma}$ will be at a point inside the curve.

On the other hand, we have seen that once γ is selected, the value of the smaller critical radius, r_s and the corresponding value of the parameter α_c is determined once and for all by Eqs. (88), (89), and (90). If the cavitation number is such that $\alpha \leq \alpha_c$, the time required for vaporous growth to r_{sc} will be logarithmically infinite and if $r_m > r_s$, the maximum radius will not be attained. Useful reference values of $K = K_r$, $\beta = \beta_r$, and $r = r_r$ are defined when Eq. (115) for the larger critical radius is solved for ξ_r and when $\beta_r = \beta_s$ corresponding to the cavitation number for the smaller critical radius. Then in Figure 13 we see that the only permissible values of r_m (or ξ_m) must lie to the left of the intersection at ξ_r between the horizontal line through $\beta = \beta_r$ and the curve of Eq. (115), provided that $\beta_r < 0$. If $\beta_r \geq 0$ the entire area corresponding to $\beta < 0$ and to the right of the minimum of $\beta\sqrt{\gamma}$ is available for Class-3 solutions. If $\beta_r < 0$, the point $(\xi_m, \beta_m\sqrt{\gamma})$ must lie within the wedge-shaped region between the horizontal line and the curve if Class-3 solutions are to be found. This restriction also limits the

the range of r_m to be within the interval

$$n < r_{sc} < r_m < r_r \quad , \tag{116}$$

where r_{sc} is the smaller critical radius defined by Eqs. (89) and (90). The condition given by Eq. (116) supplements that given by Eq. (112) if $\beta_r < 0$.

In order to explore this point in more detail, a numerical example based upon Eqs. (57a), (59), (64), and (69a) has been carried out for several cavitation numbers (or β's) and at three values of r_m in the permissible region. Since all r_m have been taken to be only slightly less than r_r, Figure 14 shows a greatly enlarged plot of the vicinity to the left of the point of intersection $(\xi_r, \beta_r\sqrt{\gamma})$. Figure 14 also shows a number of level lines bearing prescribed values of the time spent in vaporous growth for $1 \leq r \leq r_m$. These level lines of $\tau_o + \tau_g$ result from numerical integrations of Eqs. (64) and (69a). Figure 15 results from cross plotting the data given in Figure 15. This figure shows graphs of τ as a function of $\beta\sqrt{\gamma}$ for the three values of r_m selected for study. The vertical axis on the right of Figure 15 passes through the smaller critical radius line in Figure 14 so that as $K \to K_s$, $\tau \to \infty$. Similarly, the other axes, being at the intersection of r_m with β as given by Eq. (115) and the selected values of ξ_r towards the left in Figure 14. These illustrations show that the solution of the problem of matching a prescribed maximum vaporous growth and a prescribed growth time is not unique. Because of Eq. (7) it follows for given values of ξ_m and τ that the value of K which gives $\beta \to \beta_s$ will be larger than the value of K on that branch of the level line which is near $\beta_\ell\sqrt{\gamma}$. Thus if we prescribe r_m, we are tempted to let this larger value of K determine the cavitation number for inception. However, it is better to reserve this judgment until the conclusion of the investigation. Any r_m value can be prescribed provided that the prescription does not violate conditions given by Eqs. (112) and (116).

November 19, 1979
BRP:mmj

The preceding discussion centers on the case when $\beta_r < 0$. On the other hand, cases can arise in which $\beta_r \geq 0$. Nevertheless, as we have seen, $\beta < 0$ and the point $(\beta\sqrt{\gamma},\xi)$ must still be inside the critical curve of Figure 13 in order that Class-3 solutions will be found. In this case the asymptotic condition associated with the horizontal line at β_r is not meaningful and in this extended permissible region of Figure 13 the level lines of τ will parallel roughly the critical contour defined by Eq. (115). They will not double back as in Figure 14. Then the range of possible r_m values will lie between the value defined by Eq. (9) for the upper bound and, for the lower bound, the larger of $\xi = \sqrt{3}$ or r_c as given by Eq. (8). We will return to this point later.

Since Figures 14 and 15 show that we are in a canyon having very steep sides, it is important to verify that Eqs. (105) and (111) can be used to help us locate points on the steep sides. The data plotted in Figure 15 have been used for this purpose. Two of the radii, ξ_m, have been used for comparison and three pairs of test points have been used to define the time difference $\Delta\tau_2 - \Delta\tau_2$. These are the pair (a,b) on $\xi_m = 10.517705$, and the pairs (c,e) and (c,d) as marked in Figure 15. Equation (105) was evaluated for (a,b) and Eq. (111) was used for (c,e) and (c,d). The values of $\Delta\tau_2 - \Delta\tau_1$ thus computed are compared with those calculated numerically using Eqs. (64) and (69a). Table VI shows the important numerical results.

In view of the fact that the approximate relationships of Eqs. (105) and (111) were designed for scaling cliffs and not for climbing the lower slopes, the degree of agreement shown in Table VI is felt to be satisfactory.

It is believed that the accuracy of these formulae will improve greatly when these expressions are put to their intended use. One reason for this belief is that the numerical work shows that as the value of β changes and the smaller critical radius is approached along a line of prescribed r_m, the value of τ_o grows as expected while the value of τ_g is less important and shows hardly any change. Similarly, as β changes and the larger critical radius is approached, τ_g becomes large and τ_o shows very little change, and it is always smaller than τ_g. The chief finding is that one can use Eqs. (105) and (111) as supplements to the numerical integrations of Eqs. (64) and (69a) in those cases for which the value of τ_m is so large that the numerical integrations by themselves can not complete the matching.

The foregoing analysis has been restricted to the case in which α_s and the prescribed parameters are such that the corresponding value of β, as indicated by the horizontal lines in Figures 13 and 14, are such that $\beta < 0$. This will not be true in all cases. Then the entire area within the critical curve of Figure 13 to the right of a vertical line through $\xi_1 = n/\sqrt{\gamma}$ and to the left of a second vertical which intersects the critical curve at $\xi_2 = r_m/\sqrt{\gamma}$ in which r_m is now defined by the laminar bubble height in accordance with Eq. (9). In this case only the critical curve will correspond to an infinite value of τ. In either of these cases the value of β will be less than zero corresponding to cavitation numbers less than $-C_{p_s}$. In the present situation, in order that the value of K for inception is as large as possible, the inception point in the $\beta\sqrt{\gamma} - \xi$ plane will lie at a point on the vertical line through ξ_2 and as close to the horizontal axis as possible and still match the growth time available. This will be true because the level lines for various values of τ will be

almost parallel to the critical curve in Figure 13 which slopes upward towards the right. The doubling back of the τ contours caused by the smaller critical radius as illustrated in Figure 14 will no longer play a role because the value of β corresponding to α_s will be positive once the horizontal line would lie above the ξ-axis in Figure 13.

General Scheme for Matching and Inception Calculations:

When Figure 14 applies, it appears to show that when the value of τ is prescribed, the largest values of K will be found if one uses the smallest values of r_m within the permissible range because of the slope of the level lines near the line $\beta_s\sqrt{\gamma}$. Of course, this trend is discernable only in a highly enlarged plot. Therefore its practical effect on the value of the cavitation number at inception will be limited to the very last few significant figures. The important theoretical finding at this stage of the analysis is that τ_a, K, and r_m for incipient cavitation are still unknows. However, we now know the general ranges of these parameters for which the solution should be found, provided a solution for cavitation inception exists. Moreover, the best solution for cavitation inception should have the largest possible value of K and it should also involve the smallest possible value of r_m within the permissible ranges of these parameters.

In order to insure that r_m will be as small as possible, we should use the smallest possible value for r_o. This condition would put r_o at the smaller critical radius. However, since our interest centers on Class-3 trajectories, it is computationally convenient to insist that r_o coincide with r_{vm}, the radius of minimum velocity very near the smaller critical

radius. Thus we shall set $r_{vm} = r_o$ in Eq. (97) and write

$$r_o = [6\,\gamma \ln r_o + n^2 + n + 1 - 2(\alpha + \gamma)]^{1/2} \quad . \qquad (97a)$$

Equation (97a) is in a convenient form for an iterative solution if it is assumed that the cavitation number is prescribed. Once r_o has been determined Eq. (59) can be solved for r_m^3 by iteration. The value of r_m resulting from this calculation should be close to the smallest possible value for the given value of K.

Using these values of r_o, r_m, and K, we find values of τ_o and τ_g from numerical integrations of Eqs. (64) and (69a). Since Class-3 phase-plane trajectories for these calculations will all pass close to the smaller critical radius at which v = 0, it is appropriate to use Eq. (100) in the vicinity of r_o in the integration of Eq. (64) for τ_o. Moreover, since this integration stops at r_o in this case, we shall replace the factor $2r_s$ by r_o in Eq. (100).

Once τ_o and τ_a have been found, we can carry out the matching between the distance traveled by the nucleus and the time available for this travel distance. The travel time available is given by the known value of τ_m in Eq. (115). The arc length covered by the convective motion of the growing cavitation bubble for the stepwise-autonomous approximation has been given in one form just above Eq. (50). This equation can also be written as

$$(s_3 - s_0)\,\frac{2}{V_o}\sqrt{\frac{2\sigma}{\rho\, R_o^3}} = \tau_a\sqrt{1 + K} + \tau_o\sqrt{1 + b} + \tau_g\sqrt{1 - C_{p_s}} \quad . \qquad (117)$$

The lag time τ_a is the only unknown in Eq. (117) and it can be eliminated from Eq. (117) by means of Eq. (115). Thus we find for a consistent

matching that

$$\tau_o(\sqrt{1+b} - \sqrt{1+K}) + \tau_g(\sqrt{1-C_{p_s}} - \sqrt{1+K}) = (s_3 - s_0)\frac{2}{V_o}\sqrt{\frac{2\sigma}{\rho R_o^3}} - \tau_m\sqrt{1+K} \quad . \tag{118}$$

Equations (115) and (118) are a simultaneous pair involving the three variables τ_a, τ_o, and τ_g. If K is assumed known, s_0 can be found from Eq. (31) and τ_m follows from Eq. (39). The chief constraint upon the solution of these equations is that τ_a, τ_o, and τ_g can not be negative. Their solutions will be among a one-parameter family in which we use τ_a as the free parameter. It is useful to compare some examples of this solution for values of the various physical parameters, K, V_o, and so forth, which are consistent with the bubble-dynamics data illustrated in Figures 14 and 15. To this end we have selected two values of K for a free-stream velocity of 20 fps (6.096 m/s) on the two-inch diameter (0.0508 m) hemisphere. As illustrated in Figure 16, two values of K have been selected and the value for the right-hand side of Eq. (118) for each of these K-values is tabulated in Table VII. Values of τ_m are also tabulated in Table VII for use in Eq. (113). The solid lines in Figure 16 are plots of Eq. (118). Because the two values of K are so close together, we have only one value for each coefficient on the left-hand side of Eq. (118). The single value for the coefficient of τ_o is .156 and the value of the coefficient of τ_g is 0.092. The two curves which result are the solid lines shown in Figue 16. The dashed lines show values of the parameter $\tau_a (\geq 0)$ for which solutions of these two equations are found. These solutions are indicated by the points of intersection marked for the two cases. The profound influence of very small changes in cavitation number is certainly emphasized in this plot. Moreover, we see that permissible values of τ_a are limited, and

that the magnitudes of τ_g and τ_o are thousands of bubble-time units. An added feature of these equations is revealed if we take $K = -C_{p_s}$ in Eq. (118). In this case a kinematically correct solution will not depend upon τ_g and a plot of this limiting case will appear as a vertical line in Figure 16. In this case the coefficient of τ_o will equal 0.064 and the right-hand side of Eq. (118) will equal -763 and for τ_m we have 10,069. But there can be no valid solution if τ_o is negative. In this case τ_o = 11,925. Evidently we require that $K < C_{p_s}$ if kinematically correct solutions are to be found.

If the time magnitudes in Figure 16 are compared to the time units displayed in Figures 14 and 15, we see that the kinematically-determined time units in Figure 16 are an order of magnitude greater than those shown previously. This difference indicated that the dynamical equations must be considered at points in the $\xi - \beta\sqrt{\gamma}$ plot of Figures 13 or 14 which are close to a critical line. In such cases, equations such as (100) or (105), for $\alpha \to \alpha_c$ at the smaller critical radius, will be the chief factor determining the final magnitude of τ_o. Similarly, the final value of the time τ_g will be determined mainly by equations such as (109) or (111) corresponding to the maximum radius r_m being very close to the larger critical radius. As we have noted these values, τ_o and τ_g, can be selected almost independently of one another. If τ_o must be increased, we simply must change the cavitation number so that the phase-plane trajectory comes closer to the smaller critical radius. In order to increase τ_g, we must increase r_m in order to bring it closer to the larger critical radius.

On the other hand, Figure 16 shows that once a kinematically permissible value of τ_o has been found, the corresponding value of τ_g is determined from Eq. (118) and the value of r_m then follows from this value of τ_g by causing

it to be more or less close to the larger critical radius at that cavitation number. Once these adjustments have been made, the value of τ_a follows from Eq. (113) and the matching is determined.

Evidently the matching described above is not unique. In principle, one would like to adjust τ_o and τ_g so that r_m is as small as possible. This can be done if τ_o is large compared to τ_g. That is, one wants to make the cavitation number as high as possible so that the phase-plane trajectory just grazes the smaller critical radius. Then the value of τ_g must be relatively smaller and as we see from Figure 16, the value of τ_a will be larger than it would be for larger values of τ_g.

As we have noted already, the important aspect of this consideration is that in principle we have seen the way to determine the matching of nonautonomous and piecewise-autonomous systems even though the matching is not unique. As a practical matter the comparison of time magnitudes shown in Figures 14, 15, and 16 indicates that the arguments of the exponentials in Eqs. (105) and (111) will be large negative numbers so that differences between α and α_c, β and β_c will be vanishingly small. Indeed, the tabulated values of K for which Figure 16 was drawn, differ only in their $6^{\underline{th}}$ decimal places. One does well experimentally if he can measure K to three decimal places. Thus, except possibly for very small bodies immersed in very high speed flows, one is justified if he uses the asymptotic values α_c from Eqs. (88), (89), and (90) in order to fix the inception cavitation number and the smaller critical radius of the vapor bubble. On the other hand, even though in principle, r_m can have almost any value between the larger critical radius and the smaller critical radius, it appears that more often than not r_m will be close to the larger critical radius. In the $\xi - \beta\sqrt{\gamma}$

plot of Figure 14 this consideration places the largest r_m at the intersection of the horizontal and sloping critical lines. Once r_m has been found, we can calculate r_o from Eq. (59). The smallest permissible value of r_m is found when r_o equals the smaller critical radius. In those cases in which the larger critical radius exceeds the maximum radius permitted by the laminar bubble height, Eq. (9), then we use Eq. (9) to find r_m for use in Eq. (59). This procedure can be continued as the Reynolds number increases until the value of r_o found in this way equals the smaller critical radius, r_s. When r_o equals r_s as indicated, the cavitation form assumed in the present theory is no longer possible. The bubble can not have a vaporous growth followed by a gaseous-growth phase and one should not expect to observe the characteristic narrow cloudy bubble ring which typifies the form of cavitation of interest here.

In view of the influence of the relationship between r_o and r_m, as given by Eq. (59), upon the maximum vaporous bubble radius, we continue the illustrative example and show curves of r_o versus r_m for two cavitation numbers in Figure 17. The upper curve corresponds to a K-value close to the horizontal critical line in the plot of Figure 14. The larger critical radius which bounds the solid part of this curve locates r_m at the intersection of the horizontal and sloping critical lines in Figure 14. The lower end of the curve terminates when $r_m = r_o = r_s$. The lower curve corresponds to radii on a horizontal line in Figure 14 which lies below the horizontal critical. The solid part of the curve terminates on the right when r_m lies on the sloping critical line in Figure 14. The termination at the left places r_o at the smaller critical radius. When r_o is at the smaller critical, the value of r_o, and consequently τ_o,

will be as small as possible. On the upper curve this permits r_m to be equal to r_o and consequently τ_g will vanish. This situation would give points on the τ_o axis in Figure 16. The lower curve shows that as K is reduced from the critical value, r_m will be larger than r_o when r_o is at the lower critical radius so that τ_g will no longer be equal to zero, although the radius r_m will certainly be less than it would be if the value of r_o exceeds the smaller critical value, r_s. The situation with respect to calculations based upon the asymptotic formula corresponds to that illustrated by the upper curve of Figure 17. The dotted parts of the two curves to the right of the larger critical radii in Figure 14 show solutions of Eq. (59) which lie in the region of Class-4 solutions of Figure 12. These branches of the curves are not appropriate for the present considerations. They are plotted in Figure 17 in order to show that r_o reaches a maximum value on the separatrix between Class-3 and Class-4 solutions.

The preceding discussion is not complete because it applies only to the case when the value of β, corresponding to the value of α_s for the smaller critical radius, is negative. This situation applies mostly to lower free-stream velocities. In order to complete the discussion we must also consider the case in which this critical β value is positive or zero. When this latter state of affairs exists, we have already argued that the largest cavitation number will be found when r_m is given by Eq. (9) which defines the limit set by the height of the laminar bubble. The matching between τ_m for this prescribed r_m then determines the particular phase-plane trajectory, the incipient cavitation number, and so on. Since r_m in this case is determined by the free-stream

velocity V_o, it is evident that appropriate results from the preceding analyses can be organized to provide a scheme of calculations for all vapor-bubble properties of interest in the inception process for the present situation also. Since we do not plan to execute such general calculations in this report we will not list the specific equations which apply here. Instead we will content ourselves with the observation that for many experimentally interesting situations, the level lines of τ_m will be very close to the contour which defines the value of β for the larger critical radius, as already illustrated in appropriate regions in Figure 14. Since the analysis is greatly simplified and very small, error will be introduced if the analytically exact formulae are replaced by criteria which apply to the separatrices themselves. We will now turn to the exploitation of this simplification.

The Use of Asymptotic Formulae for Inception Calculations:

The preceding paragraph suggests that the formulation of inception calculations should recognize two possibilities. These are that for a given Reynolds number, inception can occur at a fairly low free-stream velocity on a large test body or at a rather high free-stream velocity on a small test body. Of course, if asymptotic formulae are to be used for the calculations, we have also noted that these formulae will not apply too well if the body is too small. In this case the value of τ_m can become rather small and the asymptotic formulae which are strictly valid for $\tau \to \infty$ will not give accurate results. Fortunately, this latter restriction will not apply in most laboratory situations of interest here.

The Cavitation Transition State

We shall define bubble-ring-cavitation transition to exist at that Reynolds number at which the laminar bubble is about to disappear. For hemispherical headforms the highest Reynolds number at which a laminar bubble can be observed is about 5×10^6. Since cavitation nuclei have some range of radii R_o and experience some vaporous growth from R_o prior to becoming stabilized in the laminar bubble, it seems likely that bubble-ring cavitation will cease and be replaced by other forms of cavitation at Reynolds numbers which are somewhat less than the value of Reynolds number at which laminar separation disappears in the noncavitating flow. Unfortunately, the author knows of no observations of incipient or desinent bubble-ring cavitation which gives the value of K and other flow parameters which define this "cavitation transition state".

Anticipating the time when such measurements will be made, we shall discuss one way by which one might estimate representative values for R_o and n from the data. In our calculations we will use Eq. (9) in order to fix r_m at the highest Reynolds number at which incipient bubble-ring cavitation is observed. At this cavitation transition Reynolds number, the larger critical radius r_ℓ, as defined by the intesection of the horizontal and sloping critical lines in Figures 13 and 14, may well be significantly larger than the maximum permissible value of r_m from Eq. (9). We note also that if there is such an intersection, the following analysis assumes that the headform is large enough and the free-stream velocity is low enough so that only negative values of β are involved. In order to test for this condition one must first find α_s

from Eqs. (88), (89), and (90). Then the corresponding value of β can be found from Eq. (47) if V_o is known from experiment.

Continuing with the analysis we recall from our decision to use asymptotic equations and the discussion surrounding Figure 17, that the smallest permissible value of r_m will be achieved when r_m is such that $r_o = r_s$, the smaller critical radius. Therefore we would expect to relate the Reynolds number at cavitation transition to the smaller critical radius by changing Eq. (59) to read

$$r_s = \left[\frac{\alpha + 1.5\, r_m^2 - 3\gamma \ln r_m - (n^2 + n + 1)/3}{\alpha + \beta}\right]^{1/3}, \qquad (119)$$

where r_m is given by Eq. (9) and we have put $\beta = 0$ in Eq. (59). The reason for putting $\beta = 0$ in order to obtain Eq. (119) is that at the high Reynolds number corresponding to cavitation transition $K = -C_{p_s}$ within experimental accuracy. And although $\beta < 0$ theoretically, it will be very small in magnitude and the experimental data will generally have too much scatter for us to determine a value of β. As Figure 13 shows, this approximation causes $r_\ell \to \infty$. In any case, since K is assumed known from the anticipated experiment it follows, when the value of r_m from Eq. (9) is used in (119), that r_s is dependent upon the unknown parameters n and R_o. The quantities α, β, and γ also depend on R_o.

On the other hand, r_s is also determined by Eqs. (88) and (89). Moreover, because of the way the parameters α and γ are defined, the ratio γ/α_c will be independent of R_o and this ratio will be known if K is known. Therefore, we can obtain an equation which relates only

r_s and n if we form the ratio γ/α_c using Eqs. (88) and (89). The result of this step is

$$n^2 + n - C = 0 \tag{120}$$

and

$$C = \left[r_s^2 - (\ln r_s)\, 6\gamma/\alpha_c r_s + (2 + 3\gamma/\alpha_c)/r_s\right]/(1 + \gamma/\alpha_c r_s^3) - 1 \quad . \tag{121}$$

The solution of Eq. (121) is

$$n = (\sqrt{1 + 4C} - 1)/2 \quad . \tag{122}$$

In the case of the spherical nucleus (air bubble) n = 1 and we see from (122) that C = 2.

In order to obtain representative values of n and R_o from cavitation-transition experimental data, one starts the calculation by finding values of n for a range of values of the critical radius r_s from Eqs. (121) and (122). Then we observe that at cavitation transition the smallest possible value of r_m will be r_s, as discussed in connection with Figure 17. Therefore we put $r_m = r_s$ in the right-hand side of Eq. (119). But according to Eq. (9) R_o will now be determined by

$$R_o = 27.8\, D/(r_s\, Re^{0.79}) \quad , \tag{123}$$

so that we can regard Eq. (119) as a second equation between r_s and n. These two relationships can be plotted in an r_s - n plane. The intersection of the two curves will provide representative values of r_s, n and then Eq. (123) can be used to obtain the representative value of R_o.

Because we lack the necessary experimental results, we must content ourselves with a range of corresponding values of R_o and n. This situation

arises because the highest velocity obtained in the experiments of Reference 3 is 70 fps (21.34 m/s). Even so, we find within experimental accuracy that at this speed $K = -C_{p_s} = 0.63$ for bubble-ring desinent cavitation. However, since the Reynolds number at this speed is only 1.25×10^6 for the 2-inch diameter (0.0508 m) models of the experiments, the conditions for cavitation transition are not attained. Therefore we can not put $r_m = r_o$ in Eqs. (9) and (119) as we can at cavitation transition. Instead we are left with a one-parameter family of solutions of Eqs. (122) and (119). We took the critical radius r_s as the free parameter in our calculations. Thus we found a curve of n versus r_s for the experimental ratio $\gamma/\alpha_c = 1.679$ in Eq. (122), as illustrated in Figure 18. Then we selected a number of R_o values starting at $R_o = 1\mu m$ and ending at $7\mu m$. For each value of R_o we used Eqs. (9) and (108) in order to calculate a family of curves of n versus r_s. Except for the curve at $R_o = 1\mu m$, this family is also shown in Figure 18. The intersections of these curves with that obtained from Eq. (122) define consistent values of n, R_o, and r_s. The final values for a spherical air nucleus at n - 1 are representative values of the sort described previously because in this case n is known along with the experimental data pertaining to this case. Therefore, R_o and r_s are determined once and for all by Eqs. (108) and (122). The result of this is that we can find r_s when n = 1 from the graph of Eq. (122). The value is $r_s = 2.2$. This value can then be put in Eq. (123) in order to obtain R_o. The results of all calculations are given in Table VIII. The fact that $\beta = 0$ in these calculations makes these values approximate because Eq. (119) does not contain the term βr_m^3.

Therefore r_s is somewhat over estimated and the R_o values which result are probably a bit too small, or conversely, the values of n are somewhat larger than they should be.

A graph of the numerical data in Table VIII is shown in Figure 19. Except for the point at n = 1, nuclei sizes in the region below and to the left of the curve will produce the characteristic bubble-ring cavitation. For example if n = 5, the largest nucleus which will lead to bubble-ring cavitation by means of gaseous growth in the laminar separation bubble after an initial period of vaporous growth, has a radius of about 5.7μm. Nuclei having this n and larger values of R_o than approximately 5.7μm will not produce bubble-ring inception, although some other form of limited cavitation might be produced upon their vaporous growth.

The foregoing calculations have been made under the assumption that α_s leads to a negative value of β. When this is not the case we may still let r_m be determined by Eq. (9) as before. Then we can calculate β from Eq. (93). Since V_o and K are known from experiment, we can find the Reynolds number and the value of β. Therefore we have two equations for the determination of r_m and R_o:

$$R_o\, r_m = \frac{27.8D}{Re^{0.79}} \tag{124}$$

and

$$\beta r_m^3 + r_m^2 - \gamma = 0 \quad . \tag{125}$$

An approximate solution of the cubic can be found from recognition of the fact that β will be close to zero and r_m must be fairly large, as illustrated

by the critical curve of Figure 13. Therefore since β is negative we put

$$r_m = x - \frac{1}{\beta}$$

in Eq. (125) where $|x| \leq r_m$. As a result the cubic becomes

$$\beta x^3 - 2x^2 + \frac{x}{\beta} - \gamma = 0$$

The term βx^3 will be less than the terms of lower order and we can get an approximate solution by solving the quadratic which results from deleting this third order term. The approximate root of interest in this case is

$$x \doteq [1 - \sqrt{1 - 8\gamma\beta^2}]/4\beta \quad .$$

When this approximation is substituted into the cubic in x, it is found that the residual by which it fails to vanish is $O[(\gamma\beta/2)^2]$. Therefore r_m will be approximated by

$$r_m \doteq \frac{1}{\beta}\left[1 - \frac{1 - \sqrt{1 - 8\gamma\beta^2}}{4}\right] \quad , \qquad (126)$$

the corresponding approximation for R_o then follows directly from the use of this value of r_m in Eq. (124). An estimate for n can then be found if we use Eq. (59) with $r_o = r_s$, as was assumed for Eq. (119).

The foregoing discussion has dealt with the case in which experimental data on a known headform defining the cavitation-transition state (V_o, K) are available. Then it is desired to find the properties of a representative nucleus in terms of the parameters R_o and n. Two cases were considered. The first occurs when α_c is such that the corresponding value of β_c is negative and the second pertains to the case when the corresponding value

of β_c equals or exceeds zero. The first case applies to larger bodies operating at rather low speeds and the second case corresponds to relatively smaller bodies in a relatively high-speed flow.

Next suppose that values of n and R_o are known. Let us find approximately the cavitation-transition state as defined by the values of K and V_o for bubble-ring inception. In the high-speed case when the value of α_s is such that the corresponding critical value of β is positive, we can calculate r_s from Eqs. (88), (89), and (90) as usual. Then we put $r_m = r_s$ as the smallest value of r_m likely to be permissible. This value of r_m can be used in Eq. (9) to calculate Re and then V_o can be found. Once V_o is known C_σ can be found from the formula just above Eq. (6). The value of r_m can also be used in Eq. (84) in order to calculate β. Then Eq. (7) gives the transition value of K. Since the high-speed case is the more likely of the two possibilities, we shall not pursue this matter further. Instead we turn to the consideration of the phenomenon of bubble-ring-cavitation cutoff.

Cavitation Cutoff

The following calculations are motivated by the fact that in the experiments of Reference 3 no bubble-ring cavitation was observed at a free-stream velocity of 30 fps (9.144 m/s), although other forms of cavitation were observed at this speed. A tunnel speed of 40 fps (12.192 m/s) was the next higher speed in these experiments and bubble-ring cavitation was observed at this speed. Thus it was found that a bubble-ring cavitation "cutoff speed" existed at some value of tunnel velocity between 30 and 40 fps (9.144 and 12.192 m/s). No systematic

experiments were carried out in order to determine the cutoff values of tunnel speed and desinent cavitation number.

As a first step in the cutoff calculation, we offer an interpretation of the experimental findings which can be expressed in terms of the present theory. One factor may be that since the cutoff speed is a relatively low speed, the cavitation number at this speed should be somewhat less than that at the inception numbers at higher speeds. Moreover, since this speed is a threshold value for bubble-ring cavitation, it seems that the cavitation number should probably be as low as possible. For bubble-ring cavitation the lowest cativation number will be accompanied by the largest permissible value of r_m. Thus r_m will be given by Eq. (9); namely,

$$r_m = \frac{27.8D}{Re^{0.79} R_o} \tag{9}$$

The idea here is that for Class-2 or Class-3 trajectories the greatest amount of vaporous growth should occur in such a way that the maximum radius is limited by the height of the laminar bubble. Moreover, since we are dealing with the asymptotic theory, the value of r_m will be a larger critical value. That is, from Eq. (93) we have

$$\beta = \frac{1}{r_m}\left(\frac{\gamma}{r_m^2} - 1\right) \quad . \tag{93}$$

Also the radii r_m and r_o must be related by Eq. (59), which we will write as

$$(\alpha + \beta)\, r_o^3 = \alpha + \beta\, r_m^3 + \frac{3}{2} r_m^2 - 3\gamma \ln r_m - \frac{n^2 + n + 1}{2} \quad . \tag{59}$$

Since r_m is a larger critical radius, the condition for vanishing slope of the phase-plane trajectory at r_m from Eq. (93) can be used in the right-hand side of Eq. (59) in order to eliminate the term βr_m^3. The result is

$$(\alpha + \beta)\, r_o^3 = \alpha + \gamma + \frac{1}{2} r_m^2 - 3\gamma \ln r_m - \frac{n^2 + n + 1}{2} \quad . \tag{127}$$

If we use the condition given by Eq. (15) and the definition for the Reynolds number, we can write Eq. (15) as

$$r_m = 27.8\nu^{0.79} D^{0.21} / (V_o^{0.79} R_o) \quad , \tag{128}$$

where V_o is now the cutoff velocity, V_{co}.

If for the moment we assume that V_{co} is known, then Eq. (128) determines r_m and since n, R_o, and γ are known quantities, β is given by Eq. (93). On the other hand, we can use Eq. (47) in order to write the quantity $(\alpha + \beta)$ in terms of the cutoff velocity as

$$\alpha + \beta = (b + C_{p_s})\, \rho\, R_o\, V_{co}^2 / (4\sigma) \quad . \tag{129}$$

Since Eq. (129) contains known quantities, the sum $\alpha + \beta$ is determined and α can now be found because β itself is known. It remains to make good our assumption that V_{co} can be found by closing the above system of equations with an additional condition.

Thus far we have required the greatest amount of vaporous growth, without producing unlimited growth as would be found in Class-4 solutions, by specifying the largest possible value of r_m. This specification is consistent with the idea that the cutoff velocity is the limiting condition

for bubble-ring cavitation, but that other forms which are independent of a laminar bubble being present may exist. The cavitation number for this condition will be as small as possible but not too small for Class-3 solutions, if the radius r_o in Eq. (127) is taken to be as small as possible. Strictly speaking, this condition will be one in which the parameter α will be close to but larger than α_c, corresponding to a smaller critical radius [see Eqs. (88), (89), and (90)]. However, the phase-plane trajectory will still show an isolated minimum at a radius slightly less than the smaller critical radius. We have seen in connection with the general structure of permissible solutions that the difference between α and α_c will be very small indeed. Therefore we can, within the framework of the present asymptotic theory, put $\alpha = \alpha_c$, $r_o = r_c$ and produce negligible error. If we adopt this proposal, we can return to Eqs. (89) and (90) and combine them into the single condition

$$r_o^2 + 2\gamma(1 - 3\ln r_o) - (n^2 + n + 1) + \frac{2}{r_o}\left(1 - \frac{\gamma}{r_o^2}\right) = 0 \quad , \tag{130}$$

For values of r_o in the range $1 < r_o < r_m$, this equation will have one root, provided that V_{co} is properly chosen. The fact that r_o depends parametrically on V_{co} suggests that one may write

$$G(V_{co}) = r_o^2 + 2\gamma(1 - 3\ln r_o) - (n^2 + n + 1) + \frac{2}{r_o}\left(1 - \frac{\gamma}{r_o^2}\right) \tag{130a}$$

and solve for $G = 0$ by iteration on V_o because the foregoing system of equations is now closed.

The preceding analysis has used formulae which have been designed for r_m and r_o both larger than or equal to n. But we have seen that as long as $r_m \geq n$, Eq. (59) is valid for any value of r_o in the range $1 < r_o < r_m$. On the other hand, if $r_o < n$ Eq. (130a) does not apply. The applicable equation can be obtained from Eqs. (90) and (89a). Upon combining these two equations we find that if $r_o < n$, the condition that $G(V_{co}) = 0$ can be expressed as

$$\alpha(r_o - 1)(r_o + 2) + 6\gamma \ln r_o = \gamma(1 - \frac{1}{r_o})(2 + \frac{1}{r_o}) \quad . \tag{131}$$

But α and γ are both positive and $r_o > 1$ for situations of physical interest. Therefore we see that Eq. (120) has no solution if $r_o < n$. Since we shall continue to impose the condition that $r_m \geq n$, it follows that admissible solutions of Eq. (119a) must lie in the range $n \leq r_o < r_m$. Therefore, if in the calculation of r_o in accordance with Eq. (59) one finds that $r_o < n$, it follows that there is no solution for V_{co} corresponding to selected values of the parameters R_o, n, and γ.

Once V_{co} has been found by the method suggested above, one can complete the calculation by finding C_σ from

$$C_\sigma = 4\sigma/(\rho R_o V_{co}^2) \quad , \tag{132}$$

and the cutoff cavitation number from either of

$$K_{co} = b - \alpha C_\sigma = \beta C_\sigma - C_{p_s} \quad . \tag{133}$$

Table IX gives numerical data from calculations as outlined above for cutoff values of V_{co} and K_{co} at a water temperature of 80°F (26.67°C). Extensive

ranges of R_o (microns) and n have been selected for two air contents in order to show the general trends forecast by the analysis as clearly as possible. All calculations pertain to $C_{p_s} = -0.630$.

As noted already, experimental observations now available [3] indicate a cutoff velocity between 30 fps (9.14 m/s) and 40 fps (12.19 m/s) for a 2-inch (0.0508 m) diameter hemispherical nose at water temperature between 78° (25.56°C) and 79°F (21.11°C). This range of possible cutoff velocities was not found to change with dissolved air content. In order to illustrate how the present numerical data fit in with the observed trends, we have extracted those values from Table IX which lie in the neighborhood of the experimental trends and presented them in the carpet plot of Figure 20. In this plot the abcissa is simply the cutoff velocity V_{co}. The ordinate is the cutoff cavitation number K_{co}. However, this ordinate has a sliding scale which depends upon the value of n chosen for each calculation of the cutoff condition (V_{co}, K_{co}). For example, suppose the value of n is 6. Then at the ordinate marked 6 in Figure 20, $K_{co} = 0.5$. At the ordinate marked 5, we would have $K_{co} = 0.4$ and at the ordinate marked 7, we would have $K_{co} = 0.6$. It is necessary to choose this kind of a sliding scale because it is found from the values given in Table IX that V_{co} is the primary quantity affecting the value of K_{co}. The values of R_o and n affect K_{co} less directly. Another interesting fact which emerges from Figure 20 is that the influence of air content, at least within the range studied, seems to have little effect upon the value of K_{co} to the accuracy of a plot to the scale of that used here. The chief differences appear in the third or fourth decimal places. For this reason each curve of K_{co} versus V_{co}, shown at the slightly sloping lines for each value of n

in Figure 20, have been faired between all points regardless of the values of R_o and air content. The more steeply sloping families of curves in Figure 20 which intersect the K_{co} curves represent constant values of the initial radius R_o (microns) for air contents of 7.5 ppm (solid curves) and 15 ppm (dashed curves). These curves show that a prescribed cutoff velocity is achieved with varying nucleus sizes which depend upon air content. Other factors being the same, one sees that as air content increases the value of R_o decreases. Figure 20 also shows that if one knows the values of V_{co} and K_{co}, he would be able to determine the nominal properties of a typical nucelus which lead to the observed cutoff in terms of R_o and n. However, at present we do not know any precise experimental condition for cutoff but we do know the free-stream velocity range in which it may be found [3], when the test conditions are those summarized above. As a result we can at least see from Figure 20 a limited range of possible nucelus properties which needs to be explored. Table X gives a few such values which have been read from Figure 20 when various values of n have been chosen and the observed extreme values of 30 fps (9.144 m/s) and 40 fps (12.19 m/s) have been chosen for comparison even though these velocities are certainly not cutoff values. Table X shows how to limit the range of parameters needing consideration in subsequent numerical work. It may be noted that the values of n and R_o in Table X do not differ too greatly from those presented in Table VIII and that the general trend of decreasing R_o with increasing n is shown in both instances.

Figure 20 and Table IX pertain to $C_{p_s} = -0.630$, corresponding to the laminar separation point. Another point taken inside the laminar separation bubble where $C_{p_s} \doteq -0.613$ as noted in Figure 5, is an alternative worth considering. Figure 21 shows one example of such comparative data calculated for cavitation cutoff. Comparison with experiment suggests that the value $C_{p_s} = -0.630$ is preferred because it leads to higher cutoff cavitation numbers.

November 19, 1979
BRP:mmj

Calculations for Prescribed Nucleus and Free-Stream Velocities

The preceding arguments have permitted some narrowing of the choices for nucleus properties and at the same time they provide the upper and lower limits on the free-stream velocity which must be considered. It now remains to give a general procedure, using the asymptotic theory, which permits the estimation of the inception cavitation number for bubble-ring cavitation when n and R_o are prescribed and V_o lies anywhere between the upper and lower bounds defined by the cavitation transition and cutoff states. Two cases will be considered in these calculations. The first of these occurs when the cavitation number for the smaller critical value of the cavitation number exceeds $-C_{p_s}$. Then the asymptotic value of K for the onset of bubble-ring cavitation is determined from Eq. (7) and

$$\beta = \frac{1}{r_m}\left(\frac{\gamma}{r_m^2} - 1\right) \quad , \tag{93}$$

where r_m is determined by Eq. (9). Having specified V_o, n, R_o, γ, and so on, we first calculate r_{m_b} from Eq. (9). Next we use Eqs. (88), (89), and (90) in order to find α_c from which K_c can be found from Eq. (46) because C_σ can be calculated at once from the prescribed data of the problem. In this case $K_c \geq -C_{p_s}$. Therefore we can use Eq. (93) in order to find β. Then the cavitation number for onset follows from Eq. (7). These calculations, being rather straightforward, permit one to write a rather simple asymptotic formula for bubble-ring onset in this case. The result is

$$K = -C_{p_s} - \frac{\sigma}{6.9\,\mu^{0.79}(\rho D)^{0.21}V_o^{1.21}}\left(1 - \frac{\gamma R_o^2 V_o^{1.58}}{772.34\,\nu^{1.58}D^{0.42}}\right) . \tag{134}$$

This result shows that the incipient cavitation number is practically independent of air content except when $K \approx -C_{p_s}$. Indeed, when $K = -C_{p_s}$ we can solve for V_o in Eq. (134) and obtain

$$V_o = \left(\frac{27.8}{R_o}\right)^{1.266} \frac{\gamma\, D^{0.266}}{\nu^{0.633}} , \tag{135}$$

which gives the lowest speed at which $K = -C_{p_s}$. This condition corresponds to $\gamma = r_m^2$ in Eq. (93) and in Figure 13 it is to be found at the point of intersection of the $\beta\sqrt{\gamma}$ versus ξ curve with the ξ-axis at $\xi = 1$, which is to the left of β_{min}, and this branch of the curve is not physically accessible to us. Therefore the interpretation of Eq. (134), which indicates that the inception of bubble-ring cavitation is independent of air content, is the correct one for our purposes and it is permissible for us to simplify Eq. (134) by neglecting the term involving γ altogether. Thus we have

$$K \doteq -C_{p_s} - \frac{\sigma}{6.9\,\mu^{0.79}(\rho D)^{0.21} V_o^{1.21}} . \tag{134a}$$

We note in passing that Eq. (134) does not depend upon n.

In the second case $K_c < -C_{p_s}$. When r_m from Eq. (9) is larger than or equal to larger critical radius corresponding to the intersection of the horizontal line resulting from $\beta = (K_c + C_{p_s})/C_\sigma$ and the critical curve of $\beta\sqrt{\gamma}$ versus ξ in Figures 13 or 14, the calculation for the inception of bubble-ring cavitation can be determined from Eqs. (134) or (134a). When r_m from Eq. (9) is to the left of the intersection, one value of K can be determined from Eq. (134) and a larger value for inception is obtained if one puts $K = K_c$, where K_c is obtained from Eqs. (88), (89), (90), and Eq. (46).

November 19, 1979
BRP:mmj

Since the inception cavitation number is to be as large as possible, we are tempted to select the larger of these two values as being the correct value for this case. Unfortunately, a simple formula such as Eq. (134) is not readily available in this case. However, this solution, leading to a horizontal line in Figures 13 or 14 above, is associated with Class-2 vaporous growth curves if the limiting value of β is approached from above. It is associated with Class-3 growth curves if it is approached from below and both positive and negative values of the limiting value of β can occur. In this latter case there is no intersection between the horizontal critical β line and the $\beta\sqrt{\gamma}$ versus ξ curve in Figure 13 for values of $r > 1$. And the K versus V_o curve associated with the critical β line is distinct from that obtained from the $\beta\sqrt{\gamma}$ versus ξ curve. This latter curve demands that $\beta < 0$ for inception and it guarantees Class-3 solutions. Therefore, if we insist that only Class-3 solutions be used to define the inception of cavitation, we will frequently find that the calculated value of K is less than it would be if the horizontal critical β line were used. For brevity we shall call these critical β solutions Class-2 solutions even though within the framework of the asymptotic theory either Class-2 or Class-3 solutions could be involved.

Once Eqs. (88), (89), and (90) have been used to define α_c and r_s, we can use Eq. (46), defining α, in order to calculate K_c for prescribed values of V_o. Indeed, if we put $K_c = -C_{p_s}$ in Eq. (46) and solve for V_o, we have the value of V_o corresponding to $\beta = 0$ in Figure 13. This value is given by

$$\tilde{V}_o = 2\sqrt{\frac{\sigma\,\alpha_c}{\rho\,R_o\,(b + C_{p_s})}}\,.$$

November 19, 1979
BRP:mmj

On the other hand, we can also find the values of V_o, K, and r_s at the intersection of Class-3 and Class-2 solutions. Since $\beta = (\gamma/r^2 - 1)/r$ and $\beta C_\sigma = K + C_{p_s}$ from Eq. (7), we can write

$$V_o = 2\sqrt{\frac{\sigma}{\rho R_o(b + C_{p_s})}\left[\alpha_c + \frac{1}{r}\left(\frac{\gamma}{r^2} - 1\right)\right]} \quad , \tag{136}$$

But

$$Re = \frac{V_o D}{\nu}$$

and

$$r = \frac{55.5D}{R_o R_e^{0.76}}$$

and these can be used in conjunction with Eq. (136) in order to solve for V_o by trial and error. This solution then permits us to find the value of K at which Class-3 and Class-2 V_o- *versus* -K *curves intersect.* Note that the value of r used here depends on the full laminar bubble height instead of the half-height as given by Eq. (9).

The foregoing calculations for Class-3 and Class-2 solutions have been programmed for execution on a computer. The cavitation cutoff curves of Figure 20 were used to select likely values of R_o and n for air contents of 7.5 and 15 parts per million. Calculations were then made in order to see which set of parameters give Class-3 solutions which seem to match the data of Holl and Carroll [3] for a water temperature of 80°F (26.67°C) and cavitation cutoff speeds between 30 and 40 fps (9.144 m/s and 12.192 m/s). The results of these calculations which gives the best agreement is shown in Figure 22. As also found

experimentally, the calculations are practically independent of dissolved air content. The best agreement is found for a spherical nucleus, n = 1, having a radius R_o of 5.18 microns. The cutoff speed is also shown in Figure 22. The agreement is best when the maximum vapor bubble radius is set equal to the full laminar bubble height. The result of using half the laminar bubble height is also shown in this figure.

Figure 23 is an enlarged plot which presents the same data as Figure 23 for the Class-3 solutions and also shows the trend found for one example of the Class-2 solution having the input parameters indicated. The similarity between the Class-2 solution shown in Figure 23 and similar trends reported in Reference 9 may be noted. The reason for this similarity is the fact that the present Class-2 solutions and the theory of Reference 9 are essentially the same.

It is believed that the comparison between the best Class-3 solution and the data is most encouraging. Insofar as it has been possible, these calculations have been carried out from first principles. Of course, the pressure distributions of Holl and Carroll together with the laminar bubble data of Figure 3 are basic to the entire calculation scheme. Certainly, we are now lead to discard the Class-2 solution compared to the results which are obtained if we insist that Class-3 solutions be required. Moreover, if we are prepared to "fudge" on the meanings of the numerical constants appearing in Eq. (134), we could fit the theory to the experiments almost exactly. However, our concern has been to obtain some justification for the basic hypotheses outlined in THE SEQUENCE OF EVENTS at the start of this report. The present comparisons tend to increase our confidence in their validity.

November 19, 1979
BRP:mmj

One of the uncertainties in the present theory has concerned the maximum vapor bubble diameter as compared to the maximum height of the laminar separation bubble. In order to examine the sensitivity with respect to this factor of calculated results for Class-3 solutions, we have changed the ratio of these two characteristic lengths by a factor of two as illustrated in Figures 22 and 23. But Class-3 solutions are characterized in the aysmptotic theory by Eqs. (134) or (134a) and these equations contain the assumpiton that the maximum vapor bubble diameter is one half of the maximum laminar separation bubble height. Suppose we let this ratio be designated by θ, where $\theta \leq 1$. Then we can rewrite Eq. (134) as

$$K = -C_{p_s} - \frac{\sigma}{13.875\theta\rho\nu^{0.79}D^{0.21}V_o^{1.21}}\left[1 - \frac{\gamma}{D^{0.42}}\left(\frac{V_o}{\nu}\right)^{1.58}\left(\frac{R_o}{55.5\theta}\right)^2\right] . \tag{137}$$

This slight extension of Eq. (134) has the virtue that the effect of ratio θ on inception is displayed explicitly.

The data on bubble-ring cavitation considered thus far are not all of the experimental findings reported by Holl and Carroll [3]. They also discovered a temperature dependence for bubble-ring desinence which is illustrated in Figure 24. In order to compare the predictions of Eq. (137) when $\theta = 1$ with the experimental findings, calculations were carried out for temperatures of 75°F, 80°F, and 93°F at a dissolved air content of 7.5 ppm. The Class-3 solution for this comparison between experiment and theory is shown in Figure 24 as dashed lines.

The agreement between theory and experiment for the highest temperature is quite good but the observed sensitivity of desinence with respect to water temperature is not well represented by the asymptotic theory. About the best that can be said is that the direction of the calculated trend is the same as that observed.

In carrying out these calculations, the spherical (n = 1) nucleus size has been selected to give agreement with the observed cavitation cutoff velocities. Since the experiments were performed using nominal velocity increments of 10 fps (3.048 m/s), the present calculations were carried out only for this level of precision. The results of this matching are given in Table XI. This table suggests that perhaps the "typical nucleus size" decreases with increasing water temperature. On the other hand, the good agreement between calculated and observed bubble-ring desinence at the temperature of 93°F suggests, if one were willing to forego the cutoff phenomenon as the main matching procedure, that one might secure better agreement between the calculated and observed trend by making further adjustments in the value of R_o. We have not made such adjustments in the present study.

CONCLUSIONS AND RECOMMENDATIONS

In the present study we have sought to use the applicable experimental data now available with regard to cavitation onset on hemispherical headforms when the process is affected by a laminar separation zone on the body. It appears that both vaporous and gaseous growth of cavitation bubbles are responsible for the appearance of the so-called bubble-ring cavitation in

this case. In order to analyze the phenomenon, a sequence of key events has been postulated which depends upon the way that cavitation bubbles originate from free-stream nuclei in the water and interact with the boundary layer on the body. A simple model of a stable "Harvey nucleus" has been used as a starting point in the formulation of the theory. This nucleus model assumes that air is stabilized on microscopic solids in the liquid so that initially the nucleus has zero surface energy. The spherical gas-bubble nucleus is included as a limiting case in this model.

The key events leading to the observed behavior appear to be that a typical nucleus moves with the boundary layer flow on the body. This nucleus first experiences a period of vaporous growth before attaining its maximum radius at a point downstream of the minimum pressure point in the laminar separation bubble. The vapor bubble becomes fixed at some point on the body inside the laminar bubble and it then can experience further growth by air diffusion from the liquid into the bubble. The phase of gaseous growth ends when the cavitation bubble radius becomes large enough to interact with the free shear layer at the edge of the laminar bubble. This interaction causes the cavitation bubble to be removed from the separation region to the turbulent boundary layer flow associated with boundary layer reattachment behind the laminar separation bubble. The turbulent eddies produce further low pressures in the water which can cause additional vaporous growth. However, because of intense shearing action within this turbulent flow the cavitation bubbles are distorted and torn apart. As a result, a white band or cloud of small but easily seen bubbles is produced. This state of desinence or inception is called bubble-ring cavitation.

Once the process of gaseous growth in the laminar separation zone is established, the conditions for the onset of bubble-ring cavitation are present and all events experienced by a typical nucleus at later stages of its development occur automatically. Only the processes of initial vaporous growth and gaseous growth require detailed analysis. In regard to gaseous growth, it is found that the separation zone does provide a favorable environment for air diffusion into the bubble because the liquid is definitely supersaturated. The most favorable condition for gaseous growth occurs when the vapor bubble just attains its maximum radius and simultaneously reaches the laminar separation bubble. The accelerations in the liquid surrounding the cavitation bubble increase the degree of supersaturation at the bubble wall over that which exists if such accelerations are negligible. Therefore, the probability that a cavitation bubble can become stabilized in the laminar separation zone at a fixed point on the body would be greatest at this instant. Once the bubble has become fixed on the body and bubble-wall accelerations are no longer appreciable, the conditions for subsequent gaseous diffusion become somewhat more demanding than those discussed above. Nevertheless, it is found that the liquid is still supersaturated at the bubble wall. It is also found that it is not possible for gaseous growth to occur under the above circumstances if the gaseous growth is not preceded by a period of vaporous growth.

With respect to the initial phase of vaporous growth, it is found that four classes of radius versus time growth histories can result from the externally applied pressure pulse on the bubble. In Class 1 the bubble simply oscillates about its initial radius and exhibits no

appreciable net growth. In Class 2 the initial small-scale oscillatory phase is followed by an appreciable increase in bubble size to a maximum radius. In these two classes of motion the small-scale oscillations are caused by the Harvey nucleus of zero initial surface energy. A spherical bubble would be less likely to have either Class 1 or Class 2 motions, although they cannot be ruled out. In Class 3 the pressure pulse imposes a sufficiently strong liquid tension to cause the vaporous growth to proceed monotonically to a maximum radius. In Class 4 the external pulse is so strong that there is no maximum radius and the vaporous growth is unbounded. It is found that the Class-3 vaporous growth solution is responsible for bubble-ring cavitation onset. The theory also requires that the cavitation number at desinence or inception be less than the magnitude of the pressure coefficient at the laminar separation point. This finding results from an approximate but fairly complete theory in which a novel procedure is developed for matching the correct nonautonomous equation of motion to a piecewise-autonomous representation. The use of the piecewise-autonomous equation in place of the correct nonautonomous equation permits one to determine at least approximately the various flow states to be associated with each of the four classes of solutions on almost an a priori basis. Once this approximation is developed, it leads naturally to a further asymptotic approximation as noted below.

As discovered by Holl and Carroll [3], there is also a cavitation-cutoff speed which defines a free-stream velocity below which bubble-ring cavitation is not observed although other forms may be present. It is now found both experimentally and theoretically that the cutoff phenomenon exists and that it is sensitive to the temperature of the water. Holl and

Carroll also found for air contents below four parts per million that bubble-ring cavitation was observed. We speculate that this result could be due to the cutoff velocity being sensitive to dissolved air content. In addition, the theory suggests that there is also a high-speed limit on bubble-ring cavitation which is associated with the Reynolds number at which the laminar separation bubble starts to disappear. It has been possible to estimate the value of the free-stream velocity and cavitation number for this "cavitation-transition" limit. No experimental data are presently available for comparison with the analytical results. The foregoing theoretical findings have been obtained by means of a simplified "asymptotic theory" which shows very encouraging agreement with the experimental data reported by Holl and Carroll [3]. It seems worth noting, when their data are supplemented by results on the geometry of the laminar separation bubble as reported by Arakeri and Acosta [1], Arakeri [2, 18], and Van der Meulen [12], that only then is there a consistent body of experimental data which permits the detailed comparisons discussed in this report. These data appear to be the only body of such experimental results now available.

The present asymptotic theory is derived from the more complete formulation which requires that both maximum vaporous cavitation bubble radius and the time available for the initial vaporous growth be considered. It has been found that the time available to a cavitation nucleus for vaporous growth from its initial size to its maximum radius is generally much greater than the characteristic time naturally associated with the motions of such small bubbles. As a result, it is possible to let the growth time be infinite. For most laboratory experiments and situations

of practical interest this very convenient approximation introduces negligible error. For example, both theory and experiment show cavitation number versus free-stream velocity curves which are almost independent of dissolved air content as long as there is appreciable dissolved air in the water. To date no calculations have been carried out for dissolved air contents which are less than 7.5 ppm, so that the findings reported by Holl and Carroll [3], that bubble-ring cavitation was not seen at air contents lower than 4 ppm, have not been investigated theoretically. With respect to agreement between measured and calculated trends of cavitation number versus free-stream velocity, it has also been found that the best results are found when the parameter $n = 1$, corresponding to a spherical air bubble nucleus of 7μm initial radius. However, comparison with results calculated for larger values of n revealed differences in cavitation numbers in the third, and occasionally in the second, decimal place. The chief trend seems to be that as the value of n increases, the nucleus size R_o decreases and the value of incipient cavitation number at a prescribed velocity shows only minor variation.

As indicated above, the formulation of a more complete theory has been carried out. An important finding of the more complete theory, which is also reflected in the asymptotic theory, is that the cavitation number for the onset of bubble-ring cavitation must be less than or equal to the magnitude of the pressure coefficient at laminar separation. However, the more complete theory has not yet been implemented in detail because it has been found that the present asymptotic theory appears to be adequate for many cases of practical importance. The more complete

theory is probably most useful for bodies of very small diameter at very high free-stream speeds, where the present asymptotic theory is not expected to apply because the time available for vaporous bubble growth will be rather short. This more complete theory should be implemented for comparison with future experiments on bubble-ring cavitation. Among the matters which further experimental and analytical work could investigate are:

(a) Bubble-ring cavitation onset on very small hemispherical headforms in very high-speed flows;

(b) More detailed investigations of cavitation cutoff;

(c) Studies of high-speed flows and cavitation transition on large and small hemispherical headforms;

(d) Bubble-ring cavitation onset on headforms of varying size in which detailed pressure distributions near $C_{p_{min}}$ and in the laminar separation bubble are considered. Experiments for these investigations should be designed in order to avoid the influence of tunnel walls, or at least to be carried out in such a way that the wall effect will be the same for all bodies tested in the experiments regardless of headform size.

Such tests, together with calculations based upon the approximate but more complete theory, would permit one to decide whether or not further elaboration of the theory developed here is warranted. It is clear that there is certainly plenty of room for improvement of the present theory. If further studies of the type indicated above should indicate that further theoretical work might be useful, they might also suggest the most promising lines of endeavor.

References

1. Arakeri, V. H., and Acosta, A. J., "Viscous Effects in the Inception of Cavitation on Axisymmetric Bodies," Transactions of the A.S.M.E., Journal of Fluids Engineering, Vol. 95, Series 1, No. 4, December 1973, pp. 519-527.

2. Arakeri, V. H., "A Note on the Transition Observations on an Axisymmetric Body and Some Related Fluctuating Wall Pressure Measurements," Transactions of the A.S.M.E., Journal of Fluids Engineering, Vol. 97, Series 1, No. 1, March 1975, pp. 82-86.

3. Holl, J. William, and Carroll, James A., "Observations of the Various Types of Limited Cavitation on Axisymmetric Bodies," International Symposium-on Cavitation Inception, The American Society of Mechanical Engineers, New York, December 1979, p. 87.

4. Holl, J. W., "Limited Cavitation," in Cavitation State of Knowledge, A.S.M.E. United Engineering Center, 345 East 47th Street, New York, New York, 1969. In particular, see pp. 46-58.

5. Plesset, M. S., "The Tensile Strength of Liquids," in Cavitation State of Knowledge, A.S.M.E., United Engineering Center, 345 East 47th Street, New York, New York, 1969, pp. 15-25.

6. Beyer, R. T., Nonlinear Acoustics, Naval Sea Systems Command, Department of the Navy, Washington, D.C., 1974, pp. 288-292.

7. Ross, Donald, Mechanics of Underwater Noise, Pergamon Press, New York, New York, 1976, pp. 203-205.

8. Knapp, R. T., Daily, J. W., and Hammitt, F. H., Cavitation, McGraw-Hill Book Co., New York, New York, pp. 51-93.

9. Parkin, B. R., "Scale Effects in Cavitating Flow," Report No. 21-8, Hydrodynamics Laboratory, California Institute of Technology, Pasadena, California, July 31, 1952.

10. Numachi, F. (Editor), Cavitation and Hydraulic Machinery, Proceedings of IAHR Symposium Published by the Local Organizing Committee, Sendai, Japan, 1963. See Parkin , B. R. and Kermeen, R. W. "The Roles of Convective Air Diffusion and Liquid Tensile Stresses During Cavitation Inception," pp. 17-36.

11. Gupta, S. K., "The Influence of Porosity and Contact Angle on Incipient and Desinent Cavitation," M. S. Thesis, Department of Aerospace Engineering, The Pennsylvania State University, University Park, PA, 1969.

12. Van der Meulen, J. H. J., "A Holographic Study of the Influence of Boundary Layer and Surface Characteristics on Incipient and Developed Cavitation on Axisymmetric Bodies," Proceedings Twelfth Symposium on Naval Hydrodynamics, National Academy of Sciences, Washington, D.C., In Press, (1978).

13. Epstein, P. S. and Plesset, M. S., "On the Stability of Gas Bubbles in Liquid-Gas Solutions, Journal of Chemical Physics, Vol. 18, 1959, pp. 1505-1509.

14. Epstein, P. S., Textbook of Thermodynamics, John Wiley and Sons, Inc., (1937), Chapter IX, p. 159.

15. Gates, E. M. and Bacon, J., "A Note on the Determination of Cavitation Nuclei Distributions by Holography," Journal of Ship Research, Vol. 22, No. 1, March 1978, pp. 29-31.

16. Plesset, M. S., "Dynamics of Cavitation Bubbles," Transactions of the A.S.M.E., Vol. 71, Journal of Applied Mechanics, Vol. 16, 1949, p. 277.

17. Van der Meulen, J. H. J., "A Holographic Study of Cavitation on Axisymmetric Bodies and the Influence of Polymer Additives," Ph.D. Thesis, Enschede, 1976.

18. Arakeri, V. H., "Viscous Effects in Inception and Development of Cavitation on Axi-Symmetric Bodies," Ph.D. Thesis, California Institute of Technology, 1973. (Also released as Report No. 3183.1, Division of Engineering and Applied Science, California Institute of Technology, 1973.)

19. Lefschetz, S., Differential Equations: Geometric Theory, Second Edition, Dover Publications, New York, 1977.

20. Davis, H. T., Introduction to Nonlinear Differential and Integral Equations, U. S. Atomic Energy Commission, U. S. Government Printing Office, Washington, D.C., 1960.

21. Dergarabedian, P., "The Rate of Growth of Vapor Bubbles in Superheated Water," Transactions of the A.S.M.E., Vol. 75, Journal of Applied Mechanics, Vol. 20, 1953, p. 537.

22. Ma, J. T. S. and Wang, P. K. C., "Effect of Initial Air Content on the Dynamics of Bubbles in Liquids," I.B.M. Journal of Research and Development, Vol. 6, No. 4, October 1962, p. 472.

23. Hart, W. L., College Algebra, D. C. Heath and Co., New York, 1926, p. 237.

November 19, 1979
BRP:mmj

Table I

Values of the Parameter $|\beta|$ when $(K + C_{p_s}) = 0.05$

V_o, fps (mps)	20(6.10)	30(9.14)	40(12.2)	50(15.2)	60(18.3)	70(21.3)
$\|\gamma - \Gamma\| = \|\beta\|$	0.013	0.029	0.051	0.080	0.115	0.156
C_σ	3.93	1.74	0.981	0.628	0.436	0.320

Table II

Pressure Distribution on a 2 in. (0.0508 m) dia. Hemisphere Headform in a 12 in. (0.3048 m) dia. Tunnel

s/D	0.557	0.617	0.674	0.715	0.748	0.765	0.705	0.798
C_p	-0.615	-0.732	-0.780	-0.746	-0.661	-0.640	-0.617	-0.613

Table III

Comparisons of $I(r_m)$ from Eq. (53) with Results Obtained by Numerical Quadrature for a Step Function Forcing Function

α	γ	r_m	$I = \frac{\alpha}{3}(r_m^3 - 1)$	$\frac{1}{2} r_m^2 - \gamma \ln r_m - \frac{n^2 + n + 1}{6}$
0.18066	0	5.52886	10.11743	10.117479
0.16406	0.6	5.95794	11.510957	11.511037
0.15034	1.2	6.42355	13.232349	13.232366

Table IV

Summary of Matching Tests ($\alpha = 0.3$, $\beta = 0.08$, $\gamma = 0.2$)

How Matched	τ_m	% error	r_m	% error	τ_a	τ_o
Test Case	36.71	-	8.490	-	0	-
Algebraic	30.68	-16.42	9.430	-11.1	-2.824	21.88
Quadrature	44.63	+21.5	8.574	+0.99	14.84	19.445

November 19, 1979
BRP:mmj

Table V

Affixes of Vortex Points in Figure 11

α	0.15	0.1667	0.175	0.18066
r	2.500	3.001	3.333	3.605

Table VI

Comparison of Numerical and Analytical Bubble-Time Differences

r_m	β_c	β_1	β_2	$\Delta\tau_2 - \Delta\tau_1$		% diff.	Fig. 14 pairs
				numerical	analytical , from Eq.		
11.334247	-0.086679417	-0.086874610	-0.086679755	196.05825	161.7056 , (96)	4.35	(a,b)
11.434247	-0.083194475	-0.088099850	-0.08170808	55.4577	53.0424 , (102)	4.35	(c,e)
"	"	"	-0.088147140	26.8163	26.7815 , (102)	0.12	(c,d)

Table VII

Numerical Data Pertaining to Figure 15

K	r.h.s. (109)	τ_m
0,38849756	1037.4	9,330
0.38849856	241.1	10,006

Table VIII

Experimentally Determined Estimates for R_o (microns) and n Using the Maximum Test Velocity of 70 fps (21.34 m/s)

R_o	1	2	3	5	7	9,79
n	16.86	12.63	9.82	6.07	3.42	1.0

Table IX

Parametric Survey of Cavitation Cutoff Conditions (V_{co}, fps; K_{co}) for Two Air Contents

and for a 2-inch (0.0508 m) Diameter Spherical Head Form in a 12-inch (0.3048 m) Diameter Test Section

Water Temperature, 80°F (26.6°C)

	DISSOLVED AIR CONTENT 15 ppm								DISSOLVED AIR CONTENT 7.5 ppm									
n	R_n = .5	1.	2.	3.	4.	5.	6.	7.	.5	1.	2.	3.	4.	5.	6.	7.	8.	9.
1		275.35 .6245	93.83 .6097	50.59 .5875	32.58 .5579	23.08 .5211	17.36 .4768	13.60 .4248		560.6 .6277	149.9 .6185	78.96 .6052	50.48 .5876	35.69 .5657	26.85 .5396	21.07 .5093	17.05 .4765	14.12 .4352
2	354.73 .6259	173.91 .6203	76.70 .6040	44.92 .5806	30.03 .5501	21.72 .5123	16.53 .4671	13.06 .4140	376.5 .6262	195.9 .6215	95.15 .6099	59.31 .5965	41.27 .5756	30.66 .5521	23.80 .5247	19.09 .4930	15.68 .4569	13.14 .4162
3	270.93 .6243	138.06 .6171	65.03 .5981	39.79 .5726	27.36 .5402	20.15 .5007	15.54 .4537		282.1 .6245	149.5 .6182	75.45 .6032	48.72 .5848	34.92 .5627	26.57 .5368	21.03 .5069	17.12 .4728	14.24 .4342	
4	222.66 .6227	115.68 .6140	56.41 .5920	35.45 .5638	24.87 .5289	18.59 .4869	14.50 .4374		229.4 .6230	122.71 .6151	63.09 .5967	41.47 .5749	30.21 .5495	23.31 .5204	18.67 .4872	15.37 .4498	12.89 .4080	
5	190.11 .6212	99.92 .6109	49.77 .5857	31.84 .5544	22.65 .5165	17.13 .4715	13.48 .4192		194.6 .6214	104.61 .6119	54.37 .5901	36.12 .5648	26.56 .5358	20.68 .5029	16.70 .4659	13.84 .4267		
6	166.38 .6197	89.09 .6077	44.50 .5793	28.82 .5446	20.72 .5032	15.81 .4548			169.5 .6199	91.41 .6087	47.82 .5834	31.97 .5563	23.67 .5216	18.53 .4845	15.05 .4434			
7	148.22 .6181	79.84 .6045	40.22 .5726	26.27 .5343	19.06 .4893	14.62 .4371			150.5 .6183	81.30 .6054	42.71 .5765	28.69 .5436	21.32 .5066	16.76 .4653	13.66 .4197			
8	133.82 .6165	71.43 .6012	36.68 .5658	24.11 .5237	17.57 .4747	13.56 .4183			135.5 .6167	73.29 .6021	38.59 .5695	25.99 .5325	19.37 .4912	15.27 .4655				
9	122.09 .6149	65.32 .5978	33.70 .5588	22.26 .5128	16.29 .4600				123.4 .6151	66.77 .5988	35.21 .5623	23.75 .5212	17.73 .4755	14.01 .4249				
10	112.36 .6134	60.19 .5946	31.16 .5517	20.65 .5015	15.16 .4439				113.4 .6135	61.35 .5954	32.37 .5551	21.86 .5097	16.34 .4592					
11	104.13 .6117	55.84 .5912	28.97 .5444	19.25 .4900	14.17 .4277				105.0 .6119	56.78 .5920	29.96 .5477	20.26 .4979	15.14 .4426					
12	97.07 .6101	52.08 .5878	27.06 .5370	18.01 .4782	13.28 .4131				97.78 .6103	52.86 .5885	27.88 .5402	18.84 .4859	14.09 .4256					
13	90.96 .6085	48.81 .5844	25.39 .5295	16.92 .4662					91.55 .6087	49.46 .5851	26.08 .5326	13.18 .4082						
14	85.60 .6068	45.94 .5809	23.90 .5219	15.94 .4539					86.10 .6070	46.48 .5816	24.49 .5249	16.53 .4611						
15	80.82 .6052	43.39 .5774	22.58 .5142	15.06 .4413					81.29 .6056	43.85 .5780	23.08 .5171	15.57 .4484						

NO SOLUTIONS IN THIS REGION

NO SOLUTIONS IN THIS REGION

Table X

Possible Nucleus Ranges R_o (microns) for Cutoff Velocities in the Test Interval.
Temperature 80°F (26.67°C), $C_{p_s} = -0.630$

	Air Content 7.5 ppm			Air Content 15 ppm		
V_{co} \ $\vec{n}$	1	5	15	1	5	15
30	5.65	3.63	1.67	4.28	3.20	1.64
40	4.71	2.78	1.64	3.61	2.54	1.16

Table XI

Calculated Cavitation Cutoff Data for Various Temperatures and for a Dissolved Air Content of 7.5 ppm

Temperature °F (°C)	V_{co} fps (m/s)	R_e	K	R_o, microns
75 (23.89)	24.7 (7.53)	4.16×10^5	0.582	9.0
80 (26.67)	33.9 (10.33)	6.07×10^5	0.595	7.0
93 (33.89)	57.2 (17.43)	1.19×10^6	0.610	4.5

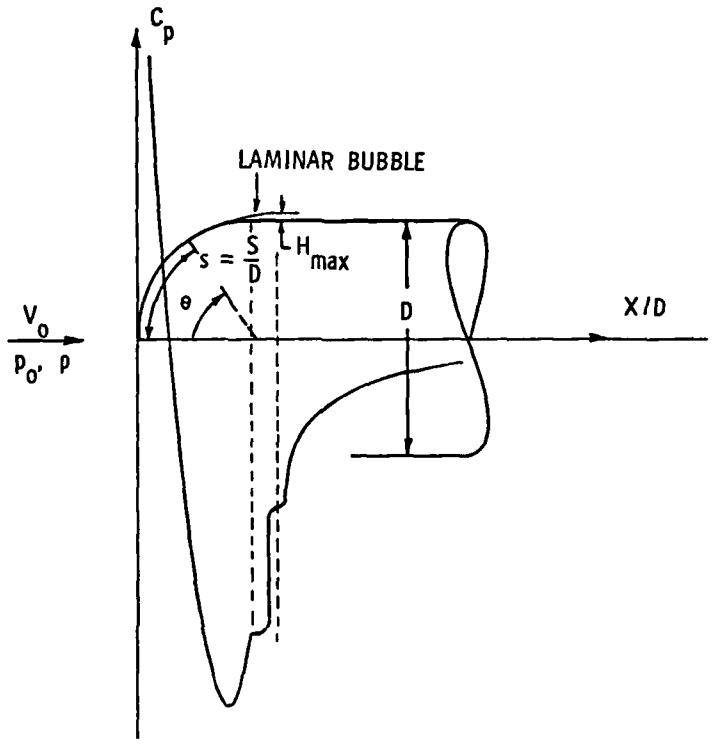

Figure 1. Schematic Diagram of Flow about a Hemispherical Headform when Laminar Separation is Present.

November 19, 1979
BRP:mmj

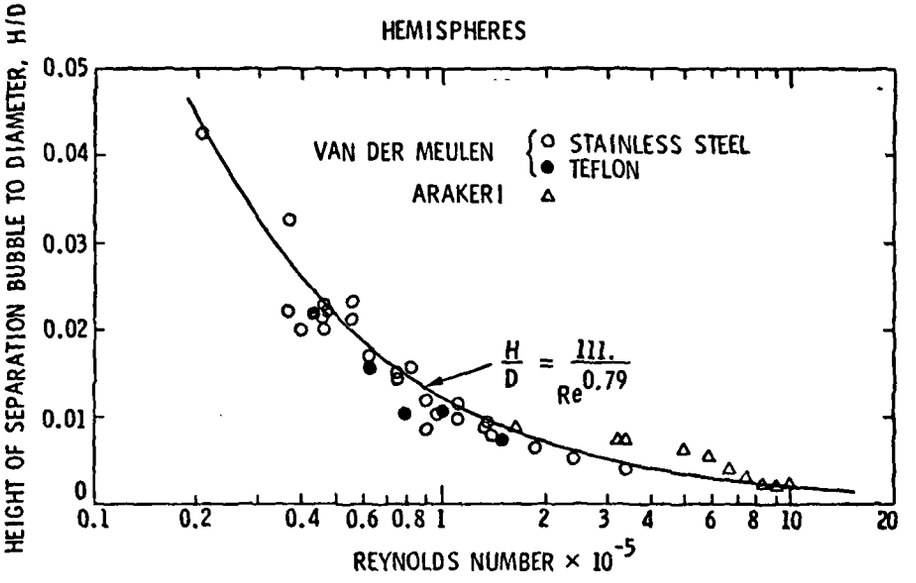

Figure 2. The Ratio of Maximum Height of Laminar Separation Bubble to Headform Diameter, H/D, as a Function of Reynolds Number.

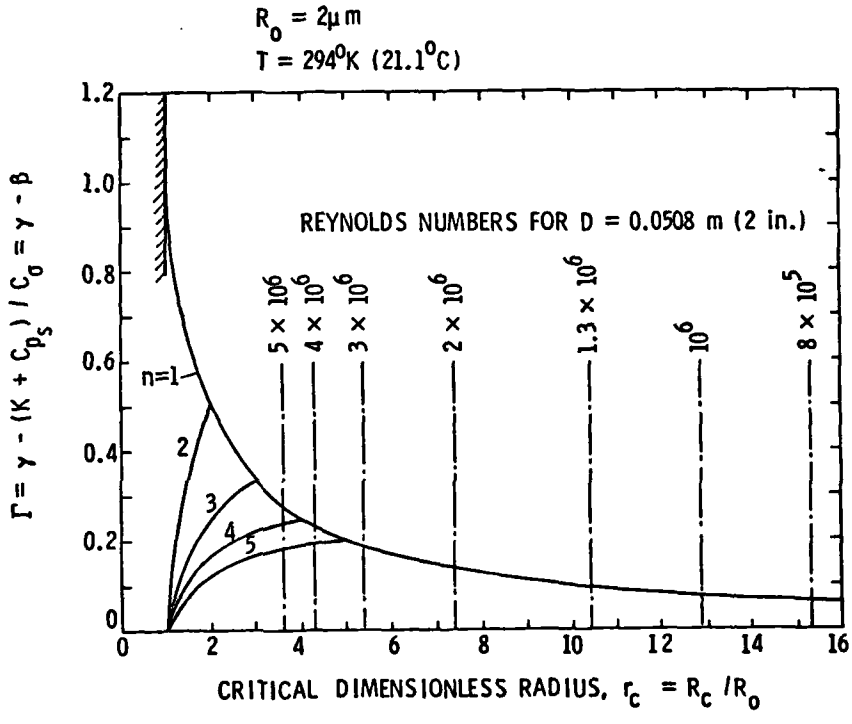

Figure 3. Critical Parameters for Subsequent Gaseous Growth after the Cavitation Bubble is Fixed in the Laminar Separation Bubble.

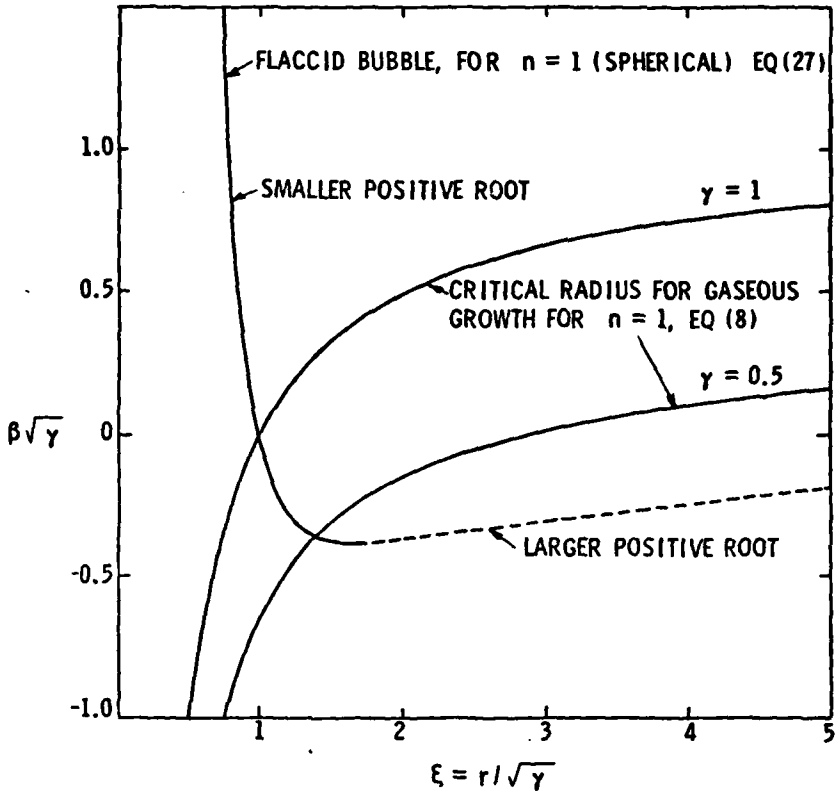

Figure 4. Comparison of Flaccid Bubble and Critical Bubble Radii in the Laminar Separation Zone.

November 19, 1979
BRP:mmj

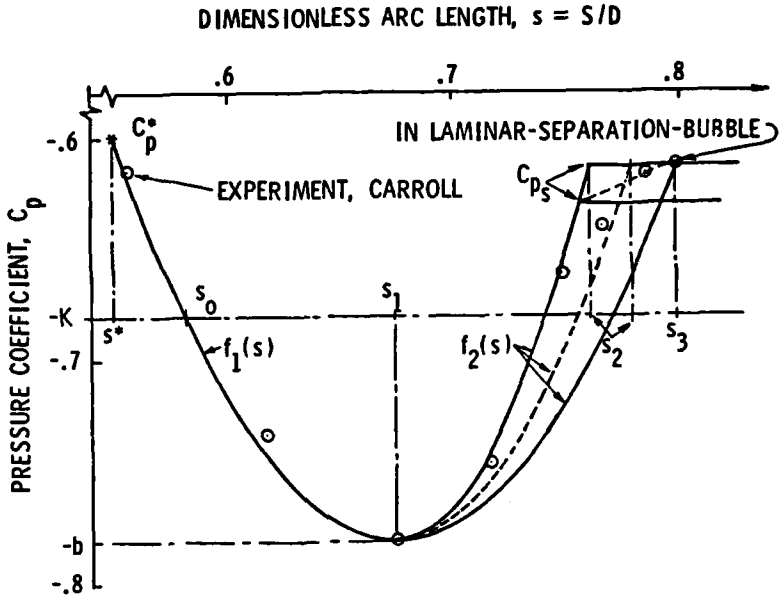

Figure 5. Measured Pressure Coefficients and Parabolic Approximations for a 2-inch Diameter (0.0508 m) Hemispherical Headform.

November 19, 1979
BRP:mmj

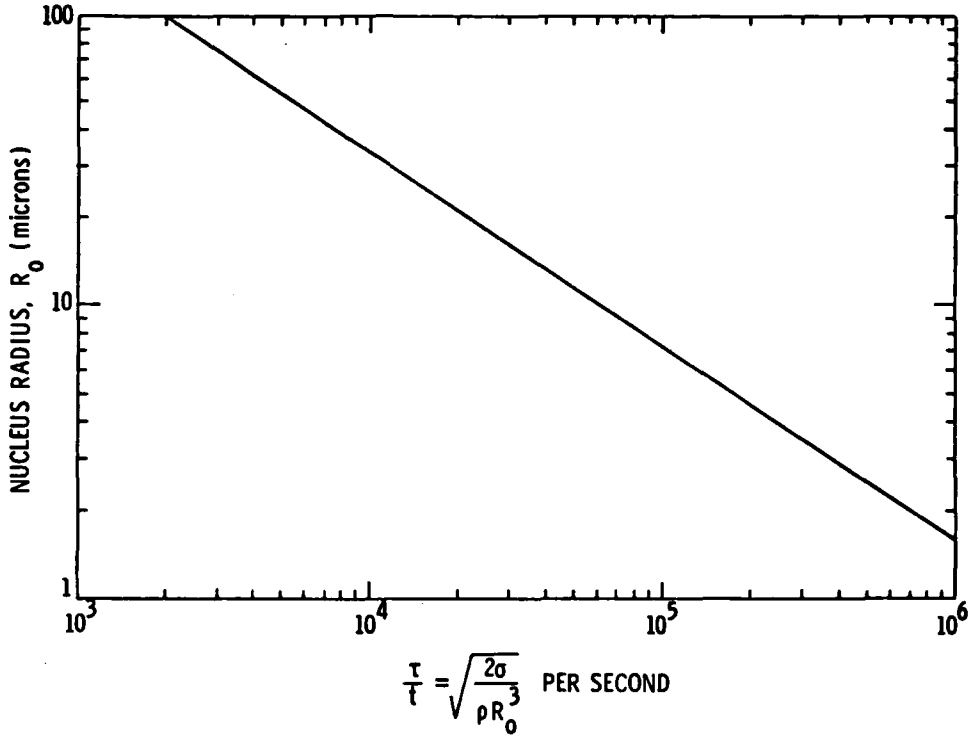

Figure 6. Ratio of Dimensionless "Bubble Time" to Laboratory Time for a Range of Nucleus Sizes.

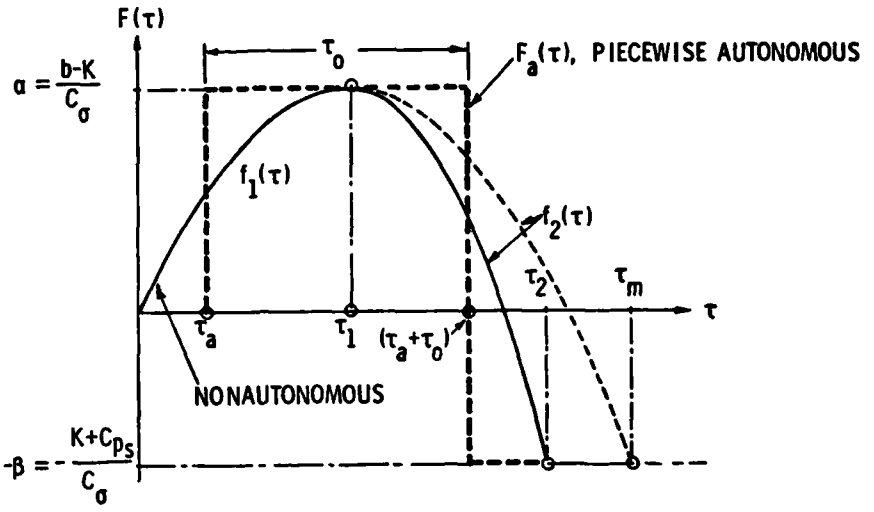

Figure 7, Schematic Diagrams of Pressure Forcing Functions for Nonautonomous and Piecewise-Autonomous Cavitation Bubble Dynamics.

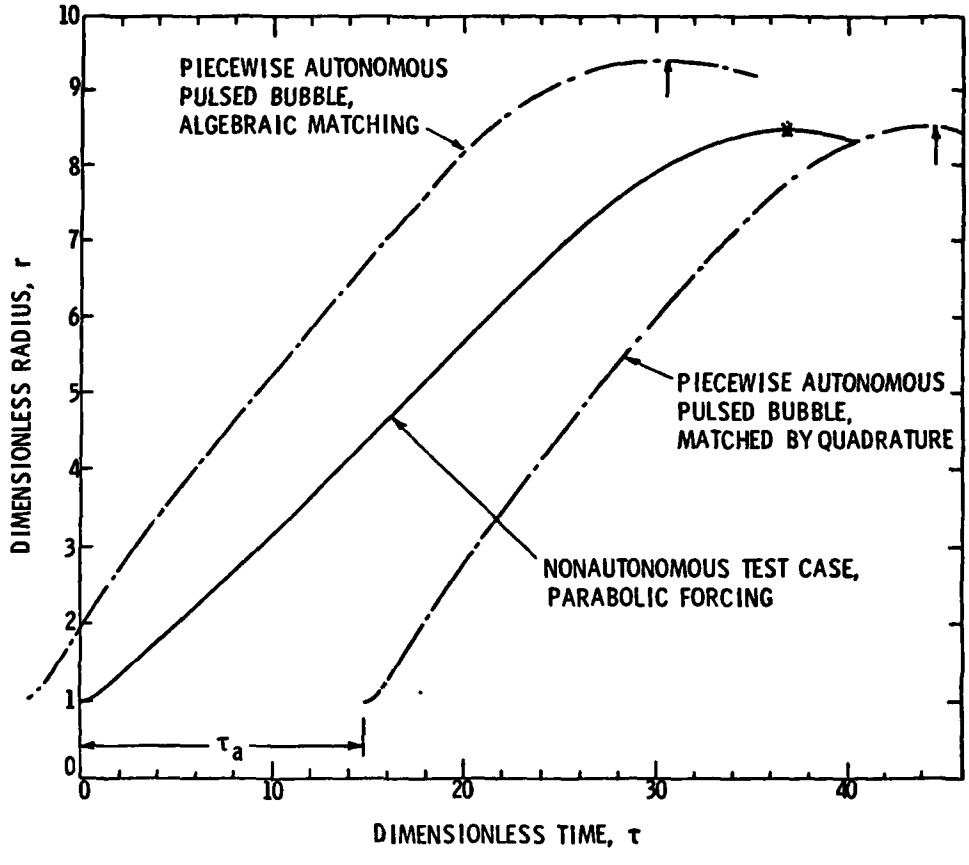

Figure 8. Comparison of Calculated Bubble Growths for Two Matching Procedures and a Nonautonomous Test Case.

November 19, 1979
BRP:mmj

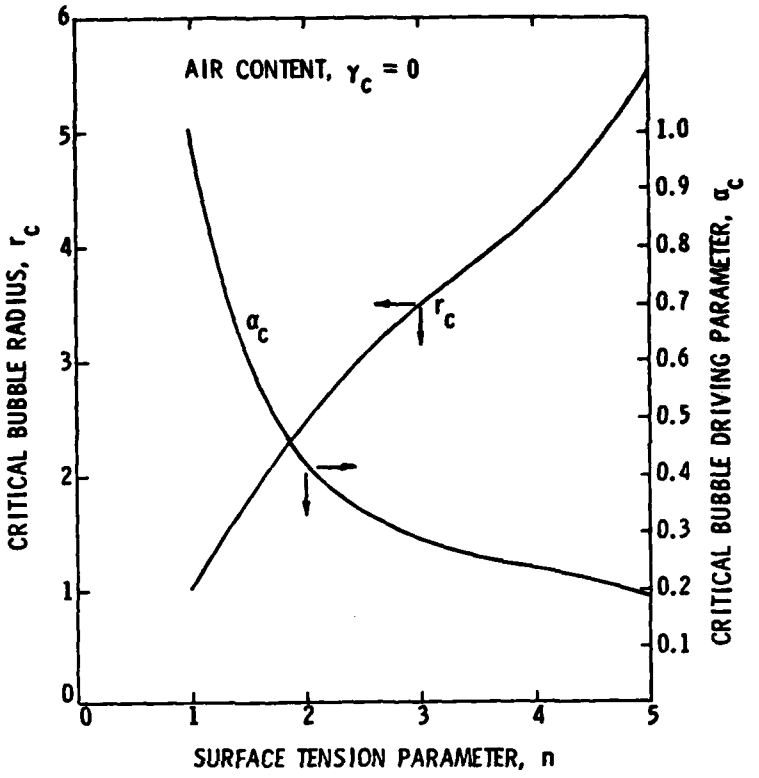

Figure 9. Threshold Values of α for Zero Air Content when a Step-Function of Strength α_c Acts on a Vapor Bubble. Under this Driving Parameter an Infinite Time is Required for the Radius to Grow from its Initial Value, r = 1, to the Size, r_c, for $r_c \geq n$.

November 19, 1979
BRP:mmj

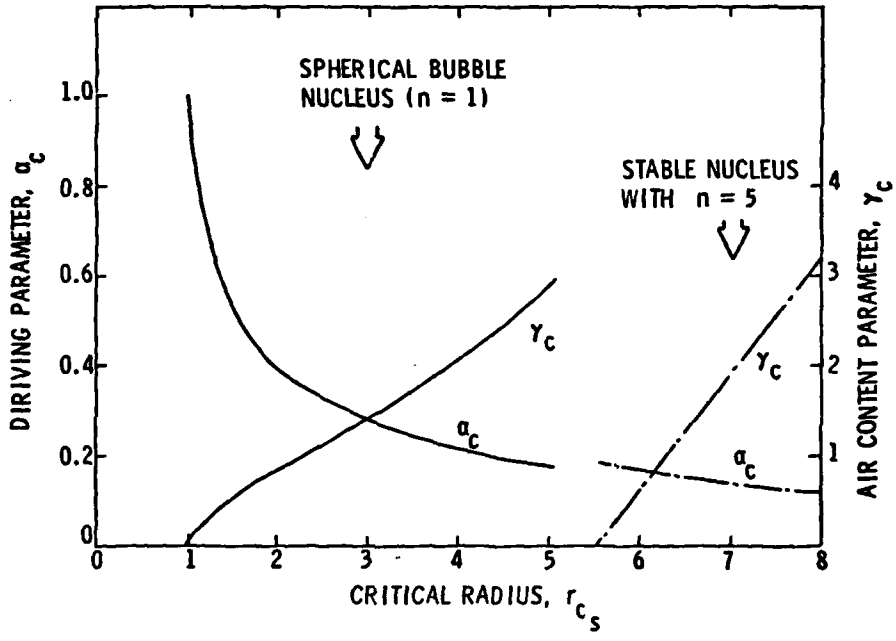

Figure 10. Values of External Driving Parameter α_c and Air Content Parameter γ_c for a Step-Function Input of Strength α_c which will Produce a Bubble Growth in Infinite Time from r = 1 to the r_c values Plotted on the Abcissa.

November 19, 1979
BRP:mmj

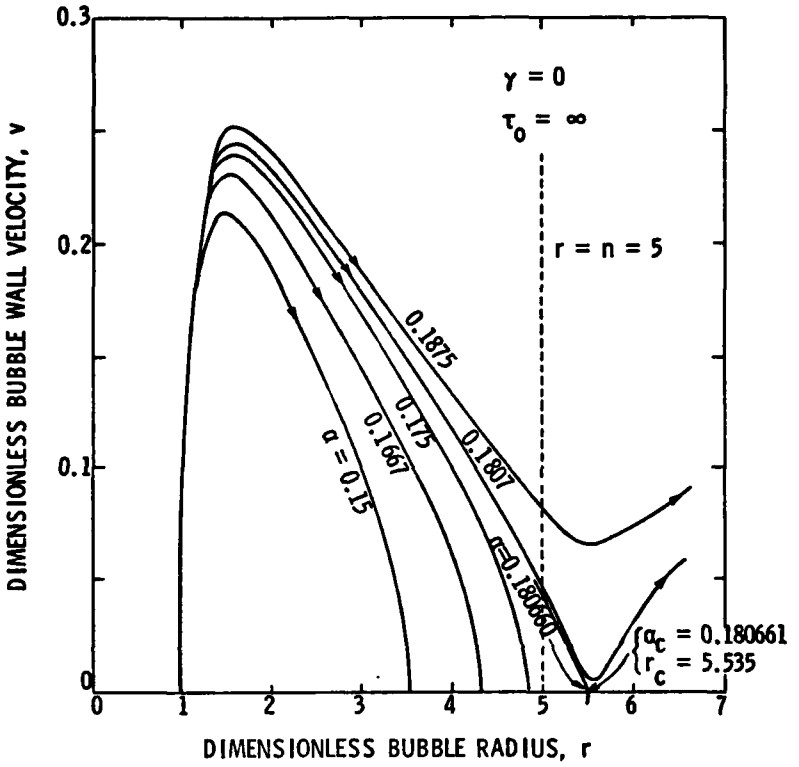

Figure 11. Phase-Plane Trajectories for Several Step-Function Driving Functions of Intensity α. The Values of α are close to the Critical Value α_c and Show that the Separatrix is a Critical Trajectory Passing Through $r = r_c$, $v = 0$.

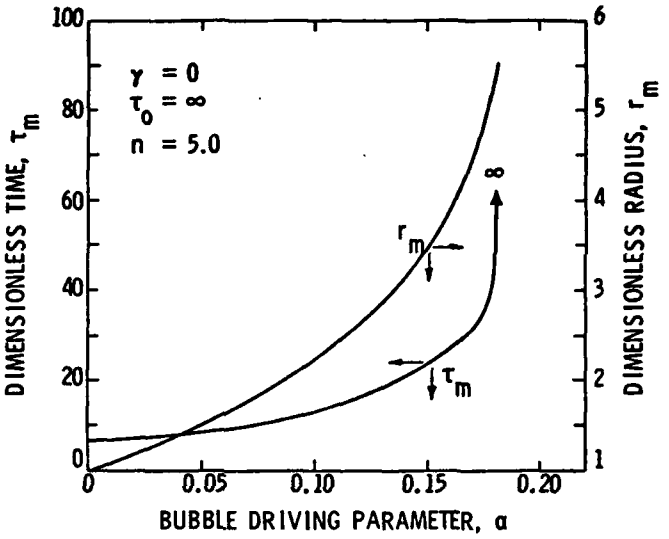

Figure 12. Dimensionless Maximum Radius, r_m, and Half Period τ_m for Step-Function Forcing Functions of Amplitudes α, Critical Radius and Driving Parameter are $r_c = 5.5352$ and $\alpha_c = 0.180661$.

November 19, 1979
BRP:mmj

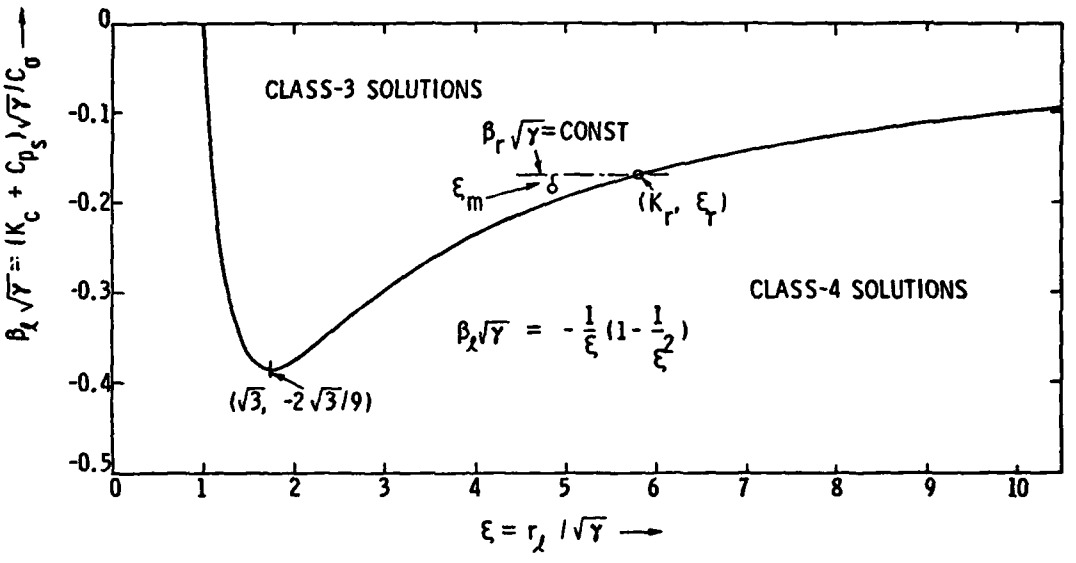

Figure 13. The Critical Curve Separating Class-3 and Class-4 Solutions for Vaporous Cavitation Bubble Growth in the Matched Piecewise-Autonomous Approximation.

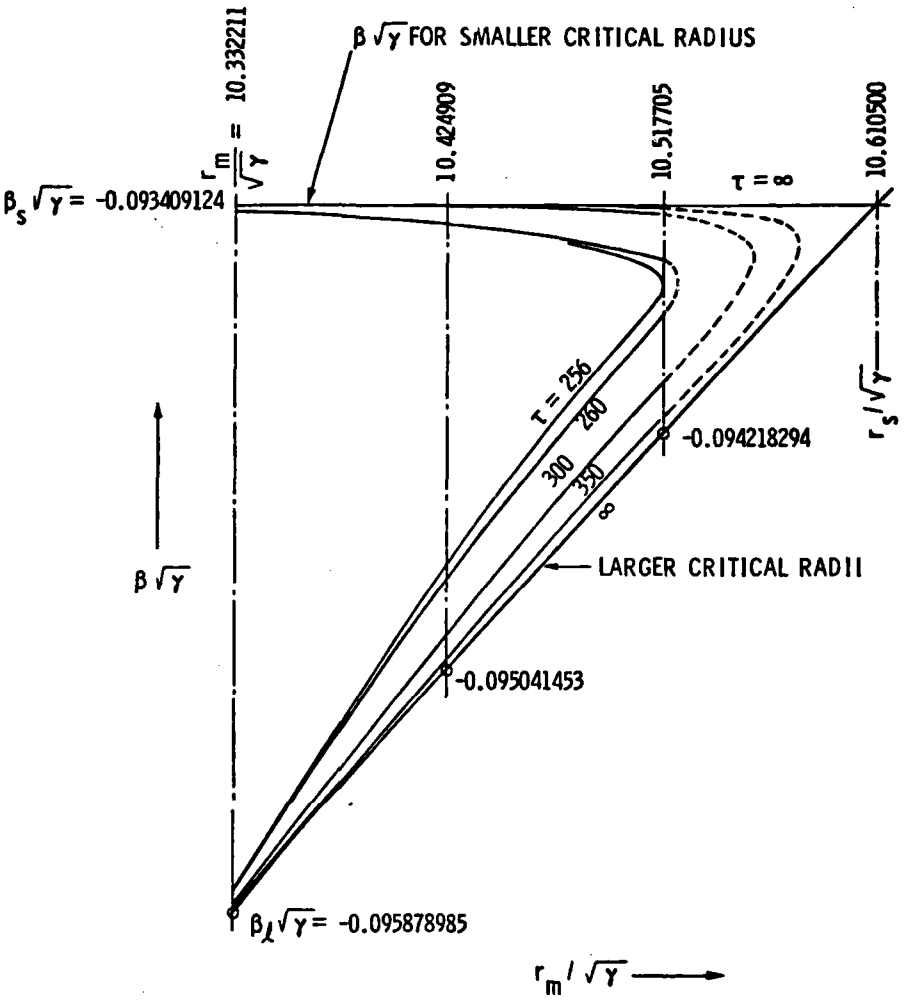

Figure 14. A Contour Plot Showing Level Lines of Dimensionless Bubble Time, τ, in the $\xi,\beta\sqrt{\gamma}$ Plane for a Region Near the Reference Critical Radius, r_r. The Dotted Portions of the Level Lines are Extrapolated Estimates.

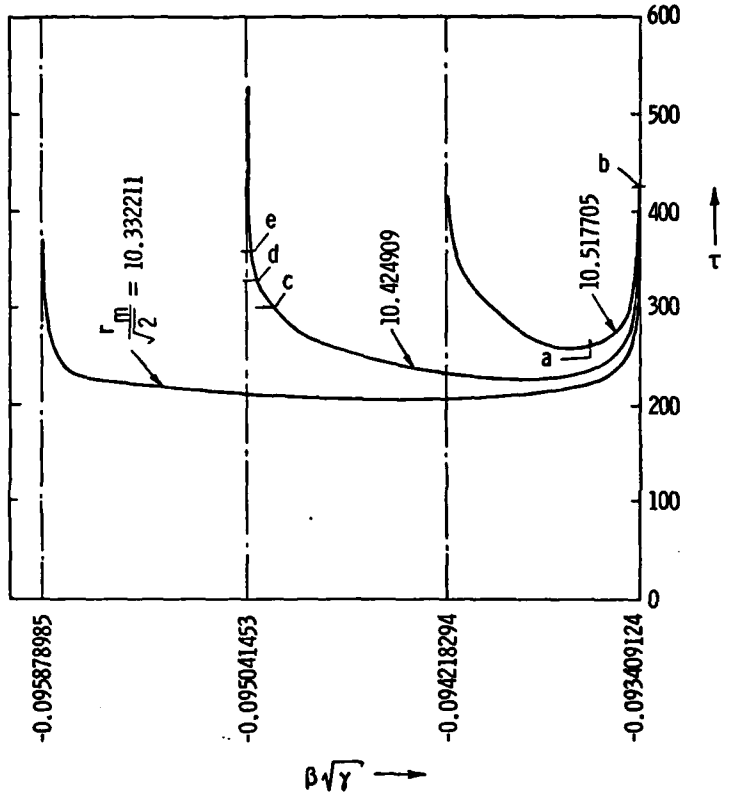

Figure 15. Plots of τ versus $\beta\sqrt{\gamma}$ Showing how Steeply τ Increases as β Approaches either the Larger or the Smaller Critical Value.

K = 0.38849756, TDIST = 1037.4, TM = 9329.9, V_o = 20 fps, 2' DIA HEMISPHERE

—— $\tau_o(\sqrt{1+b} - \sqrt{1+K}) + \tau_g(\sqrt{1-C_{p_s}} - \sqrt{1+K}) = TDIST$

---- $0.156\,\tau_o + 0.092\,\tau_g = 1037.4$

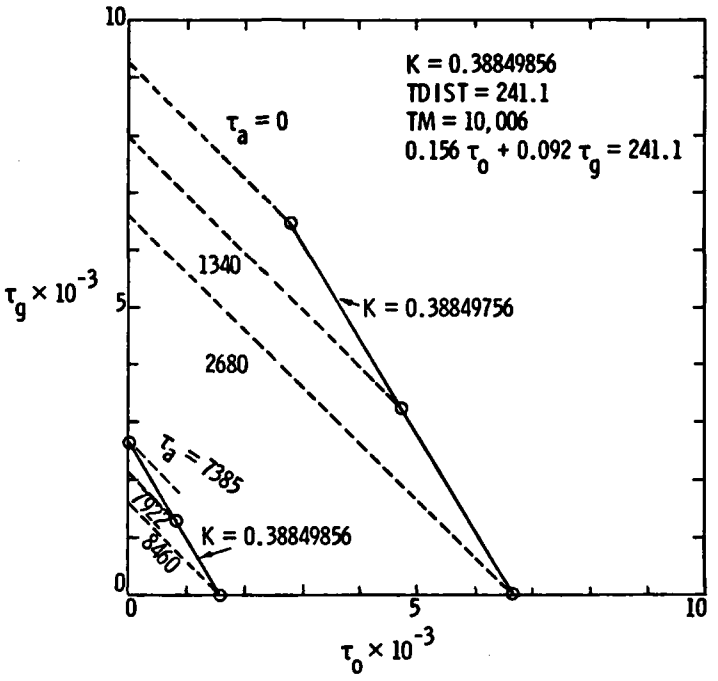

Figure 16. Matched Values of τ_a and τ_o for Two Cavitation Numbers Occur at the Circled Points of Intersection with the Other Parameters as Noted. The Lag Time is Taken as a Free Parameter.

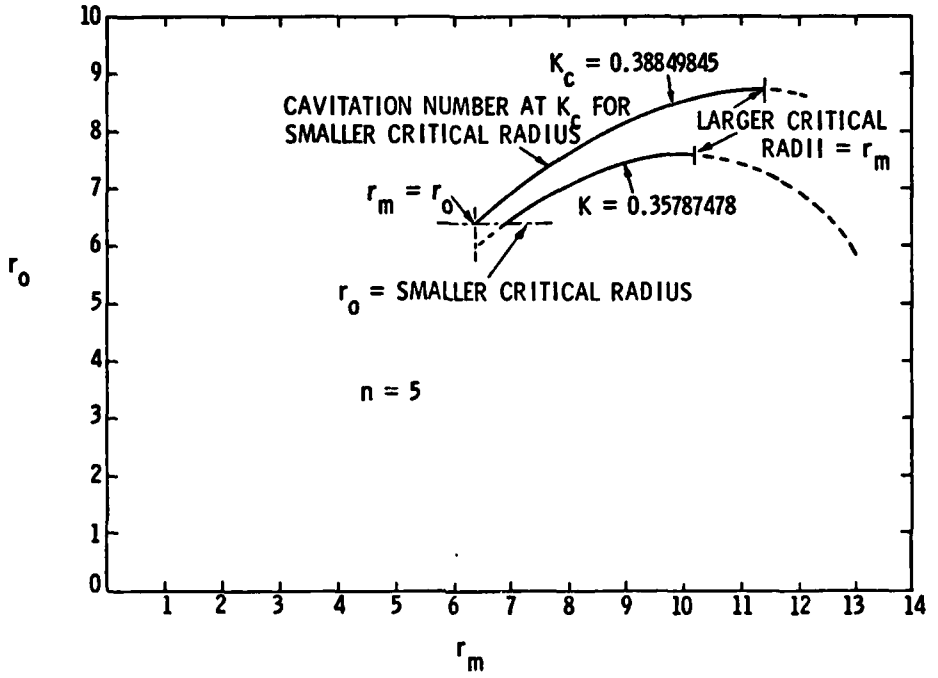

Figure 17. A Further Example, Based Upon Calculations Leading to Figure 14, which Shows the Relationship Between r_o and r_m for Two Cavitation Numbers. Since r_o can not be Less than the Smaller Critical Radius, these Curves Show the Smallest Values of r_m which can be Prescribed for the Cavitation Numbers Specified.

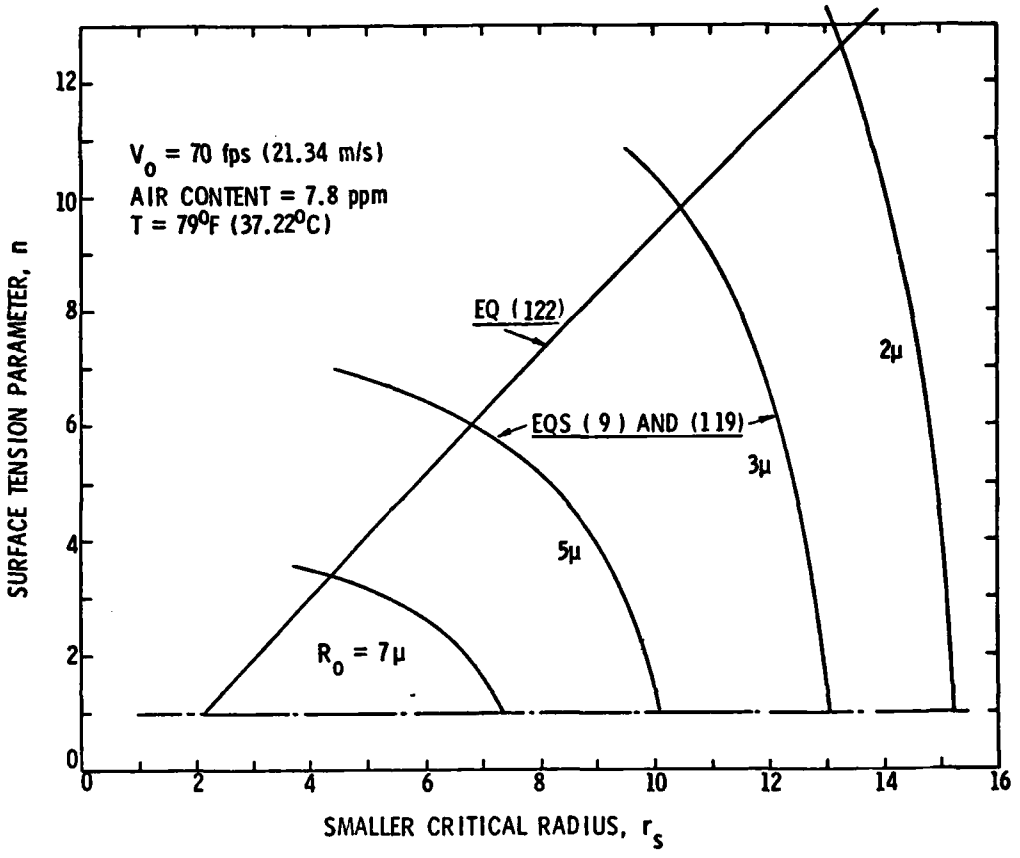

Figure 18. Consistent Values of Smaller Critical Radius and Surface Tension Parameter n at Cavitation Transition are given at the Points of Intersection for each Initial Radius Curve and the Curve of Eq. (122). V_o = 70 fps (21.34 m/s) is not a Transition Speed. C_{p_s} = -0.613.

November 19, 1979
BRP:mmj

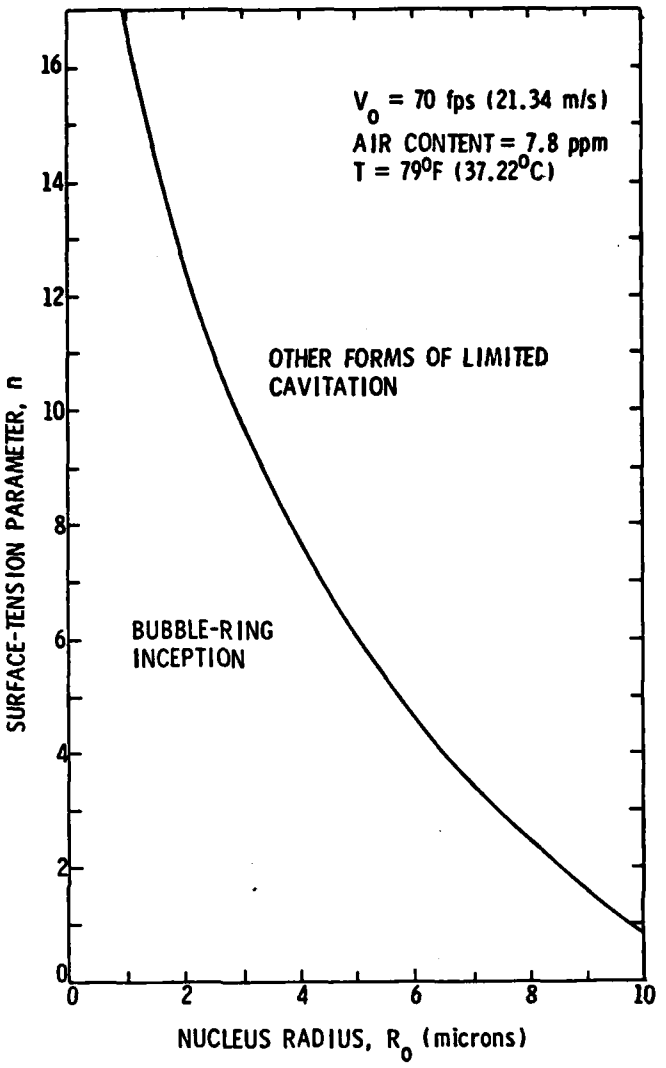

Figure 19. Boundary Between Bubble-Ring Cavitation and Other Forms at a Cavitation Transition State from Figure 18. V_o = 70 fps (21.34 m/s) is not a Transition Velocity. C_{p_s} = -0.613.

November 19, 1979
BRP:mmj

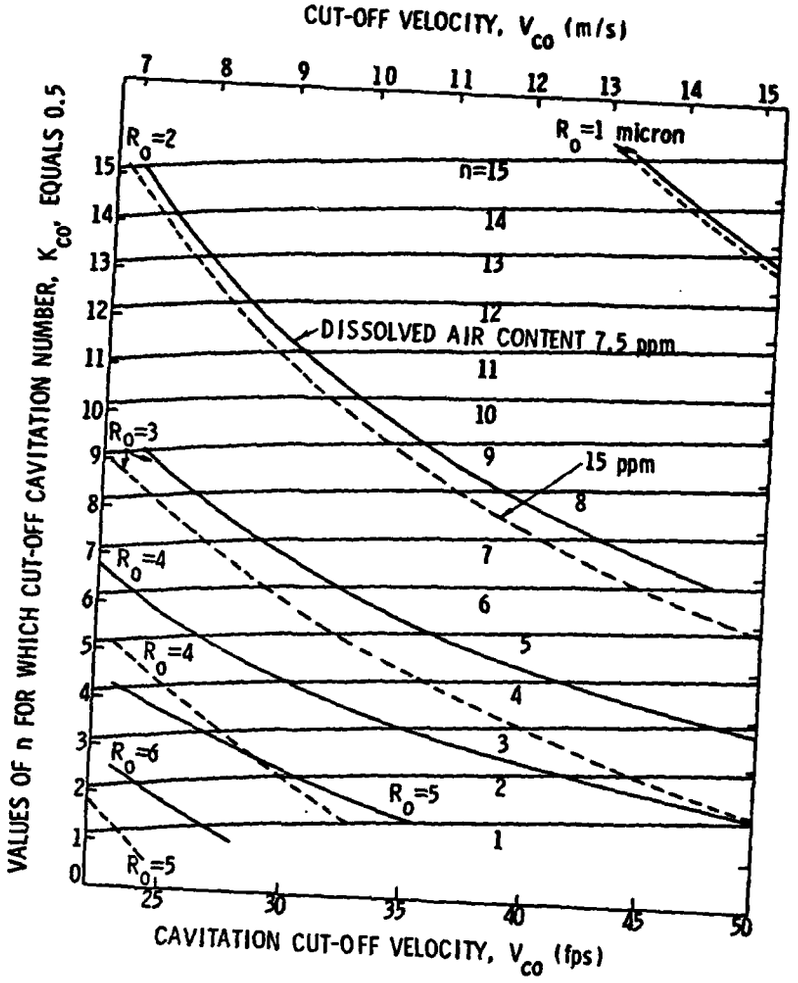

Figure 20, Cavitation Cutoff Data for Ranges in Important Physical Parameter Values, Calculations for $C_{p_s} = -0.630$.

November 19, 1979
BRP:mmj

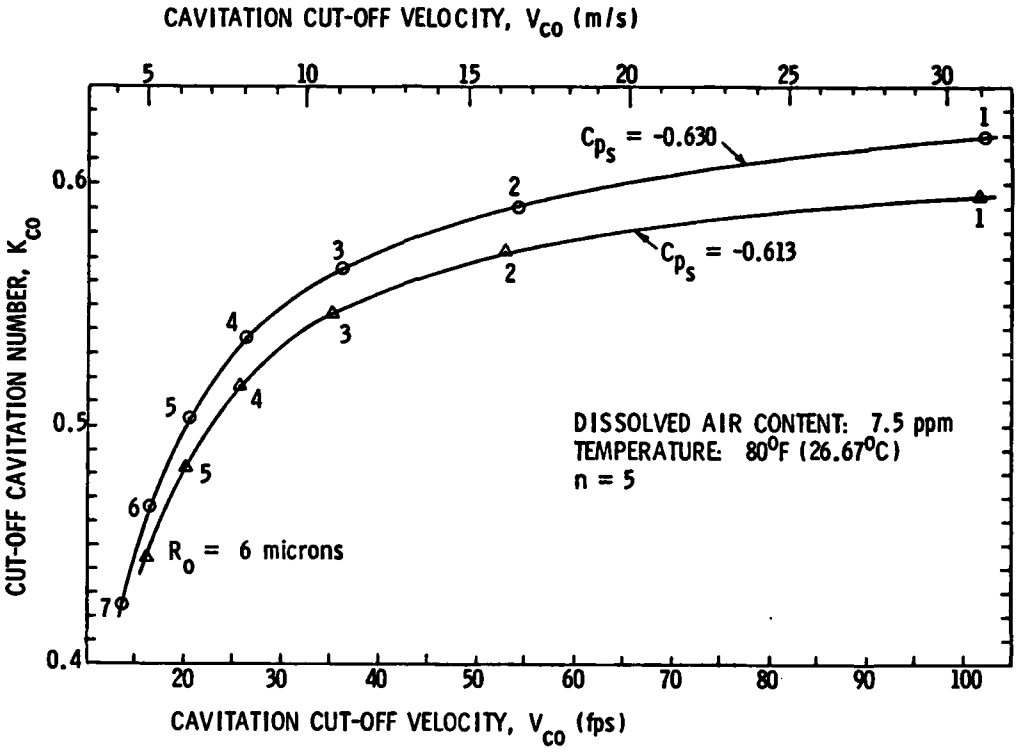

Figure 21. Effect of R_o and Alternative Values of C_{p_s} on Cavitation Cutoff Conditions.

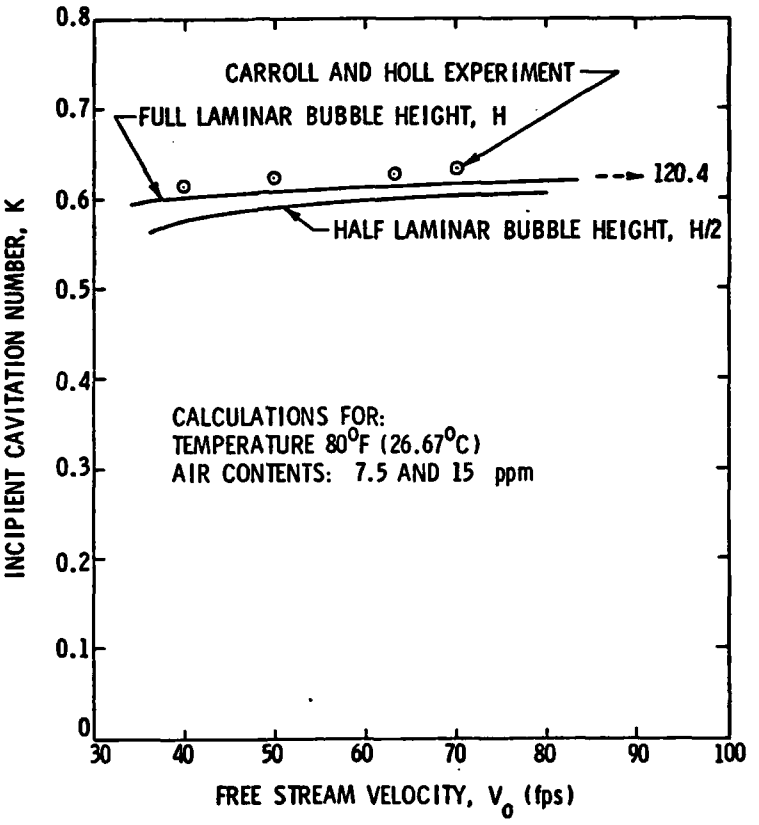

Figure 22. Comparison of Experiment and Theory for Bubble-Ring Cavitation Onset. Calculated Values of K for Maximum Vapor Bubble Radii of One Half Laminar Bubble Height and Equal to Laminar Bubble Height are Shown.

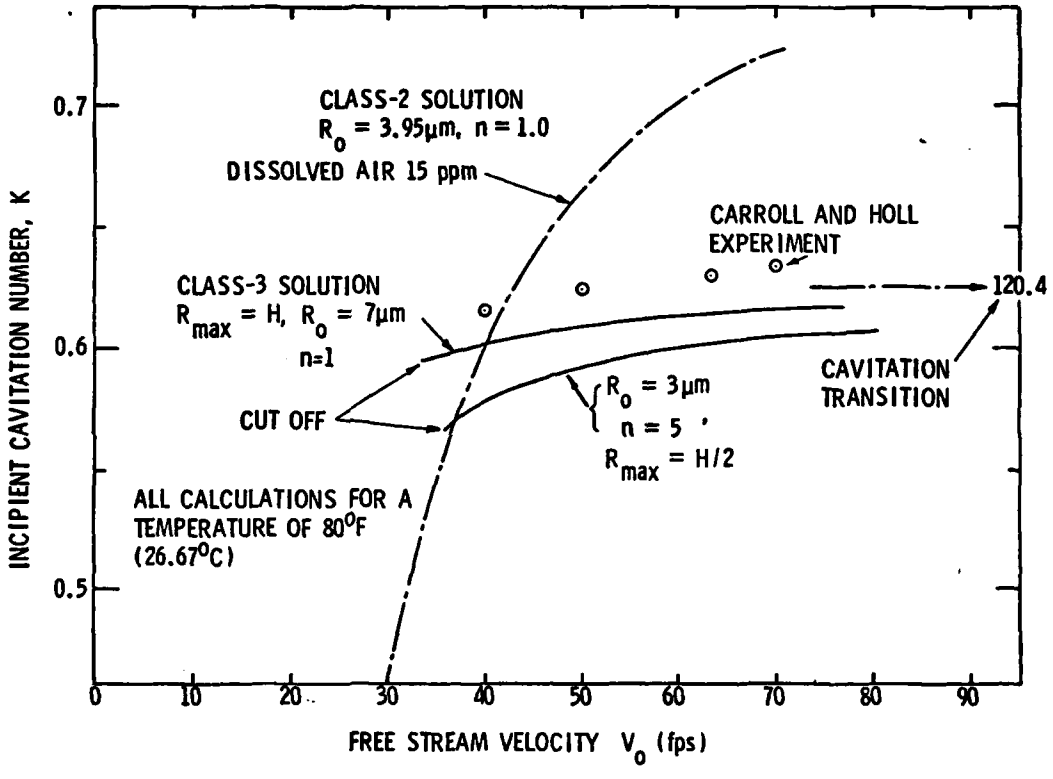

Figure 23. Comparison of Experiment and Theory for Class-2 and Class-3 Solutions for the Onset of Bubble-Ring Cavitation.

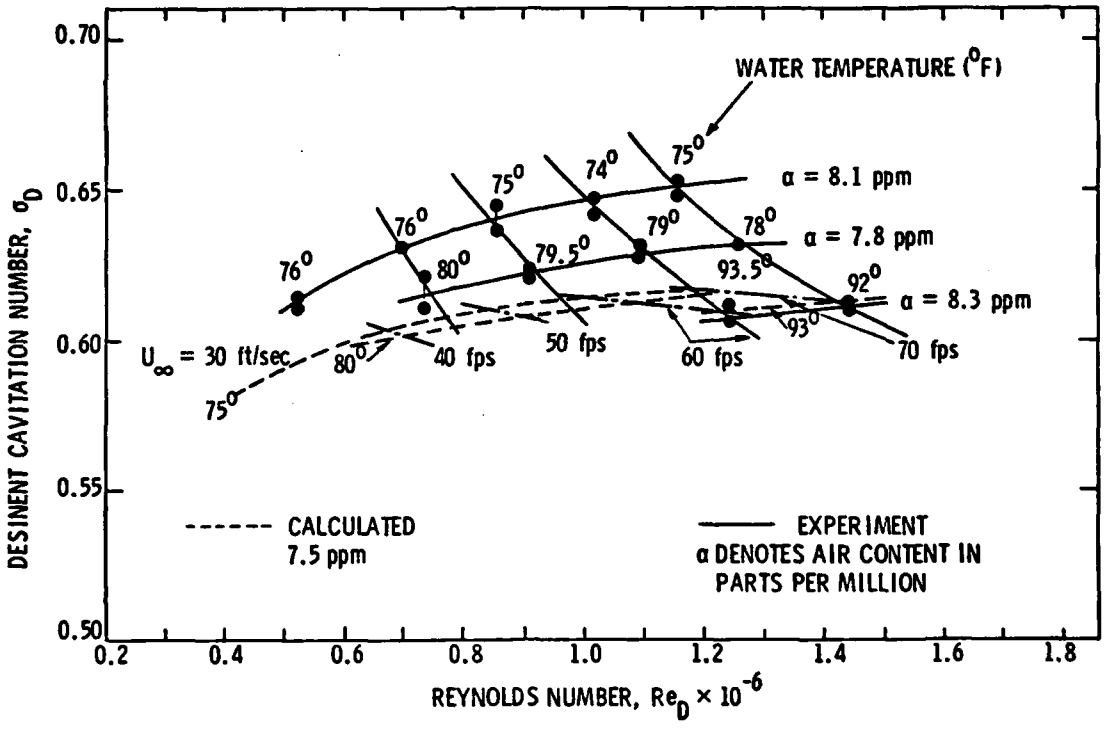

Figure 24. Comparison of Experiments of Holl and Carroll with Asymptotic Calculations for the Temperature Dependence of Bubble-Ring Cavitation Onset.

DISTRIBUTION LIST FOR UNCLASSIFIED TM 79-198 by B. R. Parkin, dated November 19, 1979

Commander
Naval Sea Systems Command
Department of the Navy
Washington, DC 20362
Attn: Library
Code NSEA-09G32
(Copy Nos. 1 and 2)

Naval Sea Systems Command
Attn: J. G. Juergens
Code NSEA-05H
(Copy No. 3)

Naval Sea Systems Command
Attn: T. E. Peirce
Code NSEA-63R3
(Copy Nos. 4 thru 8)

Commanding Officer
Naval Underwater Systems Center
Newport, RI 02840
Attn: Library
Code 54
(Copy No. 9)

Naval Underwater Systems Center
Attn: D. Goodrich
Code 3634
(Copy No. 10)

Naval Underwater Systems Center
Attn: R. H. Nadolink
Code 3634
(Copy No. 11)

Commanding Officer
Naval Ocean Systems Center
San Diego, CA 92152
Attn: D. Nelson
Code 2542
(Copy No. 12)

Naval Ocean Systems Center
Attn: M. M. Rieschman
Code 2542
(Copy No. 13)

Commander
David W. Taylor Naval Ship R&D Center
Department of the Navy
Bethesda, MD 20084
Attn: Library
Code 522
(Copy Nos. 14 and 15)

David W. Taylor Naval Ship R&D Center
Attn: Y. T. Shen
Code 1524
(Copy No. 16)

David W. Taylor Naval Ship R&D Center
Attn: Code 1505
(Copy No. 17)

Commander
Naval Surface Weapon Center
Silver Spring, MD 20910
Attn: J. L. Baldwin
Code WA-42
(Copy No. 18)

Office of Naval Research
Department of the Navy
800 N. Quincy Street
Arlington, VA 22217
Attn: R. D. Cooper
Code 438
(Copy No. 19)

Office of Naval Research
Attn: H. Fitzpatrick
Code 438
(Copy No. 20)

Defense Technical Information Center
5010 Duke Street
Cameron Station
Alexandria, VA 22314
(Copy Nos. 21 thru 32)

National Bureau of Standards
Aerodynamics Section
Washington, DC 20234
Attn: P. S. Klebanoff
(Copy No. 33)

Netherlands Ship Model Basin
Haagsteeg 2, P. O. Box 28
67 AA Wageningen, The Netherlands
Attn: Dr. Jan Van der Meulen
(Copy No. 34)

Netherlands Ship Model Basin
Attn: Dr. Peter van Oossanen
(Copy No. 35)

DISTRIBUTION LIST FOR UNCLASSIFIED TM 79-198 by B. R. Parkin, dated November 19, 1979

Dr. V. H. Arakeri
Department of Mechanical Engineering
Indian Institute of Science
Bangalore 560 012
India
(Copy No. 36)

Dr. Allan J. Acosta
California Institute of Technology
Division of Engineering for
Applied Sciences
Pasadena, CA 91109
(Copy No. 37)

Naval Postgraduate School
The Presidio
Monterey, CA 93940
Attn: Library
(Copy No. 38)

Iowa Institute of Hydraulic Research
The University of Iowa
Iowa City, Iowa 52240
(Copy No. 39)

Dr. Roger E. A. Arndt
St. Anthony Falls Hydraulic Laboratory
University of Minnesota
Mississippi River at 3rd Avenue, S.E.
Minneapolis, MN 55414
(Copy No. 40)

Dr. Y. S. Cha
U. S. Department of Energy
Argonne National Laboratory
9700 South Cass Avenue
Argonne, IL 60439
(Copy No. 41)

The Pennsylvania State University
Applied Research Laboratory
P. O. Box 30
State College, PA 16801
Attn: B. R. Parkin
(Copy No. 42)

Applied Research Laboratory
Attn: J. W. Holl
(Copy No. 43)

Applied Research Laboratory
Attn: M. L. Billet
(Copy No. 44)

Applied Research Laboratory
Attn: Garfield Thomas Water Tunnel Files
(Copy No. 45)


END
DTIC

AD-A082 851 PENNSYLVANIA STATE UNIV UNIVERSITY PARK APPLIED RESE--ETC F/6 20/4
A THEORY FOR CAVITATION INCEPTION IN A FLOW HAVING LAMINAR SEPA--ETC(U)
NOV 79 B R PARKIN N00024-79-C-6043
UNCLASSIFIED ARL/PSU/TM-79-198 NL

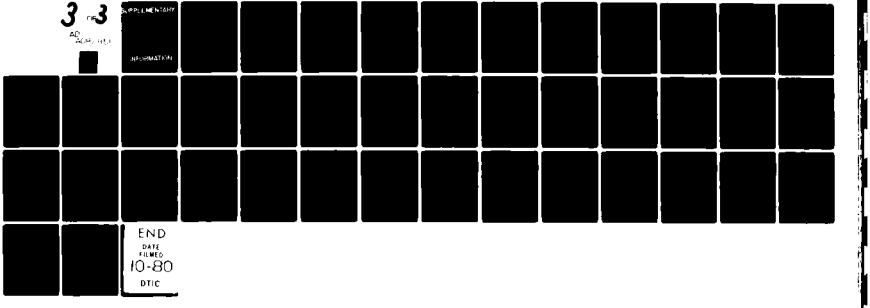


AD
AO

SUPPLEMENTARY

INFORMATION

(12)

THE PENNSYLVANIA STATE UNIVERSITY
INSTITUTE FOR SCIENCE AND ENGINEERING
APPLIED RESEARCH LABORATORY

ADDRESS REPLY TO:
APPLIED RESEARCH LABORATORY
P. O. Box 30
STATE COLLEGE, PENNSYLVANIA 16801

June 24, 1980

To Distribution List

Subject: ARL/PSU Technical Memorandum, Flie No. 79-198, "A Theory for Cavitation Inception in a Flow Having Laminar Separation," by B. R. Parkin, November 19, 1979

Enclosure: Revised pages to subject memorandum.

Dear Sir:

Please insert the enclosed revised pages into your copy(s) of the subject memorandum.

Very truly yours,

Blaine R. Parkin

Blaine R. Parkin
Director
Garfield Thomas Water Tunnel

BRP:mmj

DISTRIBUTION LIST FOR UNCLASSIFIED TM 79-198 by B. R. Parkin, dated November 19, 1979

Commander
Naval Sea Systems Command
Department of the Navy
Washington, DC 20362
Attn: Library
Code NSEA-09G32
(Copy Nos. 1 and 2)

Naval Sea Systems Command
Attn: J. G. Juergens
Code NSEA-05H
(Copy No. 3)

Naval Sea Systems Command
Attn: T. E. Peirce
Code NSEA-63R3
(Copy Nos. 4 thru 8)

Commanding Officer
Naval Underwater Systems Center
Newport, RI 02840
Attn: Library
Code 54
(Copy No. 9)

Naval Underwater Systems Center
Attn: D. Goodrich
Code 3634
(Copy No. 10)

Naval Underwater Systems Center
Attn: R. H. Nadolink
Code 3634
(Copy No. 11)

Commanding Officer
Naval Ocean Systems Center
San Diego, CA 92152
Attn: D. Nelson
Code 2542
(Copy No. 12)

Naval Ocean Systems Center
Attn: M. M. Rieschman
Code 2542
(Copy No. 13)

Commander
David W. Taylor Naval Ship R&D Center
Department of the Navy
Bethesda, MD 20084
Attn: Library
Code 522
(Copy Nos. 14 and 15)

David W. Taylor Naval Ship R&D Center
Attn: Y. T. Shen
Code 1524
(Copy No. 16)

David W. Taylor Naval Ship R&D Center
Attn: Code 1505
(Copy No. 17)

Commander
Naval Surface Weapon Center
Silver Spring, MD 20910
Attn: J. L. Baldwin
Code WA-42
(Copy No. 18)

Office of Naval Research
Department of the Navy
800 N. Quincy Street
Arlington, VA 22217
Attn: R. D. Cooper
Code 438
(Copy No. 19)

Office of Naval Research
Attn: H. Fitzpatrick
Code 438
(Copy No. 20)

Defense Technical Information Center
5010 Duke Street
Cameron Station
Alexandria, VA 22314
(Copy Nos. 21 thru 32)

National Bureau of Standards
Aerodynamics Section
Washington, DC 20234
Attn: P. S. Klebanoff
(Copy No. 33)

Netherlands Ship Model Basin
Haagsteeg 2, P. O. Box 28
67 AA Wageningen, The Netherlands
Attn: Dr. Jan Van der Meulen
(Copy No. 34)

Netherlands Ship Model Basin
Attn: Dr. Peter van Oossanen
(Copy No. 35)

DISTRIBUTION LIST FOR UNCLASSIFIED TM 79-198 by B. R. Parkin, dated November 19, 1979

Dr. V. H. Arakeri
Department of Mechanical Engineering
Indian Institute of Science
Bangalore 560 012
India
(Copy No. 36)

Dr. Allan J. Acosta
California Institute of Technology
Division of Engineering for
Applied Sciences
Pasadena, CA 91109
(Copy No. 37)

Naval Postgraduate School
The Presidio
Monterey, CA 93940
Attn: Library
(Copy No. 38)

Iowa Institute of Hydraulic Research
The University of Iowa
Iowa City, Iowa 52240
(Copy No. 39)

Dr. Roger E. A. Arndt
St. Anthony Falls Hydraulic Laboratory
University of Minnesota
Mississippi River at 3rd Avenue, S.E.
Minneapolis, MN 55414
(Copy No. 40)

Dr. Y. S. Cha
U. S. Department of Energy
Argonne National Laboratory
9700 South Cass Avenue
Argonne, IL 60439
(Copy No. 41)

The Pennsylvania State University
Applied Research Laboratory
P. O. Box 30
State College, PA 16801
Attn: B. R. Parkin
(Copy No. 42)

Applied Research Laboratory
Attn: J. W. Holl
(Copy No. 43)

Applied Research Laboratory
Attn: M. L. Billet
(Copy No. 44)

Applied Research Laboratory
Attn: Garfield Thomas Water Tunnel Files
(Copy No. 45)

Nomenclature - Continued

r	dimensionless radius $= R/R_o$
r_b	denotes the limiting value of r_m as limited by the height of the laminar separation bubble
r_c	critical dimensionless bubble radius
r_e	equilibrium dimensionless radius
r_m	maximum dimensionless bubble radius
r_{m_b}	maximum dimensionless radius as limited by height of laminar separation bubble $= r_b$
r_{max}	maximum dimensionless radius $= r_m$
r_o	value of dimensionless radius when $\tau = \tau_o$
r_ℓ	larger critical dimensionless radius
$r(\tau)$	dimensionless radius as a function of bubble time, τ
r_{vm}	the radius of minimum velocity very near the smaller critical radius
r_s	smaller critical dimensionless radius
R	bubble radius
R_e	equilibrium bubble radius
Re	Reynolds number based on body diameter
R_m	maximum bubble radius
R_o	"radius" of typical nucleus
$R(t)$	bubble radius is time dependent
s	dimensionless arc length along the body surface $= S/D$
s_0, s_1, s_2, s_3	particular points on the body
s^*	dimensionless arc length at a point upstream of the minimum pressure point
S	arc length along surface of head form

Nomenclature - Continued

$S(n,\sigma)$ value of surface tension law when $r = n$ then $S = \sigma$

$S(r,\sigma)$ surface tension law

t laboratory or "real" time

t_m time available for vaporous growth

T temperature

v dimensionless bubble-wall velocity

v_o dimensionless bubble-wall velocity when $\tau = \tau_o$

$v(r_o)$ dimensionless bubble-wall velocity when $r = r_o$

$v(\tau)$ dimensionless bubble-wall velocity as a function of dimensionless time

V_{co} cutoff velocity

V_o free-stream velocity

α driving parameter, $\alpha = \dfrac{b - K}{C_\sigma}$

α_c critical value of α corresponding to $r = r_c$

α_s value of the bubble driving parameter at the smaller critical radius r_s as defined by Eq. (88a) in which case $r_s = r_c$

β dimensionless parameter characterising static pressure in laminar separation zone,

$$\beta = \frac{K + C_{p_s}}{C_\sigma}$$

β_e value of β when $r = r_e$

β_c value of β when $r = r_c$

γ dimensionless air content parameter, $\gamma = p_a/(2\sigma/R_o)$

γ_c critical value of γ corresponding to $r = r_c$

Γ $\gamma - \beta$

Equations (22) and (23) can be combined to give

$$p_a R_o^3 = (p_s - p_v + \frac{2S}{R}) R^3 \quad . \tag{24}$$

Upon introducing the dimensionless quantities r, β, and γ from Eqs. (5), (6), and (7), we find

$$\frac{\gamma}{r^3} = \beta + \frac{S(r,\sigma)}{r} \quad . \tag{25}$$

Thus, the new radius is given by

$$\left.\begin{aligned} r^3 - \frac{r^2}{1 + (n-1)\beta} - \frac{(n-1)\gamma}{1 + (n-1)\beta} = 0 \quad , \quad r < n \quad , \\ r^3 + \frac{1}{\beta} r^2 - \frac{\gamma}{\beta} = 0 \quad , \quad r \geq n \quad . \end{aligned}\right\} \tag{26}$$

The equilibrium radius, r_e, is found from these cubics as the smaller real root for which $r_e \geq 1$. If this radius is less than r_m from Eq. (8) when $r_m \geq n$, the bubble will dissolve. Otherwise, subsequent diffusive growth is possible. In order to investigate the conditions leading to diffusive growth when $r_e \geq n$, let us rewrite the second of Eqs. (26) as

$$\beta \sqrt{\gamma} = \frac{\sqrt{\gamma}}{r_e} \left[\left(\frac{\sqrt{\gamma}}{r_e} \right)^2 - 1 \right] \quad , \quad n \leq r_e < r_b \quad , \tag{27}$$

where r_b denotes the limiting value of r_m given by Eq. (9). In terms of the variables $\beta\sqrt{\gamma}$ and $(r_e/\sqrt{\gamma})$, Eq. (27) defines a single curve. When this equation is satisfied, since r_e and γ are positive and $\gamma < r_e^2$ in

most instances, we see that this flaccid bubble result can give negative values of β although $\beta \geq 0$ if $r_e^2 \leq \gamma$. This result contrasts with the form of Eq. (8) for $r_m \geq n$; namely,

$$\beta = \gamma - \frac{1}{r_m} \quad . \tag{8}$$

As long as $\gamma - \beta > 0$ in Eq. (8), r_m will be positive and β can have positive or negative values. Moreover, β will be positive as long as $r_m^2 > 1/\gamma$. But the flaccid bubble equation (27) can be rewritten as

$$\beta + \frac{1}{r_e} = \frac{\gamma}{r_e^3} \quad ,$$

and from (8), if we replace r_m with r_e, we have

$$\beta + \frac{1}{r_c} = \gamma \quad .$$

In a particular flow these equations will apply for identical values of R_o, V_o, γ, and so forth. But the values of β will be different in these two cases. Designate them by β_e and β_c, respectively. We have argued above that the cavitation number K_c, corresponding to r_c, will be associated with a previous history of vaporous bubble growth even though Eq. (8) defines r_c as the critical radius with respect to air diffusion. Of course, r_c may not be the same as the maximum radius r_m actually achieved after vaporous growth. The equilibrium radius r_e for the flaccid bubble is not associated with vaporous growth and the cavitation number K_e will be greater than K_c. Therefore, $\beta_e > \beta_c$ as can be seen from the definition Eq. (7).

In order to investigate the implications of this state of affairs, Figure 4 presents a plot of $\beta\sqrt{\gamma}$ versus $\xi = r\sqrt{\gamma}$ of Eqs. (8) and (27). As noted above, the equilibrium condition for a spherical flaccid bubble, Eq. (27) with n = 1, is represented by a single curve in this plot. Equation (8), also for n = 1, appears as a one-parameter family of curves which depends upon $\gamma^{3/2}$. For negative values of β_e we expect the root of interest for the flaccid bubble to be along the dashed part of the curve in Figure 4 corresponding to $r_e > 1$. Nonetheless, we will consider radii on either side of r = 1. Figure 4 shows two members of the family of critical curves intersecting the equilibrium curve.

If we select an air content γ, we can draw a vertical line at a prescribed value of ξ to the right of the intersection of the equilibrium curve and the prescribed critical curve. In this case the vertical will cut the critical curve at $\beta_c\sqrt{\gamma}$ and it cuts the equilibrium curve at $\beta_e\sqrt{\gamma}$ with $\beta_c > \beta_e$ in contradiction with the inequality noted above. The physical implication of this finding is that since $K_e < K_c$ and we have associated K_c with vaporous growth, it is not possible for a flaccid bubble to survive a passage through the low pressure region upstream of the separation zone on the head form without vaporous growth. Thus, we see that if $r_c = r_e$ and corresponding to the class of larger radii, this value lies to the right of the intersection. Then a flaccid bubble cannot reach the laminar separation zone and experience subsequent gaseous growth. On the other hand, suppose we imagine a horizontal line drawn through the point $(\xi_e, \beta_e\sqrt{\gamma})$ defined by the intersection of the vertical line with the equilibrium curve as noted above. This horizontal will cut the critical curve at a point at which $r_c < r_e$ and gaseous growth of

a flaccid bubble would certainly be possible except for the fact that in this case when $\beta_e = \beta_c$ the cavitation number is less than the onset cavitation number and the flaccid bubble would experience vaporous growth. If we consider a horizontal line through the point $(\xi_c, \beta_c\sqrt{\gamma})$ defined by the intersection of the vertical line above with the critical curve, we find that this upper horizontal cuts the equilibirum curve at a value of ξ_e such that $r_e < r_c$. In this case a flaccid bubble would dissolve even if it could reach the laminar bubble without first experiencing vaporous growth. Evidently, if the vertical reference line is to the right of the intersection, it is generally true that a flaccid bubble can not settle in the separation bubble, experience subsequent gaseous growth, and thereby cause the onset of cavitation.

Turning next to a reference line to the left of the intersection, we see that this line will cut the equilibrium and critical curves at points corresponding to $K_e > K_c$ and since K_c corresponds to cavitation onset, cavitation will not occur at K_e even though the flaccid bubble might experience gaseous growth in the laminar separation zone. A lower horizontal line through the intersection of this new reference vertical with the critical curve leads to two possible values for the flaccid bubble which have $r_e > r_c$ and gaseous growth is possible. But once again such a flaccid bubble would be interrupted in its passage to the laminar separation zone by vaporous growth. Along the upper horizontal we find $r_e < r_c$ and the flaccid bubble will dissolve.

We conclude therefore that flaccid bubbles which drift into the laminar bubble will not lead to incipient (or desinent) cavitation. Either they will dissolve or they will experience vaporous growth before reaching the laminar separation zone.

Matching Conditions:

The way in which the forcing function, Eq. (49), of the piecewise-autonomous system is used to match the parabolic approximation for the forcing function of the nonautonomous system of Eqs. (42) and (44) is illustrated in Figure 7. The quantities τ_a and τ_o remain to be determined by the matching procedure. One condition which is required for matching is that a bubble will move downstream in the boundary layer from the point s_0, where the static pressure on the body first falls to vapor pressure and $\tau = 0$, to the point s_3, where it is stabilized in the boundary layer, within the time interval, τ_m as given by Eq. (39). The distance along the arc of the body which is traversed by the nucleus during this time is $s_3 - s_0$. In terms of the piecewise autonomous approximation, this distance is the sum of three subintervals,

$$(s_3 - s_0)\sqrt{\frac{2\sigma}{\rho R_o^3}} = (\tau_a V_o\sqrt{1 + K})/2 + (\tau_o V_o \sqrt{1+ K + \alpha C_\sigma})/2$$

$$+ [(\tau_m - \tau_o - \tau_a) V_o \sqrt{1 + K - \beta C_\sigma}]/2 \quad .$$

Therefore we can solve for τ_m and introduce the values of αC_σ and βC_σ from the definitions of β, Eq. (7), and α, Eq. (46), in order to write

$$\tau_m = \frac{2(s_3 - s_0)}{V_o\sqrt{1 - C_{p_s}}}\sqrt{\frac{2\sigma}{\rho R_o^3}} - \tau_a\left(\sqrt{\frac{1 + K}{1 - C_{p_s}}} - 1\right) - \tau_o\left(\sqrt{\frac{1 + b}{1 - C_{p_s}}} - 1\right) \quad . \tag{50}$$

As we have noted, the value of τ_m is given by Eq. (39) so that the matching condition (50) contains only two unknows, τ_a and τ_o.

In following sections the value of radius, r_o, when $\tau = \tau_a + \tau_o$ will be needed. Strictly, this value should be obtained from the integration of the equation of motion in the interval, $\tau_a \leq \tau \leq \tau_a + \tau_o$, with $F_a = \alpha$ as indicated by Eq. (49) and with $r(\tau_a) = 1$, $v(\tau_a) = 0$. However, as we have noted, τ_m is prescribed. Moreover, $r_m = r(\tau_m)$ is also specified and r_m is a maximum radius so that $v(\tau_m) = 0$. Therefore, a simple approximation for the solution in the interval $\tau_a \leq \tau \leq \tau_m$ could be given by the parabola,

$$r = 1 + (r_m - 1) \frac{\tau - \tau_a}{\tau_m - \tau_a} \left(2 - \frac{\tau - \tau_a}{\tau_m - \tau_a} \right) \quad . \tag{51}$$

Evidently Eq. 51 does satisfy the conditions that $r(\tau_a) = 1$ and that $r(\tau_m) = r_m$. Moreover,

$$\frac{dr}{d\tau} = \frac{2(r_m - 1)}{\tau_m - \tau_a} \left[1 - \frac{\tau - \tau_a}{\tau_m - \tau_a} \right] \quad . \tag{52}$$

Equation (52) shows that $v(\tau_m) = 0$ as anticipated, but that $v(\tau_a) \neq 0$. In view of the approximations already noted with respect to the piecewise autonomous representation, the violation of the initial condition that $v(\tau_a) = 0$ can be accepted. The appropriate inversion of Eq. (51), after we put $r = r_o$ and $\tau = \tau_a + \tau_o$, is

$$\tau_o + \tau_a \left[1 - \sqrt{\frac{r_m - r_o}{r_m - 1}} \right] = \tau_m \left[1 - \sqrt{\frac{r_m - r_o}{r_m - 1}} \right] \quad . \tag{53}$$

Equations (51) and (53) contain three unknows: τ_a, τ_o, and r_o.

Continuing with the matching, we employ the dynamical Equations (42), (43), and (45). We see that if we write $v = dr/d\tau$, then the differential operator on the left-hand side of Eq. (42) can be written as

$$r \frac{dv}{d\tau} + \frac{3}{2} v^2 = \frac{1}{2r^2} \frac{d}{dr}(r^3 v^2) \quad . \tag{54}$$

Then we can write the first integral of Eq. (42) in terms of indefinite integrals as

$$r^3 v^2 = 2 \int r^2 F(\tau) \frac{dr}{d\tau} d\tau + 2 \gamma \ln r - 2 \int r S(r,n) dr + \text{const} \quad , \tag{55}$$

where the function $S(r,n)$ is given by Eq. (43). Consider the nonautonomous system, in which case $F(\tau)$ is given by Eq. (41), or at least it is closely approximated by Eq. (44). Using the initial conditions (45) and the surface tension law of Eq. (43), we can evaluate the constant of integration in Eq. (55) as well as the second integral on the right-hand side of the equation. Denoting the first integral on the right-hand side of Eq. (55) by $I(r)$, we have

$$r^3 v^2 = 2I(r) + 2 \gamma \ln r - \begin{cases} \frac{2}{n-1} \left(\frac{r^3 - 1}{3} - \frac{r^2 - 1}{2} \right) & , \quad 1 < r < n \quad , \\ \left(r^2 - \frac{n^2 + n + 1}{3} \right) & , \quad n \leq r \quad . \end{cases} \tag{56}$$

But when $r = r_m$, $v = 0$ as we have noted. Therefore, when $r_m \geq n$, in accordance with the discussion surrounding Figure 3, we have

$$2I(r_m) = -2\gamma \ln r_m + r_m^2 - \frac{n^2 + n + 1}{3} \quad . \tag{57}$$

Since our interest is centered upon the maximum radius, $r_m \geq n$, we shall use Eq. (57) in order to evaluate $I(r_m)$.

In order to check the proposed use of Eq. (57), we have considered the case in which the forcing function $F(\tau)$ is a simple step function of strength α. In this case

$$I = \frac{\alpha}{3}(r_m^3 - 1) \quad .$$

We have integrated a number of bubble histories, $r(\tau)$, for various values of air content parameter γ, driving parameter α, and with $n = 5$ using a Hewlett-Packard HP 97 programmable calculator. Many of these trajectories exhibited a maximum radius r_m. For such trajectories values of α, γ, and r_m obtained for three values of air content are entered in the first three columns of Table III. The value of I, which can be computed directly in this case, is shown in the fourth column of Table III. The right-hand side of Eq. (56) is evaluated for $n = 5$ in the fifth column. Comparison of the values contained in the fourth and fifth columns shows excellent agreement. As a further check we have integrated Eq. (42) using a Runge-Kutta routine. The initial values were $r(0) = 1$, $v(0) = 0$, and we put $n = 5$. For the forcing function we took

of the algebraic matching have shown that both positive and negative values of τ_o can occur, The negative values appear in those cases for which τ_o, if known precisely, would be small. Therefore, it seems best to restrict all matching calculations to those which depend upon a quadrature.

Singular Points and Stability:

The rules relating to translation of the cavitation bubble along the surface of the body and for matching the forcing functions of the piecewise-autonomous and nonautonomous systems have been established. It is now necessary for us to explore the properties of the piecewise-autonomous system because its use in place of the more exact nonautonomous formulation will allow us to develop some criteria about ranges of the physical parameters leading to the various classes of solution, $r(\tau)$. The development of such conditions from autonomous forms of Eq. (12) certainly contains no novelty, [9], [21], and [22], but the piecewise-autonomous representation adopted here requires further study.

In order to carry out the following analysis, we return to Eq. (42), the initial conditions (45), and we use the transformation of Eq. (54). In this way we can rewrite (42) as

$$\frac{d}{dr}\,(r^3\,v^2) = 2\frac{\gamma}{r} - 2rS(r,n) + 2r^2F_a(\tau) \quad , \qquad (66)$$

where the forcing function $F_a(\tau)$ is illustrated in Figure 7 and defined by Eq. (49). When $0 \leq \tau \leq \tau_o$ the first integral of Eq. (66) which satisfies the initial conditions (45) is given by Eq. (56). Since $v = dr/d\tau$ the solution in terms of r and τ is given by

$$\tau = \int_1^r \frac{x^{3/2}\,dx}{\sqrt{\frac{2}{3}\alpha(x^3-1) + \gamma \ln x - \begin{cases} \frac{2}{n-1}\left(\frac{x^3-1}{3} - \frac{x^2-1}{2}\right), & x < n \\ x^2 - \frac{n^2+n+1}{3}, & x \geq n \end{cases}}} \quad . \tag{67}$$

In Eq. (67) when $r = r_o$, $\tau = \tau_o$, and $v_o = v(r_o)$ in accordance with Eq. (58). The quantities r_o and v_o are the initial conditions for the second part of the solution in which $\tau > \tau_o$ and $F_a = -\beta$. From Eq. (60) we can write the first integral of Eq. (66), accounting for these new initial conditions, as

$$r^3 v^2 = r_o^3 v_o^2 - \frac{2}{3}\beta(r^3 - r_o^3) + 2\gamma \ln\frac{r}{r_o} + \begin{cases} -\frac{2}{n-1}\left(\frac{r^3-r_o^3}{3} - \frac{r^2-r_o^2}{2}\right), & r < n \\ -r_o^2 - \frac{2}{n-1}\left(\frac{r_o^3}{3} - \frac{r_o^2}{2}\right) + \frac{n^3}{3(n-1)}, & r \geq n \end{cases} . \tag{68}$$

and from Eq. (68) we have

$$\tau - \tau_o = \int_{r_o}^r \frac{x^{3/2}\,dx}{g(\beta,\gamma,v_o,r_o;x)} \quad , \tag{69}$$

in which g is of obvious definition. Although we have reduced the problem to a quadrature, the solutions must be obtained numerically. Therefore, questions relating to the stability of various solutions are certainly of interest and we shall examine this matter further.

When one applies Liapounoff's method to the real root for case (i), this root being at $v = 0$ and

$$r = \frac{1}{3\alpha} + \left[\frac{1}{27\alpha^3} - \frac{\alpha}{2\alpha} + \frac{1}{27}\sqrt{\left(\frac{27\gamma}{2\alpha}\right)^2 - \frac{27\gamma}{\alpha 4}}\right]^{1/3}$$

$$+ \left[\frac{1}{27\alpha^3} - \frac{\gamma}{2\alpha} - \frac{1}{27}\sqrt{\left(\frac{27\gamma}{2\alpha}\right)^2 - \frac{27\gamma}{\alpha 4}}\right]^{1/3} , \qquad (81)$$

he finds that the two characterisitc values are real. Therefore, the singularity is a saddle point as it was in the case of $\gamma = 0$. We also note that Eq. (81) leads to $r = 1/\alpha$ when $\gamma = 0$ in agreement with the initial consideration of Eq. (80) for $\gamma = 0$.

For case (ii) the distinct root is found to be negative at $r = -1/3\alpha = -\sqrt{3\gamma/2}$. In this study all trajectories start from $r = 1$, $v = 0$, and proceed to phase-plane regions for which $r > 1$. Therefore this negative root will have little or no influence on the trajectory $v(r)$. On the other hand, the double root is found to be at $r = 2/3\alpha = \sqrt{3\gamma}$. Because this is a double root and the associated characteristic values are both zero, this singularity is not an elementary singularity which can be investigated by the usual methods. We shall therefore be content with the observation that for cases (i) and (ii) the defining condition, $\gamma\alpha^2 \geq \frac{4}{27} = 0.1481$, implies values of γ and α which will not be encountered in the examples of interest here.

In case (iii) there are real and unequal roots which are located at

$$\left.\begin{aligned} r_i &= \frac{1}{3\alpha} - \frac{2}{3\alpha}\cos\psi_i \quad , \quad i = 1, 2, 3, \\ \text{with} \quad \psi_i &= \frac{\phi + 2\pi(i-1)}{3} \text{ and } \phi = \cos^{-1}\left[\frac{27\gamma\alpha^2}{2} - 1\right] \quad . \end{aligned}\right\} \tag{82}$$

Study of these roots shows that r_1 and r_2 are saddle points and that r_1 is negative. We also find that r_3 is a vortex point. Thus in the right half of the phase plane there are two singularities which are at locations on the r-axis given by r_2 and r_3 in Eq. (82). We will find that the vortex point is nearer to the origin than the saddle point in most of the examples which we shall consider. Moreover, the root r_3 changes character, from vortex point to saddle point when $\alpha = 0$. Also when $\gamma = 0$ it becomes a double root at the origin as already discussed in connection with case (i).

The foregoing discussion summarizes the situation with respect to the singularities of the piecewise-autonomous system, Eq. (70), which corresponds to that phase of the bubble motion for which $F_a = \alpha$ (see Eq. 57). Because of the surface tension law employed in the theory, two separate phase-plane characteristics are required. For early phases of bubble growth when $1 \leq r(\tau) < n$, the only singularity in the right half of the r-v plane is a vortex point, located on the r-axis in accordance with the formulae of Eqs. (74) and (75). For bubble radii larger than n the preceding situation no longer applies. Instead the phase-plane picture changes instantaneously when $r = n$ to one in which there are two singularities in the right half plane. The signularity on the r-axis near the origin will generally be a

vortex point. The second singularity, which is more distant from the origin than the first will generally be a saddle point. Depending on the air content this situation can be reversed. This is the case (for $n = 1$) studied previously by Dergarabedian [21] and by Ma and Wang [22]. The present study is more restrictive than those cited in the sense that the only trajectories of interest here will be those which start from $r = 1$, $v = 0$. We may also claim an extension of previous work because of the inclusion of the surface tension law $S(n,\sigma)$ and the fact that here a piecewise-autonomous system is being considered. In fact, our next step is to study that part of the solution for which $F_a = -\beta$ in Eq. (55).

The phase-plane trajectories for this case are indicated by Eq. (59) if r_m and v_m are replaced by r and v and we do not set the product $r_o^3 v_o^2$ equal to zero. Alternatively if we replace the zero on the left-hand side of Eq. (59) by $r^3 v^2$ and put r instead of r_m on the right-hand side, we have the trajectories resulting from Eq. (68) after the term $r_o^3 v_o^2$ has been eliminated from Eq. (68) by using Eq. (58). The relationship $\tau = \tau(r)$ for this phase of the motion is an obvious extension of Eq. (67).

The analysis for stability of the system parallels that given above for $F_a = \alpha$. In this case, since $F_a = -\beta$, the equations indicated by Eq. (70) can be changed by replacing the term $+\alpha$ by $-\beta$. Therefore we have for $r < n$

$$\left.\begin{aligned} P(r,v) &= -[(n-1)\beta + 1]\, r^3 + r^2 + \gamma\,(n-1) - \frac{3}{2}(n-1)\, v^2 r^3 \\ \text{and} \\ Q(r,v) &= -\,vr^4\,(n-1) \quad . \end{aligned}\right\} \tag{83}$$

Or when $r \geq n$ we have

$$\left.\begin{aligned} P(r,v) &= -\beta r^3 - r^2 + \gamma - \frac{3}{2} v^2 r^3 \\ \text{and} \\ Q(r,v) &= vr^4 \quad . \end{aligned}\right\} \tag{84}$$

In either case, when $r < n$ or $r \geq n$, the fact that $F_a = -\beta$ indicates that the cavitation bubble will collapse provided that β is a sufficiently large positive number. Thus it is not surprising when we find for the case $r < n$ that there is only one singular point on the r-axis and that it is a vortex located at

$$r = \frac{1}{3[1 + (n-1)\beta]} [\, 1 + A + B] \quad , \tag{85}$$

where

$$\left\{ \begin{matrix} A^3 \\ B^3 \end{matrix} \right\} = 1 + \frac{27}{2} \gamma (n-1) [1 + (n-1)\beta]^2$$

$$\pm [1 + (n-1)\beta] \sqrt{27(n-1)\gamma \left\{ 1 + \frac{27}{4} (n-1)\gamma [1 + (n-1)\beta]^2 \right\}} \quad .$$

when $\gamma = 0$, Eq. (85) reduces to

$$r = \frac{1}{1 + (n-1)\beta} \quad . \tag{86}$$

When $r \geq n$ one must consider the three cases corresponding to those studied above when $F_a = \alpha$. However, in the present case it turns out that only one of the several possible real roots is in the positive half of the plane and

this root is a vortex point when $(27\gamma\beta^2/4) > 1$ and it is located at

$$r = -\frac{1}{3\beta}(1 + 2\cos\psi) \quad , \text{with } \psi = \frac{1}{3}\left[2\pi + \cos^{-1}\left(1 - \frac{27\gamma\beta^2}{2}\right)\right] \quad . \quad (87)$$

This finding is consistent with the physical behavior one expects in a region having an unfavorable environment for bubble growth. The other singular points, being in the negative half of the phase plane, should have no effect on the solution.

Thus far the analysis has been restricted to $\beta > 0$. If β should change sign, it is evident that the general features of the phase plane studied previously for $\alpha > 0$ will be regained. If one makes the change in sign of the β term in the various formulae given above, he can see the ranges for the various parameters which lead to a single vortex for $r > 1$ or for vortex and saddle points on the r-axis as before.

Limiting Trajectories:

While the locations and the character of the singularities in the phase plane help us to understand the stability and general shapes of the trajectories near these points, we still need to know what particular type of solution we might expect for prescribed values of the governing physical parameters α, β, γ, and τ_o. We can obtain some guidance in this matter by using an approach suggested previously in Ref. [9].

For example, it is clear from the development of Eq. (55) that the first integral of the equation of motion is an energy integral. The left-hand side of this equation is the change in kinetic energy. The right-hand side is the work done by the external environment, the air inside the bubble

and the surface tension forces. As long as we maintain a constant value of α the formulation adopted here allows for no change in the total energy of the system.

As the bubble grows, the logarithmic effect of air content in Eq. (56) will be much smaller than the polynomial terms on the right-hand side of Eq. (56). Therefore, the work done will have a general shape of a cubic in r. In a plot of work done against the radius r, one would see a curve which starts from $W(1) = 0$. As r increases $W(r)$ rises to a maximum and subsequently descends to an isolated minimum at some critical radius, $r = r_c$. It can be shown for n greater than unity that the minimum of W occurs at a value of r_c greater than n as long as $\tau_o \to \infty$. Since the kinetic energy is zero for $r = 1$ it will be zero again if $W_{min} = 0$. The fact that r_c is a minimum of W insures that the time required for the bubble to grow to r_c is logarithmically infinite. Thus, if α and γ are chosen so as to make $W_{min} = 0$, appreciable growth will not occur, although Class-1 solutions are certainly not ruled out. Then for the step function input, corresponding to $\tau_o \to \infty$, we might say that cavitation might not occur for values of α and γ which are less than or equal to these critical values. However, this statement requires some further qualification.

We can denote these critical values of α and γ, corresponding to $r = r_c$, by α_c and γ_c. Moreover, within the range of bubble radii under consideration here, the phase-plane trajectories must share the cubic appearance of $W(r)$. Therefore they too, often have isolated minima at certain radii r_c and when a particular trajectory is just tangent to the r-axis in the phase plane the values of α and γ will have assumed their critical values as described above. Generally we envisage that this limiting trajectory will be approached from a sequence of trajectories upon which $\alpha > \alpha_c$. On any one of these

trajectories a bubble would grow without limit and we would say for the step function driving parameter that Class-4 solutions are obtained. On the other hand, as we shall see when $\alpha < \alpha_c$, the phase plane trajectories are closed and Class-1 solutions are found. Evidently the critical trajectory, upon which $\alpha = \alpha_c$ and $\gamma = \gamma_c$, is a separatrix between Class 1- and Class-4 solutions for a step function driving parameter. Therefore we should not necessarily regard these values of α_c and γ_c as being those which would preclude cavitation in all circumstances. We must await the outcome of the entire analysis before we can decide this point.

Continuing with the case in which $\tau_o \to \infty$, we must find the specific relationships between the critical values of r, α, and γ. These follow from the conditions

$$W(r_c) = 0 \;\rightarrow\; v(r_c) = 0$$

and

$$\left.\frac{dW}{dr}\right|_{r_c} = 0 \;\rightarrow\; \left.\frac{dv}{dr}\right|_{r_c} = 0 \quad .$$

The two equations which result from these conditions are

$$\frac{2\alpha_c}{3}(r_c^3 - 1) + 2\gamma \ln r_c - r_c^2 + \frac{n^2 + n + 1}{3} = 0$$

and

$$\alpha_c r_c^3 - r_c^2 + \gamma = 0 \quad .$$

These equations account for the fact that $r_c \geq n$ as noted previously, and these conditions will certainly apply to spherical bubble nuclei when $n = 1$. We observe that these equations, being linear in α_c and γ_c, can be solved for these parameters in terms of r_c. The solution is

$$\alpha_c = \left[(2\ln r_c - 1)\, r_c^2 + \frac{n^2 + n + 1}{3}\right]/(2\Delta) \qquad (88)$$

and

$$\gamma = r_c^2 \left[r_c^3 - (n^2 + n + 1)\, r_c + 2\right]/(6\Delta) \quad , \qquad (89)$$

where

$$\Delta = (\ln r_c - \tfrac{1}{3})\, r_c^3 + \tfrac{1}{3} \quad . \qquad (90)$$

When $r_c < n$ we can proceed formally using the same criteria on v and dv/dr as for $r_c \geq n$. In this case the fundamental equations become

$$\alpha_c\, r_c^3 + \gamma = \frac{r_c^2 (r_c - 1)}{n - 1} \qquad \text{(from } dv/dr = 0\text{)}$$

and

$$\alpha_c\, (r_c^3 - 1) + 3\gamma \ln r_c = \frac{(r - 1)^2\, (2r + 1)}{2\,(n - 1)} \qquad \text{(from } v = 0\text{)} \quad .$$

Solving for α_c and γ as before, we get

$$\alpha_c = \frac{(r_c - 1)}{\Delta\,(n - 1)} \left[3 \ln r_c - \frac{(r_c - 1)(2r_c + 1)}{2}\right] \qquad (88a)$$

and

$$\gamma = - \frac{r_c^2\, (r_c - 1)^2\, (r_c + 2)}{2\Delta\,(n - 1)} \quad , \qquad (89a)$$

where the value of Δ is given by Eq. (90). These results will be used at a later point in the argument.

Returning to the physically important case of $r_c \geq n$ [Eqs. (88) and (90)], we see that the smallest physically admissible value of the air content parameter is $\gamma = 0$. From Eq. (89) we see when $\gamma = 0$ that r_c values are found as roots of a cubic. The root of interest must satisfy $r_c \geq n$ and it can be found numerically. Figure 9 shows values of α_c and r_c versus n when $\gamma = 0$ in accordance with Eqs. (88), (89), and (90). Figure 10 shows α_c and γ as functions of r_c for a spherical nucleus, n = 1, and for a stable nucleus, n = 5.

It remains to make good our assertion that the separatrix corresponding to α_c, γ which passes through the phase-plane point $(r_c,0)$ does separate Class 1 from Class-4 solutions when the external driving parameter $F_a(t)$ is a step function. In order to illustrate these points, we have simply obtained some numerical results for zero air content and for a stable nucleus having n = 5. These trajectories were calculated on a Hewlett-Packard HP 97 programmable calculator. Since the calculator is limited to programs which contain no more than 125 steps, the step function input, $F_a(t) = \alpha \cdot H(t)(\text{for } \tau_o \to \infty)$,* is about the most elaborate trajectory calculation that could be performed using only a single program. The program was designed to calculate the phase-plane trajectories for various values of α and γ in accordance with Eq. (56) and to determine the growth time to any $r(\tau)$ by a numerical integration as discussed in connection with Eq. (58) and shown explicitly in Eq. (67). An example of several phase-plane trajectories at $\gamma = 0$ and with n = 5 is shown in Figure 11. Only the upper half of the phase plane is shown in Figure 11. If the trajectories shown are reflected in the r-axis, the phase-plane representation would be complete.

---

*H(t) denotes the Heaviside function.

November 19, 1979
BRP:mmj

A general finding illustrated by this figure is that the critical trajectory corresponding to $\alpha_c = 1/r_c = 0.180661$ and $r_c = 5.5352$ does separate the form of solutions to be expected from the autonomous equation of motion. When $\alpha < \alpha_c$, Figure 11 shows that the complete trajectories are closed loops so that these solutions are periodic. The amplitudes r_m and the half-periods, τ_m, for these solutions are shown in Figure 12. This figure shows how the amplitude and half-period increase with increasing α until the critical value $\alpha_c = .180661$ is reached. It can also be seen that τ_m does not vanish at $\alpha = 0$. In order to see how this nonzero limit occurs, we return to the autonomous form of Eq. (42) and write $r = 1 + x$. Near $\alpha = 0$, r is close to one so that we can assume that $x << 1$. Therefore, if we retain only first order terms in x, the equation of motion is linearized. These steps result in

$$\frac{dx^2}{d\tau^2} + \left(\alpha + \frac{1}{n-1} + 4\gamma\right) x = \alpha + \gamma$$

and

$$x(0) = \dot{x}(0) = 0 \quad .$$

The solution of this equation is

$$x = \frac{\alpha + \gamma}{\alpha + \frac{1}{n-1} + 4\gamma} \left[1 - \cos\left(\tau \sqrt{\alpha + \frac{1}{n-1} + 4\gamma}\right)\right] \quad .$$

The maximum value of x occurs when

$$\tau_{max} \sqrt{\alpha + \frac{1}{n-1} + 4\gamma} = \pi$$

so that

$$x_{max} = \frac{2(\alpha + \gamma)}{\alpha + \frac{1}{n - 1} + 4\gamma} \quad .$$

For the situation of present interest we have $\alpha = \gamma = 0$ and $n = 5$. Therefore $x_{max} = 0$ and $\tau_{max} = \pi\sqrt{n - 1} = 2\pi$ as shown in Figure 12.

We also note from Eq. (73) and the considerations which follow from it that the "closed loops" in Figure 11 are centered about vortex points which are positioned at $r = [1 - (n - 1)\alpha]^{-1}$, $v = 0$, provided that $r_m < 5$. Locations of the singular points on the r-axis for various values of α are given in Table V. The location r given for the last entry at $\alpha = 0.8066$ in Table V is valid only for those points along the trajectory for which $r(\tau) < n$. When $r \geq n$, the singularities are located in accordance with Eq. (80). In the case $\gamma = 0$, we have seen that the singularity is a saddle point at $r = 1/\alpha = 5.5353$. This saddle point is nearly coincident with the critical value r_c corresponding to $\alpha_c = 0.80661$. We note, however, that $r_m = 5.52886$ lies inside the position of the saddle point for this case so that this particular trajectory must be a closed loop. It is worth noting that as $\alpha \to \alpha_c$ the saddle point location coincides with the critical point location $r_c = 1/\alpha_c$ as indicated in the discussion leading to Eq. (88). Evidently the critical point is a saddle point and the limiting trajectories through this point are separatricies which, for the case of $\tau_o = \infty$, separates Class 1 from Class-4 solutions. Solutions of this latter type are shown in Figure 11 by the trajectories for $\alpha = 0.1807$ and 0.1875. The trajectory denoted by $\alpha = 0.18066$ is one of the Class-1 solutions used previously in Table III.

Continuing with the example for $\tau_o = \infty$, but extending our considerations to air contents exceeding zero, we find phase-plane plots to have trajectories of the same general appearance as those of Figure 11. All considerations discussed above for the case when $\gamma = 0$ apply as well to these more general cases. The chief difference pertains to the location of the critical point r_c and the value of α_c as γ varies. Again, these critical values separate solutions of Class 1 from those of Class 4. Previously we had discussed Figure 10 which shows plots of α_c and r_c for a range of air contents. These data permit one to place a lower bound on conditions for significant vaporous bubble growth because we shall, for the most part, be interested in how the solutions corresponding to unlimited growth, such as those trajectories for $\alpha > \alpha_c = 0.180661$ in Figure 11, are converted into Class-3 solutions when τ_o is finite. However, as we have seen from the preceding considerations on gaseous growth, there will be cases in which only modest vaporous growth will be needed to initiate vaporous cavitation. In such cases solutions of Class 1 may be of interest.

Suppose next that $\alpha > \alpha_c$ and that τ_o has a prescribed finite value and that n and γ are prescribed as before. Then one can inquire as to the values of β and a new value of r_c for which the time required for growth is infinite. As will be shown later, the preceding critical values of r_c and α_c and the new pair of critical values, $\beta_c(\alpha,\gamma)$ and $r_c(\alpha,\gamma)$, put limits on the range of physical parameters within which Class-3 solutions are to be expected. (See the discussion of solution types following Eq. (45).) The second pair of critical values are determined from the first integral of the equation of motion as indicated by Eq. (56). The form of the equation of interest here is

and that the final determination of r_m must await other considerations which are given later.

Once r_m is prescribed, we must match the nonautonomous and the piecewise-autonomous systems. We shall replace the nonautonomous equations with those derived for the piecewise-autonomous system on the basis that the matching between the two identifies the values of r_m and τ_m as being equals. Thus we calculate

$$I = \frac{1}{2} r_m^2 - \gamma \ln r_m - \frac{n^2 + n + 1}{6} \quad . \tag{57a}$$

Then we have

$$r_o = \left[\frac{\alpha + \beta r_m^3 + 3 I(r_m)}{\alpha + \beta} \right]^{1/3} \quad . \tag{59}$$

Since α and β are known (at least for the value of K selected), Eq. (59) determines r_o "once and for all." The time for the first phase of vaporous growth (in the region of favorable environment for growth where $F_a = \alpha$) is

$$\tau_o = \begin{cases} \displaystyle\int_1^{r_o} \frac{dr}{\sqrt{g_1(\alpha,\gamma,n;r)}} \quad , & r_o < n \quad , \\ \displaystyle\int_1^{n} \frac{dr}{\sqrt{g_1(\alpha,\gamma,n;r)}} + \int_n^{r_o} \frac{dr}{\sqrt{g_2(\alpha,\gamma,n;r)}} \quad , & r_o \geq n \quad , \end{cases} \tag{64}$$

where

$$g_1(\alpha,\gamma,n;r) = \frac{2\alpha}{3}\left(1 - \frac{1}{r^3}\right) + \frac{2\gamma}{r^3}\ln r - \frac{2}{n-1}\left[\frac{1}{3}\left(1 - \frac{1}{r^3}\right) - \frac{1}{2}\left(\frac{1}{r} + \frac{1}{r^3}\right)\right] ,$$

and

$$g_2(\alpha,\gamma,n;r) = \frac{2\alpha}{3}\left(1 - \frac{1}{r^3}\right) + \frac{2\gamma}{r^3}\ln r - \frac{1}{r} + \frac{n^2 + n + 1}{3r^3} .$$

The next phase of growth takes place when $F_a = -\beta$ and the bubble attains its maximum radius. Let this interval be designated by τ_g. Then

$$\tau_g = \int_{r_o}^{r_m} \frac{dr}{g(\beta,\gamma,v_o,r_o;r)} \tag{69a}$$

and from Eq. (69) when suitable modifications are introduced, g is defined by

$$g^2 = \frac{2}{3}(\alpha + \beta)\frac{r_o^3}{r^3} - \frac{2}{3}\alpha\frac{1}{r^3} - \frac{2}{3}\beta + \frac{2\gamma}{r^3}\ln r - \frac{1}{r} + \frac{n^2 + n + 1}{3r^3} , \quad r_o \leq r \leq r_m .$$

(69b)

Equation (69b) holds for $1 \leq r_o < n$ for $r_o \geq n$, but with $r \geq n$. The matching is completed when we put

$$\tau_m = \tau_a + \tau_o + \tau_g , \tag{113}$$

where τ_m is given by (31a), τ_a is the interval between the time when the static pressure outside the bubble first equals the vapor pressure and

The limiting condition between these two solution classes corresponds to an equality in Eq. (114). Thus

$$\beta \sqrt{\gamma} = -\frac{1}{\xi}\left(1 - \frac{1}{\xi^2}\right) \quad , \tag{115}$$

where $\xi = r_m/\sqrt{\gamma}$. Equation (115) is plotted in a ξ, $\beta\sqrt{\gamma}$ - plane in Figure 13. Since $r_m \geq n$, ξ will generally be found on that branch of Eq. (115) which is to the right of the minimum and K will be such that $\beta \sqrt{\gamma}$ will be at a point inside the curve.

On the other hand, we have seen that once γ is selected, the value of the smaller critical radius, r_s and the corresponding value of the parameter α_c is determined once and for all by Eqs. (88), (89), and (90). If the cavitation number is such that $\alpha \leq \alpha_c$, the time required for vaporous growth to r_s will be logarithmically infinite and if $r_m > r_s$, the maximum radius will not be attained. Useful reference values of $K = K_r$, $\beta = \beta_r$, and $r = r_r$ are defined when Eq. (115) for the larger critical radius is solved for ξ_r and when $\beta_r = \beta_s$ corresponding to the cavitation number for the smaller critical radius. Then in Figure 13 we see that the only permissible values of r_m (or ξ_m) must lie to the left of the intersection at ξ_r between the horizontal line through $\beta = \beta_r$ and the curve of Eq. (115), provided that $\beta_r < 0$. If $\beta_r \geq 0$ the entire area corresponding to $\beta < 0$ and to the right of the minimum of $\beta\sqrt{\gamma}$ is available for Class-3 solutions. If $\beta_r < 0$, the point $(\xi_m, \beta_m\sqrt{\gamma})$ must lie within the wedge-shaped region between the horizontal line and the curve if Class-3 solutions are to be found. This restriction also limits the

the range of r_m to be within the interval

$$n < r_s < r_m < r_r \quad , \tag{116}$$

where r_{sc} is the smaller critical radius defined by Eqs. (89) and (90). The condition given by Eq. (116) supplements that given by Eq. (112) if $\beta_r < 0$.

In order to explore this point in more detail, a numerical example based upon Eqs. (57a), (59), (64), and (69a) has been carried out for several cavitation numbers (or β's) and at three values of r_m in the permissible region. Since all r_m have been taken to be only slightly less than r_r, Figure 14 shows a greatly enlarged plot of the vicinity to the left of the point of intersection $(\xi_r, \beta_r\sqrt{\gamma})$. Figure 14 also shows a number of level lines bearing prescribed values of the time spent in vaporous growth for $1 \leq r \leq r_m$. These level lines of $\tau_o + \tau_g$ result from numerical integrations of Eqs. (64) and (69a). Figure 15 results from cross plotting the data given in Figure 14. This figure shows graphs of τ as a function of $\beta\sqrt{\gamma}$ for the three values of r_m selected for study. The vertical axis on the right of Figure 15 passes through the smaller critical radius line in Figure 14 so that as $K \to K_s$, $\tau \to \infty$. Similarly, the other axes, being at the intersection of r_m with β as given by Eq. (115) and the selected values of ξ_r towards the left in Figure 14. These illustrations show that the solution of the problem of matching a prescribed maximum vaporous growth and a prescribed growth time is not unique. Because of Eq. (7) it follows for given values of ξ_m and τ that the value of K which gives $\beta \to \beta_s$ will be larger than the value of K on that branch of the level line which is near $\beta_\ell\sqrt{\gamma}$. Thus if we prescribe r_m, we are tempted to let this larger value of K determine the cavitation number for inception. However, it is better to reserve this judgment until the conclusion of the investigation. Any r_m value can be prescribed provided that the prescription does not violate conditions given by Eqs. (112) and (116).

of β_c equals or exceeds zero. The first case applies to larger bodies operating at rather low speeds and the second case corresponds to relatively smaller bodies in a relatively high-speed flow.

Next suppose that values of n and R_o are known. Let us find approximately the cavitation-transition state as defined by the values of K and V_o for bubble-ring inception. In the high-speed case when the value of α_s is such that the corresponding critical value of β is positive, we can calculate r_s from Eqs. (88), (89), and (90) as usual. Then we put $r_m = r_s$ as the smallest value of r_m likely to be permissible. This value of r_m can be used in Eq. (9) to calculate Re and then V_o can be found. Once V_o is known C_σ can be found from the formula given by Eq. (6). The value of r_m can also be used in Eq. (93) in order to calculate β. Then Eq. (7) gives the transition value of K. Since the high-speed case is the more likely of the two possibilities, we shall not pursue this matter further. Instead we turn to the consideration of the phenomenon of bubble-ring-cavitation cutoff.

Cavitation Cutoff

The following calculations are motivated by the fact that in the experiments of Reference 3 no bubble-ring cavitation was observed at a free-stream velocity of 30 fps (9.144 m/s), although other forms of cavitation were observed at this speed. A tunnel speed of 40 fps (12.192 m/s) was the next higher speed in these experiments and bubble-ring cavitation was observed at this speed. Thus it was found that a bubble-ring cavitation "cutoff speed" existed at some value of tunnel velocity between 30 and 40 fps (9.144 and 12.192 m/s). No systematic

experiments were carried out in order to determine the cutoff values of tunnel speed and desinent cavitation number.

As a first step in the cutoff calculation, we offer an interpretation of the experimental findings which can be expressed in terms of the present theory. One factor may be that since the cutoff speed is a relatively low speed, the cavitation number at this speed should be somewhat less than that at the inception numbers at higher speeds. Moreover, since this speed is a threshold value for bubble-ring cavitation, it seems that the cavitation number should probably be as low as possible. For bubble-ring cavitation the lowest cativation number will be accompanied by the largest permissible value of r_m. Thus r_m will be given by Eq. (9); namely,

$$r_m = \frac{27.8D}{Re^{0.79} R_o} \tag{9}$$

The idea here is that for Class-2 or Class-3 trajectories the greatest amount of vaporous growth should occur in such a way that the maximum radius is limited by the height of the laminar bubble. Moreover, since we are dealing with the asymptotic theory, the value of r_m will be a larger critical value. That is, from Eq. (93) we have

$$\beta = \frac{1}{r_m}\left(\frac{\gamma}{r_m^2} - 1\right) \quad . \tag{93}$$

Also the radii r_m and r_o must be related by Eq. (59), which we will write as

$$(\alpha + \beta)\, r_o^3 = \alpha + \beta\, r_m^3 + \frac{3}{2} r_m^2 - 3\gamma \ln r_m - \frac{n^2 + n + 1}{2} \quad . \tag{59}$$

Since r_m is a larger critical radius, the condition for vanishing slope of the phase-plane trajectory at r_m from Eq. (93) can be used in the right-hand side of Eq. (59) in order to eliminate the term βr_m^3. The result is

$$(\alpha + \beta)\, r_o^3 = \alpha + \gamma + \frac{1}{2} r_m^2 - 3\gamma \ln r_m - \frac{n^2 + n + 1}{2} \quad . \tag{127}$$

If we use the condition given by Eq. (9) and the definition for the Reynolds number, we can write Eq. (9) as

$$r_m = 27.8\nu^{0.79} D^{0.21} / (V_o^{0.79} R_o) \quad , \tag{128}$$

where V_o is now the cutoff velocity, V_{co}.

If for the moment we assume that V_{co} is known, then Eq. (128) determines r_m and since n, R_o, and γ are known quantities, β is given by Eq. (93). On the other hand, we can use Eq. (47) in order to write the quantity $(\alpha + \beta)$ in terms of the cutoff velocity as

$$\alpha + \beta = (b + C_{p_s})\, \rho\, R_o\, V_{co}^2 / (4\sigma) \quad . \tag{129}$$

Since Eq. (129) contains known quantities, the sum $\alpha + \beta$ is determined and α can now be found because β itself is known. It remains to make good our assumption that V_{co} can be found by closing the above system of equations with an additional condition.

Thus far we have required the greatest amount of vaporous growth, without producing unlimited growth as would be found in Class-4 solutions, by specifying the largest possible value of r_m. This specification is consistent with the idea that the cutoff velocity is the limiting condition

for bubble-ring cavitation, but that other forms which are independent of a laminar bubble being present may exist. The cavitation number for this condition will be as small as possible but not too small for Class-3 solutions, if the radius r_o in Eq. (127) is taken to be as small as possible. Strictly speaking, this condition will be one in which the parameter α will be close to but larger than α_c, corresponding to a smaller critical radius [see Eqs. (88), (89), and (90)]. However, the phase-plane trajectory will still show an isolated minimum at a radius slightly less than the smaller critical radius. We have seen in connection with the general structure of permissible solutions that the difference between α and α_c will be very small indeed. Therefore we can, within the framework of the present asymptotic theory, put $\alpha = \alpha_c$, $r_o = r_c$ and produce negligible error. If we adopt this proposal, we can return to Eqs. (89) and (90) and combine them into the single condition

$$r_o^2 + 2\gamma(1 - 3\ln r_o) - (n^2 + n + 1) + \frac{2}{r_o}\left(1 - \frac{\gamma}{r_o^2}\right) = 0 \quad . \tag{130}$$

For values of r_o in the range $1 < r_o < r_m$, this equation will have one root, provided that V_{co} is properly chosen. The fact that r_o depends parametrically on V_{co} suggests that one may write

$$G(V_{co}) = r_o^2 + 2\gamma(1 - 3\ln r_o) - (n^2 + n + 1) + \frac{2}{r_o}\left(1 - \frac{\gamma}{r_o^2}\right) \tag{130a}$$

and solve for $G = 0$ by iteration on V_o because the foregoing system of equations is now closed.

The preceding analysis has used formulae which have been designed for r_m and r_o both larger than or equal to n. But we have seen that as long as $r_m \geq n$, Eq. (59) is valid for any value of r_o in the range $1 < r_o < r_m$. On the other hand, if $r_o < n$ Eq. (130a) does not apply. The applicable equation can be obtained from Eqs. (90) and (89a). Upon combining these two equations we find that if $r_o < n$, the condition that $G(V_{co}) = 0$ can be expressed as

$$\alpha(r_o - 1)(r_o + 2) + 6\gamma \ln r_o = \gamma(1 - \frac{1}{r_o})(2 + \frac{1}{r_o}) \quad . \tag{131}$$

But α and γ are both positive and $r_o > 1$ for situations of physical interest. Therefore we see that Eq. (131) has no solution if $r_o < n$. Since we shall continue to impose the condition that $r_m \geq n$, it follows that admissible solutions of Eq. (130a) must lie in the range $n \leq r_o < r_m$. Therefore, if in the calculation of r_o in accordance with Eq. (59) one finds that $r_o < n$, it follows that there is no solution for V_{co} corresponding to selected values of the parameters R_o, n, and γ.

Once V_{co} has been found by the method suggested above, one can complete the calculation by finding C_σ from

$$C_\sigma = 4\sigma/(\rho R_o V_{co}^2) \quad , \tag{132}$$

and the cutoff cavitation number from either of

$$K_{co} = b - \alpha C_\sigma = \beta C_\sigma - C_{p_s} \quad . \tag{133}$$

Table IX gives numerical data from calculations as outlined above for cutoff values of V'_{co} and K_{co} at a water temperature of 80°F (26.67°C). Extensive

ranges of R_o (microns) and n have been selected for two air contents in order to show the general trends forecast by the analysis as clearly as possible. All calculations pertain to $C_{p_s} = -0.630$.

As noted already, experimental observations now available [3] indicate a cutoff velocity between 30 fps (9.14 m/s) and 40 fps (12.19 m/s) for a 2-inch (0.0508 m) diameter hemispherical nose at water temperature between 78° (25.56°C) and 79°F (21.11°C). This range of possible cutoff velocities was not found to change with dissolved air content. In order to illustrate how the present numerical data fit in with the observed trends, we have extracted those values from Table IX which lie in the neighborhood of the experimental trends and presented them in the carpet plot of Figure 20. In this plot the abcissa is simply the cutoff velocity V_{co}. The ordinate is the cutoff cavitation number K_{co}. However, this ordinate has a sliding scale which depends upon the value of n chosen for each calculation of the cutoff condition (V_{co}, K_{co}). For example, suppose the value of n is 6. Then at the ordinate marked 6 in Figure 20, $K_{co} = 0.5$. At the ordinate marked 5, we would have $K_{co} = 0.4$ and at the ordinate marked 7, we would have $K_{co} = 0.6$. It is necessary to choose this kind of a sliding scale because it is found from the values given in Table IX that V_{co} is the primary quantity affecting the value of K_{co}. The values of R_o and n affect K_{co} less directly. Another interesting fact which emerges from Figure 20 is that the influence of air content, at least within the range studied, seems to have little effect upon the value of K_{co} to the accuracy of a plot to the scale of that used here. The chief differences appear in the third or fourth decimal places. For this reason each curve of K_{co} versus V_{co}, shown at the slightly sloping lines for each value of n

November 19, 1979
BRP:mmj

On the other hand, we can also find the values of V_o, K, and r_s at the intersection of Class-3 and Class-2 solutions. Since $\beta = (\gamma/r^2 - 1)/r$ and $\beta C_\sigma = K + C_{p_s}$ from Eq. (7), we can write

$$V_o = 2\sqrt{\frac{\sigma}{\rho R_o(b + C_{p_s})}\left[\alpha_c + \frac{1}{r}\left(\frac{\gamma}{r^2} - 1\right)\right]} \quad . \tag{136}$$

But

$$Re = \frac{V_o D}{\nu}$$

and

$$r = \frac{55.5D}{R_o R_e^{0.76}}$$

and these can be used in conjunction with Eq. (136) in order to solve for V_o by trial and error. This solution then permits us to find the value of K at which Class-3 and Class-2 V_o- versus -K curves intersect. Note that the value of r used here depends on the full laminar bubble height instead of the half-height as given by Eq. (9).

The foregoing calculations for Class-3 and Class-2 solutions have been programmed for execution on a computer. The cavitation cutoff curves of Figure 20 were used to select likely values of R_o and n for air contents of 7.5 and 15 parts per million. Calculations were then made in order to see which set of parameters gives Class-3 solutions which seem to match the data of Holl and Carroll [3] for a water temperature of 80°F (26.67°C) and cavitation cutoff speeds between 30 and 40 fps (9.144 m/s and 12.192 m/s). The results of these calculations which gives the best agreement is shown in Figure 22. As also found

experimentally, the calculations are practically independent of dissolved air content. The best agreement is found for a spherical nucleus, n = 1, having a radius R_o of 5.18 microns. The cutoff speed is also shown in Figure 22. The agreement is best when the maximum vapor bubble radius is set equal to the full laminar bubble height. The result of using half the laminar bubble height is also shown in this figure.

Figure 23 is an enlarged plot which presents the same data as Figure 22 for the Class-3 solutions and also shows the trend found for one example of the Class-2 solution having the input parameters indicated. The similarity between the Class-2 solution shown in Figure 23 and similar trends reported in Reference 9 may be noted. The reason for this similarity is the fact that the present Class-2 solutions and the theory of Reference 9 are essentially the same.

It is believed that the comparison between the best Class-3 solution and the data is most encouraging. Insofar as it has been possible, these calculations have been carried out from first principles. Of course, the pressure distributions of Holl and Carroll together with the laminar bubble data of Figure 2 are basic to the entire calculation scheme. Certainly, we are now lead to discard the Class-2 solution compared to the results which are obtained if we insist that Class-3 solutions be required. Moreover, if we are prepared to "fudge" on the meanings of the numerical constants appearing in Eq. (134), we could fit the theory to the experiments almost exactly. However, our concern has been to obtain some justification for the basic hypotheses outlined in THE SEQUENCE OF EVENTS at the start of this report. The present comparisons tend to increase our confidence in their validity.

November 19, 1979
BRP:mmj

Table I

Values of the Parameter $|\beta|$ when $(K + C_{p_s}) = 0.05$

V_o, fps (mps)	20(6.10)	30(9.14)	40(12.2)	50(15.2)	60(18.3)	70(21.3)
$\|\gamma - \Gamma\| = \|\beta\|$	0.013	0.029	0.051	0.080	0.115	0.156
C_σ	3.93	1.74	0.981	0.628	0.436	0.320

Table II

Pressure Distribution on a 2 in. (0.0508 m) dia. Hemisphere Headform in a 12 in. (0.3048 m) dia. Tunnel

s/D	0.557	0.617	0.674	0.715	0.748	0.765	0.705	0.798
C_p	-0.615	-0.732	-0.780	-0.746	-0.661	-0.640	-0.617	-0.613

November 19, 1979
BRP:mmj

Table III

Comparisons of $I(r_m)$ from Eq. (53) with Results Obtained by Numerical Quadrature for a Step Function Forcing Function

α	γ	r_m	$I = \frac{\alpha}{3}(r_m^3 - 1)$	$\frac{1}{2} r_m^2 - \gamma \ln r_m - \frac{n^2 + n + 1}{6}$
0.18066	0	5.52886	10.11743	10.117479
0.16406	0.6	5.95794	11.510957	11.511037
0.15034	1.2	6.42355	13.232349	13.232366

Table IV

Summary of Matching Tests ($\alpha = 0.3$, $\beta = 0.08$, $\gamma = 0.2$)

How Matched	τ_m	% error	r_m	% error	τ_a	τ_c
Test Case	36.71	-	8.490	-	0	-
Algebraic	30.68	-16.42	9.430	-11.1	-2.824	21.88
Quadrature	44.63	+21.5	8.574	+0.99	13.81	19.445